THE FORMATION OF PLATINUM ALUMINIDE COATINGS ON IN-738 AND THEIR OXIDATION RESISTANCE

by

Muayyad Dawood Hanna, B.Sc., (Baghdad), D. de Specialite (Nancy)

A thesis submitted in fulfilment
of the requirements for the degree
of Doctor of Philosophy at the
Department of Metallurgy, University
of Sheffield.

OCTOBER, 1982.

TO MY WIFE AND SON

CONTENTS

'THE FORMATION OF PLATINUM ALUMINIDE COATINGS ON IN-738 AND THEIR OXIDATION RESISTANCE'

by Muayyad Dawood Hanna - October, 1982

SUMMARY

Platinum aluminide coatings have been produced by first plating a thin layer of platinum using a fused salt platinum plating technique and then pack aluminizing using powder packs containing Al, NH_4Cl and Al_2O_3 or Ni_2Al_3, NH_4Cl and Al_2O_3. The chemistry and morphology of these coatings on IN-738 superalloy both in the as-coated and in the subsequently heat treated condition have been studied. The coating morphology and chemistry are highly dependent upon the thickness of the platinum layer, pack activity and time of processing. A relatively thick platinum layer (~10 μm) produced a coating with an outer Pt_2Al_3 layer above other narrow layers. The Pt concentration decreases towards zero as the diffusion zone is approached. A second type, usually formed with a thin (5 μm) Pt layer is characterised by a marked interaction with the substrate. An outer $PtAl_2$ layer is followed by a layer of NiAl containing fine precipitates of a chromium-tungsten rich phase. A lamella-like layer high in chromium and other refractory elements exists at the coating/substrate interface in most of the as-coated samples.

A third type of coating has been produced by a post-platinising heat treatment process prior to aluminizing. This type of coating is characterised by an outer duplex layer of $PtAl_2$ and NiAl. Heat treatment of the as-formed coating results in interdiffusion between Al, Ni and Pt to produce an overall thickening of the coating layer and a decrease in the coating Al concentration. Thus a (Pt,Ni) Al or (Ni,Pt) Al outer layer may develop after heat treating these types of coatings at 1000°C for up to 1200 hours. In addition to this Widmanstatten

sigma phase plates extending into the substrate are normally found beneath the outer layer after several hours of heat treatment. Diffusion paths on pseudo-ternary phase diagrams are made to represent the phase constitution of the as-formed coatings.

Isothermal oxidation tests in an oxygen atmosphere between 800 - 1000^{o}C of different Pt-Al surfaces have been studied and the result of tests showed that the incorporation of Pt into the aluminide coatings enhance the oxidation resistance (particularly at 1000^{o}C). Furthermore, thermal cyclic oxidation tests showed a remarkable improvement in oxide adherence over the simple aluminides.

INTRODUCTION

The majority of gas turbines in current service rely upon the use of conventional nickel aluminide diffusion coatings to protect superalloy turbine components from both oxidation and hot corrosion, but in the more extreme environments, predicted turbine blade lives are not being achieved. This breakdown of the protective coating may result in severe metal loss from the blade alloy.

One of the solutions to this problem is to develop improved coating systems. At the present time interest is centred around further developments of MCrAlY overlay and platinum aluminide systems. Platinum aluminides show a real cost advantage when compared to the overlays for the same applications. They are also in strong competition with the overlay coatings where the reduced ductilities of the platinum aluminide coatings can be tolerated.

A knowledge of the constitution and structure of Pt-Ni-Al coatings developed by diffusion processing is an important aspect of this type of coating technology but has had little attention over the last ten years. Chapter One presents a review of aluminide coatings including a general background to the coating technology and methods by which various coatings can be produced. Following this, the Pt-Al system is considered. The structures of the platinum-aluminide coatings on nickel base superalloys are described. Finally in the Review, oxidation and hot corrosion improvements due to the incorporation of platinum in the coating are presented.

In this study platinum-aluminide coatings have been formed by first plating a thin layer of platinum onto the IN-738 coupon, and then aluminizing by a pack process.

The coatings formed show that different microstructures can be produced depending on the thickness of the platinum plate and the temperature and time of aluminizing. Details of the different microstructures have been studied using metallographic techniques including X-ray diffraction, SEM and electron probe microanalysis. Results are presented which led to the identification of the coating phases and their distribution in these coatings.

Results obtained for the effect of heat treatment on the development of coating microstructure and the distribution of elements throughout the heat treated coating are also given. Finally, the oxidation behaviour of these coatings has been studied in the temperature range 800-1000^{o}C in an atmosphere of pure oxygen. Results of these studies are also presented.

CHAPTER ONE

REVIEW OF ALUMINIDE COATINGS

1.1. PURPOSE OF COATING

1.1.1. Introduction to Ni-base superalloys

Ni-base superalloys are generated principally from the Ni-Cr-Co ternary system. To provide better creep strength Al and Ti are added. These two additions contribute to the formation of the precipitate strengthening phase (γ') $Ni_3(AlTi)$ which precipitates coherently with the γ (Ni) matrix. The γ' provides, perhaps, the most unique alloy system strengthening to temperatures as high as 90% of the alloy melting point (Sims (1)).

Refractory metal elements are added and provide solid solution strengthening. These elements (such as tungsten and molybdenum) partition between the matrix and precipitate phases in superalloys and lead to solid solution strengthening of the matrix austenitic phase as well as strengthening and perhaps ordering in the γ' precipitate phase.

Carbides of chromium, titanium and sometimes other refractory elements are also present. These carbides are usually formed during the solidification of the alloys and are randomly distributed in the alloy matrix

1.1.2 Investment Castings IN-738

Nickel base investment cast alloys are the strongest widely used high-temperature alloys, serviceable up to 95% of their melting point (Sims (1)). Undoubtedly, they represent the most complex alloy development and technology of all alloy systems. IN-738 (composition given in Table 1) as an example, is in present production for buckets, in many industrial gas turbines. Further, it has a microstructure expected to be characteristic of many future alloys. The major strengthener is γ', grain boundaries are often jagged, contain a few dispersed $M_{23}C_6$ carbides and intercept large MC carbides and eutectic 'islands' of excess γ' precipiated from the melt. The MC acts as a source of carbon, slowly dissolving in service to maintain a controlled level of $M_{23}C_6$ - M_6C type carbides, which also interact with dislocation. Unlike other recent alloys, the grain boundary is not engloved in a layer of γ'. Ductility of the alloy is probably close to minimum acceptable level, while strength is close to a maximum. The limiting mechanical property in service is usually low-cycle fatique, and the limiting chemical property is hot corrosion.

1.1.3. A general background to coating technology

The most important requirements for corrosion-resistant coatings for industrial gas turbines are as follows :-

1.1.3.1. Corrosion resistance

Protective coatings are used for blades of industrial gas turbines in order to extend their life. This is done by red-

ucing the oxidation and hot corrosion rate at the blade surface. Aluminium base coatings applied by different methods have been used in jet turbines for some time but they do not give the required long term protection under sulphidation conditions and cyclic oxidation conditions.

1.1.3.2. Erosion Resistance

It is impossible to prevent particles of different sizes hitting the coated blade surface. The coating should not be completely destroyed by this process, leaving the base alloy unprotected from the corrosive attack. Ductile coatings are advantageous in this respect because an impact would deform but not destroy them.

1.1.3.3. Thermal Stability

Coatings should be stable under any service conditions, so that the protective elements of the coating responsible for the corrosion resistance remain in the coating and are not lost by diffusion into the base alloy. Such diffusion may also have a detrimental effect on the mechanical properties of the blade alloy.

1.1.3.4. Mechanical Strength

The coating must be able to withstand all the stresses which can occur on the blade surface during operation of a turbine. Cracks in the coatings caused by creep stresses or fatigue stresses could be dangerous. In this respect it is important to have coatings and base alloys with similar thermal expansion coefficients in order to minimize the risk of thermal fatigue damage in the coating during start-up and shut-down procedures.

1.1.3.5. Adhesion

The coating must be locked to the substrate material so that neither mechanical nor thermal stresses cause it to flake off. General experience has shown that usually only coatings which are bonded to the base alloy by diffusion can meet this requirement.

1.1.3.6. Influence on base alloy properties

The influence of the effects of the coating on the mechanical properties of the blade alloys has only recently been recognized. It seems that due to the increased temperatures, the difference between the necessary strength and the strength available has become smaller and smaller, i.e. in today's turbines the material properties are better utilized than in older turbines. On the other hand it seems that the modern superalloys, especially developed for the highest possible strength, are more sensitive to composition, heat treatment, etc. than older materials.

1.1.3.7. Influence on blade functions

Not as critical as the effect mentioned above, but still to be considered, is the effect of the coating on the functions of the blade. It seems to be obvious that the coating should not change the shape of the blade aerofoil in such a way that the aerodynamic behaviour of the blade should be distorted.

1.1.3.8. Economics

Economic factors have to be investigated when evaluating protective coatings. Coatings are usually not an absolute necessity for running a gas turbine but a measure to extend the blade life. Therefore, it has to be calculated whether the savings due

to a lower blade consumption, less maintenance costs, etc.justify the coating or not.

This list shows that it is important not to select or evaluate coatings alone but always as part of the coating-base-alloy-blade system.

The most widely used coating technique in current operation is that of pack cementation. This is generally considered a chemical vapour deposition process in which the element to be deposited is transferred to the surface of components by means of volatile metal halide. The production of aluminide coatings by this method is one of the most economical and well proven process routes (Sivakumar, et al (2)).

The observed microstructure formed in aluminizing IN-738 superalloy, is illustrated in Figure 1 (Jackson et al (3)). The ternary diagram shown is based on information in the literature, but is hypothetical for Al-rich compositions beyond the $\beta + \alpha$ field (Janssen et al (4)). The $\delta + \alpha(Ni_2Al_3 + Cr$ solid solution) field is observed experimentally in aluminized structures, while the higher Al fields are assumed.

The path shown in Figure 1a is for the coating formed by aluminizing IN-738 at 1060^{o}C. The initial couple can be considered as between IN-738 and Al. For IN-738 (11.8 at pct Al, 19.5 at pct Cr in the ternary approximation), it is desirable to minimize the rate of equilibration of the coating with the substrate and to retain the high Al β (NiAl) phase for long service life. During coating formation, the outermost part of the coating corresponds in the phase diagram to the first two phase

field intersected by a line joining the terminals of the couple IN-738 and Al. The remainder of the path is governed by the relative diffusivities and solubilities of Ni, Cr and Al in γ , γ' as well as β phases. Presumably, Cr is slowest in diffusion in the phases formed in the coating (Dehoff et al (5)), so the path swings away from the Cr corner of the diagram initially and then swings back towards the Cr corner, crossing the line joining the terminals of the couple in order to maintain the Cr mass balance.

During coating degradation, the β phase is seen to grow at the expense of δ as Al is reduced at the surface.The disappearance of the δ phase in service generally occurs rapidly. The IN-738 terminal of the couple does not change location, but the Al-rich terminal migrates towards the IN-738 terminal, as shown in Figure 1b. In a closed system, the diffusion path would have to cross the line joining Al and IN-738 so that mass balance would be maintained. Although spallation of oxidized material eases that restriction, the general observation is that the path does cross that line throughout the useful service life of the coating. Since current commercial coatings do not possess sufficient corrosion resistance, particularly when used in the more severe environments, coating technology is in a state of continual development. During the past decade, numerous attempts have been made to improve the oxidation and hot corrosion resistance of diffusion aluminide coatings. A moderate increase in hot corrosion at intermediate (800-900^{o}C) temperatures can be achieved by increasing the chromium concentration over that normally derived from the superalloy substrate. This can be

accomplished by a chromizing process, such as pack cementation or electroplating prior to aluminizing. Because chromium has only limited solubility, about 6-8%, in NiAl, additional amounts of this element exist in such coatings as a second phase which can be deleterious to high temperature oxidation resistance, (Goward (6)).

A number of years ago, the American Aero-engine industry expressed a desire for so-called diffusion barriers, which should prevent aluminium diffusing further into the substrate metal, when operating the turbine at high temperatures. The element inhibiting the secondary diffusion of aluminium being a part of the coating, should be a metal, Lehnert et al (7) proposed the following requirements :-

a. Solubility with the substrate metal.
b. Difference in atomic radii in comparison with aluminium, in order to obstruct its diffusion paths in an inward direction.
c. A high melting point which should lessen the danger of formation of low melting phases.
d. A good resistance to high temperature oxidation.
e. A possibility of being deposited by well-known and not too intricate methods.

As a result of such considerations (some of which were of doubtful validity), Lehnert et al (7) proposed that the material coming closest to complying with these requirements were certain metals of the platinum group and in particular, platinum itself.

1.2. Platinum-Aluminium System

The platinum-aluminium system (figure 2) comprises a wide range of platinum-based solid solution and nine intermetallic phases namely : Pt_3Al, Pt_5Al_3, PtAl and Pt_2Al_3 which melt congruently at temperatures of 1556, 1465, 1554 and 1521°C, respectively. The phases Pt_3Al_2, $PtAl_2$, $PtAl_3$ and $PtAl_4$ are formed according to peritectic reactions at temperatures of 1397, 1406, 1121 and 806°C respectively (Huch et al (8)). A tetragonal superlattice $Pt_{13}Al_3$ was observed at 80 at% Pt by the same authors, however, no other study has supported its existence. These authors have also noticed that some of the compounds of the system are coloured. The accepted crystalline structure of the intermediate phases is given in Table 2. The maximum solubility of aluminium in platinum is 16 at%. It drops sharply to roughly 3 at% at 500°C. According to Darling et al (9), platinum dissolves at room temperature 2.16% by mass (13.7 at%) Al ! The authors inferred from their data that alloys with up to 2% by mass Al are solid solutions.

Calorimetry techniques were used to determine the heat of formation of Pt-Al alloys containing 5.8 to 82.3 at% Al (Ferro et al (10)). The heat of formation vs composition curve features maxima of about 25 K cal/gm. atom for alloys corresponding to Pt_2Al_3 and PtAl (sufficient details are not available). Magneli et al (11) reported eight intermediate phases, the powder pattern of an alloy having the nominal stoichiometry Pt_2Al_3 after annealing at 800 or 600°C was apparently unrelated to that obtained from the as-cast alloy, which suggest that this may indicate the

existence of a low temperature phase.

In another study of the system (Arzhanyi et al (12)) where an iron-aluminium alloy was used for the thermo diffusional aluminizing which was carried out at 900 - 1000°C the alloy with composition Pt_2Al_3 was found to be two-phase, and in addition to a phase with a hexagonal structure (a = 4.19 Å., c = 10.48 Å) there was also a small amount of a second phase which was not identified. However, it has been suggested that this phase could be a distorted or high temperature form of $PtAl_2$, since it is indexed as a cubic material with a = 5.96 Å (Chatterji et al (13)). A recent study appears to give the best definition of the system (Chatterji et al (13)) in which the diffusion-couple technique was used. The system clearly develops the nominal phases $PtAl_3$, $PtAl_2$, Pt_2Al_3, PtAl and Pt_3Al, in agreement with previous work and the Huch and Klemm diagram (8). As a result of the comparison of the thermal analysis and diffusion couple techniques, the authors concluded that there is a need for a more definitive study of -

1. The extent of solution of Al in Pt.

2. The phase relations between 60 and 75 at% Pt. in which this method has revealed evidence - both compositional and microstructural - for a single phase of nominal composition, Pt_2Al. Comer (14) in his electron diffraction studies of thin-film alloys has suggested the existence of Pt_2Al phase and at the same time confirmed the structure of $PtAl_2$, PtAl, Pt_5Al_3 and Pt_3Al. At the same time Chattopadhyay et al (15) found that

Pt_3Al is isotypic or at least closely related to Pt_3Ga, which has a tetragonal variant structure of the Cu_3Au structure. Two types of Pt_2Al structures, namely, Pt_2Al (h) (Ni_2Si type) and Pt_2Al (r) (Pt_2Ga(r) type) were reported. Pt_2Al_3 was proved to crystallize in the Ni_2Al_3 type of structure.

Jackson et al (16) studied the aluminization of platinum using the pack cementation method at 1060°C and found that all but one of the phases shown in the binary Pt-Al phase diagram were observed for at least one aluminizing temperature. One phase Pt_3Al_2 or Pt_5Al_3, was absent. It is clear that Hugh and Klemm's (8) version of Pt-Al phase diagram is the principal base for the accepted phase diagram, but discrepancies cannot be ignored, and modifications of the phase diagram would be necessary.

1.3. Platinum-Aluminide Coatings

The concept of the platinum aluminide coating system is historically attributed to Dr. Lehnert. The first commercial coating system, designated LDC-2, was developed jointly by Lehnert and Meinhardt (17). This first commercial coating system was produced by initially electrodepositing a platinum layer less than 10 microns thick onto a nickel base alloy and subsequently aluminizing the platinised component for several hours at approximately 1050°C. This concept of using platinum in such a coating system can be attributed to the belief that it would form the basis of a diffusion barrier system that would over-come the problem of aluminium migration to the substrate,

and hence maintain the high activity of aluminium at the surface where it is essentially required. It is known now that platinum itself does not act as a diffusion barrier for aluminium but more as a diffusion medium which, during processing, allows aluminium to establish a nickel aluminide subsurface structure and simulteneously generate a platinum-aluminium intermetallic skin.

There is little published information on the exact microstructure, but it appears that Pt is present either as a distinct Pt-Al intermetallic, in solution in NiAl or both (Goward (18)). The concentration of the noble metal (Pt) is usually greater at the external surface and decreases towards zero as the diffusion zone is approached.

The coating system described by Lehnert and Meinhardt (17)) (LDC-2 type coating) is reported to give a 230 pct improvement in hot corrosion resistance over simple aluminide coatings.

Next to the surface, the LDC-2 Duplex coating contains approximately 30% Pt, 32%Al and 35%Ni (by weight), the outer, about 15 μm, part of the coating has an average platinum content of about 20%, in this zone the nickel content is about 20% lower than in the simple aluminide coating, where as the Al content remains the same. Compared with the pure aluminide layer, part of the Ni has been replaced in LDC-2 by platinum. It is also shown that for a coating thickness of 50 μm, the ratio of the total coating thickness to the thickness of platinum layer previously deposited is about 7:1.

This process has been licenced by two American based companies and each has produced its own commercial platinum aluminide coating designated RT-22 and LDC-2A respectively. The structure and chemical composition of RT-22 type shows a major duplex layer of $PtAl_2$ in NiAl matrix (Seelig et al (19), followed by a second layer of NiAl with Cr, Mo, Ti and Co in solution and finally an interfacial zone (MC, $M_{23}C_6$ in NiAl matrix). The microprobe traces of RT-22 type coating after 120 hours of rig testing shows the same sequence of layers with an outer layer of about 38%Ni, 30%Pt and 18%Al by weight.

Another example is the development under NASA Contract (20) of a coating system for the protection of an advanced directionally solidified eutectic alloy, the most promising coating was one synthesized by sputtering a thin layer of Pt over a Ni-18%Cr-12%Al, 0.3%Y,coating applied by electron beam physical vapour deposition. Further evaluation of the coating was accomplished by burner rig oxidation testing at 1050^{o}C. Thermo-mechanical fatigue testing was also performed, it was concluded that thermal fatigue resistance of the coating alloy system could be a limiting factor in practical application.

Recently, a collaborative effort between Rolls-Royce and Johnson Matthey (Wing et al (21)) resulted in a new type of platinum aluminide coating of consistent quality and microstructure, with no detriment to blade alloy properties. This development system was designated JML-1. Further development produced a second system with different element profiles, this being designated JML-2. The constitution of JML-1 may be treated for convenience as a series of intermetallics associated with the nickel-aluminium-platinum ternary system. Within the total

coating thickness of nominally 60 microns, the first 2 μm of surface structure consists of a continuous layer of Pt_2Al_3, this is followed by 12 μm of duplex $\left[Pt(Ni)\right]_2 Al_3$ + PtAl structure zone, the next 6 μm would indicate a duplex PtAl + $\left[Ni\ (Pt)\right]$ Al zone. The central portion of the coating structure consists of β-NiAl; then a finger-like sub-structure (the diffusion zone) occupying some 15 μm of the total coating is sequentially composed of β-NiAl + αCr and γ' (Ni_3Al) + αCr. The technique of fused salt platinum plating has been used to overcome the problems of deposit adherence, porosity and hardness associated with an electroplating technique.

Jackson et al (16) studied the aluminization of Pt-coated IN-738. The platinum layer varied in thickness from zero to 25 μm, the Pt-coated IN-738 was aluminized at 1060°C in argon using pack containing 3 pct Al. After aluminization, a single microsection contained a large spectrum of Pt/Al ratios. Several paths have been mapped onto the unfolded quaternary Ni-Al-Pt-Cr (figure 3) to show some of the possible coating/substrate systems. Paths through the interior of the quaternary cannot be mapped on the unfolded diagram. However, most paths observed traversed the pyramid along ternary faces or just below the faces. The path marked 1 is for the case of Pt coating that is thick relative to diffusion distances. The initial part of the path is that seen for aluminization of bulk Pt, and the remainder is for diffusion that occurs between bulk Pt and IN-738. Path 2 is for 1060°C aluminization of ∿25μm thick-Pt coated IN-738 just as the pack reaches temperature.

The path departs from that of bulk Pt below the Al layer and enters the two phase PtAl + βNiAl phase field, but it quickly crosses to Pt-rich γ and finally to γ+ γ' substrate. Path 3 is based on observations of the 3-hour aluminization of the thick-Pt coated IN-738. Diffusion of Al inwards has eliminated the outer $PtAl_2$ region and γ has been replaced with β(Ni,Pt) Al. The path leaves β to form the β + α Cr finger zone, and then goes to the γ+ γ' substrate. The dashed lines indicate that β + α and γ + γ' have a planar interface.

Path 4 describes the aluminization of thin Pt-coated IN-738 just as the pack reaches temperature. The path begins along the Pt-Al binary but quickly moves into the Ni-Pt-Al ternary isotherm. The Pt content reaches zero in the β phase, so path 4 is expected to be entirely in the Ni-Cr-Al ternary isotherm from that point on, the path exhibits two finger zones : β + α and γ + α . Path 5 for the 3-hour condition, thin Pt-coated IN-738, begins well into the ternary Ni-Pt-Al. Again, Pt drops to zero in β, and the remainder of the path duplicates Path 4. Path 6 is the path for 0 Pt; i.e. for aluminization of bare IN-738. For very thin Pt coatings on IN-738, the microstructure would be expected to follows Path 6. It was concluded that the coating morphology and chemistry are highly dependent upon the thickness of the platinum layer. The study has demonstrated that the deposition of a platinum layer onto IN-738 prior to aluminization leads to the reduction, or even elimination of refractory metal elements in the outer region of the final coating. It is suggested that this lowering or elimination of certain refractory elements may account at least in part for the

improved hot-corrosion resistance of platinum-aluminized coatings on nickel-base superalloy. In a recent study (Corti et al (22)), the concept of the use of platinum and other platinum group metals as alloying constituents has been described and several platinum enriched superalloys for specific industrial and aerospace applications have now developed. These alloys have been shown to promote a considerable enhancement in oxidation and corrosion properties for nickel-based superalloys. It was concluded that platinum additions not only increase hot su lphidation corrosion resistance but also improve oxidation resistance, particularly at the higher temperatures. The presence of platinum does not present problems in terms of sigma and other close packed phase formation which are deleterious to mechanical properties. This is because platinum is considered to have the same electron vacancy number as nickel and so, direct substitution for nickel in an alloy should not affect microstructural stability.

1.4. Coating processes

Coating processes are classified in two main categories (Cappelli (23)) :-

A. The first category includes all the processes which result in a so-called overlay coating, that is where an alloy or a compound with intrinsic higher corrosion resistance is deposited on a base material with minimal interaction or interdiffusion phenomena taking place. This category typically includes hot spraying, chemical vapour deposition and physical vapour deposition.

B. The second category includes those processes which imply the modification of the composition and/or of the microstructure of the surface of a material in order to improve its corrosion resistance. This category typically includes pack cementation, slurry, hot dipping and surface alloying.

1.4.1. Overlay coatings

1.4.1.1. Hot spraying

The three processes which are of major interest in the hot spraying category are flame spraying, plasma spraying and detonation coating.

i. Flame spraying

In the flame spraying process, a fine powder is carried in a gas stream and is passed through an intense combustion flame, where it becomes molten. The gas stream, expanding rapidly because of the heating, then sprays the molten powder onto the substrate, where it solidifies. This process as well as other spraying processes, is considered a 'cold' process in the sense that the substrate material experiences only a very limited temperature rise. Flame sprayed coatings are usually not fully dense and bonding to the substrate is only of a mechanical nature.

ii. Plasma spraying

A limitation of flame spraying, that is only those materials which will melt in the combustion flame can be sprayed, is removed in plasma spraying. The process is very similar to flame spraying, except that the powder is now passed

through an electrical plasma produced by a low voltage, high current electrical discharge. This process therefore, increases enormously the range of materials which may be used to produce coatings. Coatings produced are more dense and well bonded to the substrate than those obtained by the flame spraying.

iii. Detonation Coating

Detonation coating is somewhat similar to flame spraying, a measured amount of powder is injected into what is essentially a gun, along with a controlled mixture of oxygen and acetylene. The mixture is ignited and the shock waves which follow microseconds after ignition, attain a velocity of about 3000 m/s. The high kinetic energy of the particle, is converted to additional heat on impact with the surface. This allows the particles to completely deform and 'wet' the surface, to produce extremely high bond strengths between coating and substrate.

1.4.1.2. Chemical vapour deposition

CVD uses a chemical process occurring between gaseous compounds when in contact with a heated material. The deposition takes place as long as the reaction produces a solid. The CVD process can be used to produce very pure, homogeneous and controlled coatings. The structure of deposits is closely related to the rate determining step of the reaction happening on contact with the substrate surface and not of the homogeneous reactions which might take place in the bulk of the vapor phase.

1.4.1.3 Physical Vapor Deposition

Even if PVD has been used to indicate a specific process, we will indicate with it those processes which are based on physical principles or phenomena. These processes include Thermal Evaporation, Ion Sputtering and Ion Plating.

i. Thermal evaporation

Under conditions of high vacuum (10^{-5} - 10^{-6} torr) metals begin to evaporate when their temperature is raised (the metal passes into the vapour phase at a temperature considerably lower than its normal boiling point). This vapor traverses the vacuum chamber and condenses on any cool surface encountered. In order to produce a uniform coating, the work to be coated needs to be rotated. Depending on the nature of both source and substrate materials and on the operating parameters, the process can achieve deposition rate in the order of micron per minute.

ii. Ion Sputtering

When the gas pressure in a chamber is reduced to a fraction of a torr. and a cold cathode discharge is excited between heated metal electrodes inserted in the chamber, the cathode electrode begins to emit atoms and atomic clusters, i.e. 'sputter'. Cathode material is ejected by the bombardment of positive ions and energetic particles in the electrical discharge and the sputtered substance is condensed on adjacent receivers to form a coating. This method provides an even deposit without

the work piece having to be rotated. A wide range of substances can be sputtered to form coatings of metals, alloys, metal oxides and carbides.

iii. Ion Plating

When partial ionization of the metal vapor is used to increase the adhesion of the film to the substrate the thermal evaporation process becomes Ion plating.
The use of an electron beam to evaporate the metal source increases significantly the average energy of the metal atoms. The result is an improvement in adhesion with respect to both Thermal Evaporation and Ion Sputtering.
The ion plating process can be considered to be composed of three stages :-
pre-plating, ion plating and evaporation.
There are advantages and disadvantages in ion plating.
An advantage shared with other vacuum deposition processes, is that it is cleaner as the film is deposited directly without using a carrier. The technique usually gives a higher adhesion than a directly evaporated film without the necessity of using the much slower sputtering process.
Deposition rates of microns per minute are easily obtained. The disadvantage of a vacuum environment is that the process is relatively costly and is only likely to be economic for small parts, where many can be plated together.

1.4.2. Surface Modification Coatings

These processes, which imply phenomena such as diffusion: reaction or fusion, can be considered to include -

- pack and slurry cementation
- metalliding
- hot dipping
- surface alloying

1.4.2.1. Pack and Slurry Cementation

Diffusion is probably the single most important physical concept in the production of surface coatings. Pack and slurry cementation are both coating processes based on a thermochemical treatment which utilizes the influence of a diffusion process. This implies an interaction between coating and substrate on a physical/chemical level. The unique aspect of a diffusion coating is the fact that the substrate is incorporated as a component part of the coating, and is reacted or dissolved into it. The properties of the coating are equally dependent on the substrate composition. Pack cementation is the technique presently most utilized to produce high temperature corrosion resistant coatings. The process is indeed very simple, the part to be coated is immersed in a powdered compound containing the coating material (s). Usually this is done in a retort but fluidized bed versionsof the process are also known. In the semi-closed retort system, the sequence which follows on heating the charge can be described as follows :- The halide decomposes and the nitrogen and hydrogen act to purge the retort of air and produce reducing conditions within it. The halogen reacts, with other

constituents in the compound to form metal halides. As heating progresses, these halides vaporize and a continuous exchange reaction among part, atmosphere and compound occurs.

A quantitative model for the pack coating process has been proposed by Levine and Caves (24) and recently by Marijnissen et al (25). In this model two regions can be distinguished, namely the region of gas diffusion and the region of solid state diffusion. At the surface of the coating there must be equilibrium between these two types of mass transport (see figure on Page 23. In our experiments ammonium chloride is used as the activator. Above 700°k this compound decomposes completely according to :

$$2NH_4Cl \rightarrow N_2 + 3H_2 + 2HCl \quad ....(1)$$

At higher temperatures the nitrogen will react completely with the aluminium in the pack.

$$N_2 + 2Al \rightarrow 2AlN \quad ....(2)$$

The hydrogen chloride produces with the aluminium grains thermodynamic equilibrium pressures of the chloride compounds.

$$2Al + 2HCl \rightarrow 2AlCl + H_2 \quad ....(3)$$

$$Al + 2HCl \rightarrow AlCl_2 + H_2 \quad ....(4)$$

$$2Al + 6HCl \rightarrow 2AlCl_3 + 3H_2 \quad ....(5)$$

With the aid of thermochemical tables, the equilibrium constant (kp) can be calculated. These constants are related to the partial pressures by the following equations : -

$$\frac{P^2_{AlCl} \quad P_{H_2}}{P^2_{HCl} \quad a^2_{Al}} = K_{P_1} \quad ....(6)$$

$$\frac{P_{AlCl_2} \quad P_{H_2}}{P^2_{HCl} \quad a_{Al}} = K_{P_2} \qquad ....(7)$$

$$\frac{P^2_{AlCl_3} \quad P^3_{H_2}}{P^6_{HCl} \quad a^2_{Al}} = K_{P_3} \qquad ....(8)$$

together with the sum of all partial pressures is equal to 1 atm.

$$\Sigma P_i = 1 \qquad ....(9)$$

and the chlorine balance

$$P_{HCl} + P_{AlCl} + 2P_{AlCl_2} + 3P_{AlCl_3} = P^o_{HCl} \quad ....(10)$$

where P^o_{HCl} is the pressure of HCl after reaction (1) before reaction with the aluminium. At the temperature of 1273K where our experiments were done the partial pressure of Al_2Cl_6 is negligible. For (10) we can write, because $P_{HCl} << P_{H_2}$,

$$P_{HCl} + P_{AlCl} + 2P_{AlCl_2} + 3P_{AlCl_3} = \tfrac{1}{2} P_{H_2} \quad ....(11)$$

Now we have five equations (6), (7), (8), (9) and (11) and 6 unknowns P_{H_2}, P_{HCl}, P_{AlCl}, P_{AlCl_2}, P_{AlCl_3} and a_{Al}.

In the pack $a_{Al} = 1$ and all pressures can be calculated. At the surface of the substrate the aluminium activity is unknown but it is apparent that this activity is equivalent to the observed surface phase (unfortunately Al activity data for the Pt-Al comoounds are not available). If the surface activity

quickly approaches that of the pack and remains constant with time, then diffusion in the solid is controlling the rate of coating formation. Otherwise, vapour transport in the pack or surface reaction has significant influence on the kinetics. In the figure below the coating process is shown schematically. There is a region adjacent to the surface of the substrate where the aluminium in the pack is depleted. This is the distance to be covered by gas diffusion.

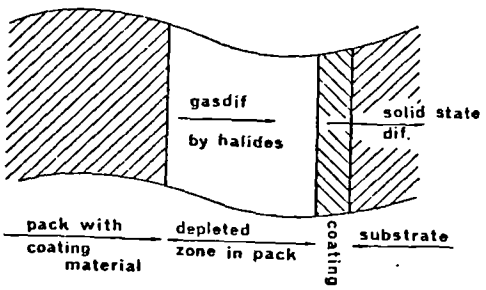

Schematic view showing the coating process.

Even though this aluminium depleted zone has been observed experimentally, it has been assumed that this depleted zone thickness increases parabolically with time, which has not been tested by experiments.

Levine and Caves (24) derived from the depletion in the pack material a parabolic Law for the aluminium deposition.

$$g^2 = k_m t \qquad \ldots.(12)$$

in which g is the amount of aluminium transported from the pack to the substrate and

$$k_m = \frac{2\rho_p \cdot \varepsilon \cdot M_{Al}}{RT\mathcal{L}} \Sigma D_i \Delta P_i \quad \ldots.(13)$$

in which ρ_p = aluminium content in the pack

ε = pack porosity

M_{Al} = molecular weight of aluminium

$\mathcal{L}$ = correction factor for non-linear transport

D_i = gas diffusion coefficient for component i.

ΔP_i = pressure difference between pack and surface for the partial pressures of component i.

It is to be noted that as Al is consumed, the particle size decreases and, consequently, the vapour pressure increases (Sivakumar (26)), Al adjacent to the samples is fully consumed and further Al deposition occurs from the areas adjacent to the depleted zone. However, an analysis of the growth of this depleted zone is quite complex and requires further detailed investigation. The activity of aluminium in the cement may be adjusted to the desired value by modifying the composition of the metallic powder, it is thereby possible to obtain more or less aluminium-rich coatings. When the aluminium activity in the cement is low, the processes using these type of cements are frequently designated as 'low activity process'. It is also said the coating forms by outward diffusion of Ni to form NiAl. When the aluminium activity in the cement is higher, it is said that the coating is formed by inward diffusion of aluminium (Pichoir (27)).

Depending on the type of growth of the compound formed, 'nickel diffusion or aluminium diffusion' the alloying elements may intervene in more or less important manner. In the first

case (nickel diffusion) they diffuse from the alloy during the formation of the coating; their content in the coating is limited by their solubility in the compound formed. In the second case, the alloying elements both enter solid solution in the compound constituting the layer and are also present in the form of precipitates throughout the layer. These precipitates are those initially existing in the alloy and those formed during the aluminizing treatment.

The slurry cementation process is based on the preparation of a slurry where metal powders and the halides are suspended in an organic binder. The slurry is then applied to the part to be coated through dipping or spraying, depending on its size and geometry. The next step, as in pack cementation, is a heat treatment which brings about the formation of the actual coating

1.4.2.2. Metalliding

A relatively recent process, utilizes molten alkali and alkaline earth fluorides as solvents to produce electrolytically diffusion coatings. The process is carried out between 500°C-1200°C in metal vessels under inert atmospheres, principally argon. The coatings can usually be formed with quantitative coulombic efficiency and a high degree of thickness control. The coatings are comprised of solid solutions, intermetallic compounds, and mixtures of solutions and compounds.

1.4.2.3. Hot Dipping

Practically the same principles as pack and slurry cementation are at the base of the hot dipping process, the immersion of a part into a molten metal will create a surface coating through the

mechanism of liquid state reaction at the substrate interface. During the first stage the liquid reacts with the substrate forming an intermetallic compound, and this reaction can continue until the substrate is completely consumed, since the bath is never depleted and particle migration is not hindered.

1.4.2.4. Surface alloying

By surface alloying, the present review means any other coating process whose surface is modified by the utilization of means other than diffusion. With the obvious limitations of such schematization, surface alloying can be considered to include ion implantation and laser alloying.

i. Ion Implantation

Ion implantation should rather be considered a technique to dope other coatings than a coating process itself. Ion implantation consists essentially of the introduction of atoms in the surface layer of a solid substrate by bombardment of the solid with ions in the Kev to Mev ranges. Essentially, ion implantation has all the advantages of an externally controlled, non-equilibrium process. Furthermore ion implantation can be performed at temperatures for which normal diffusion is totally negligible.

ii. Laser surface alloying

Finally the utilization of high power laser must be mentioned as a means of great potential in coating process development. This process brings the metal surface to very high temperature which results in a thin molten surface layer. Then the desired amounts of additive elements are introduced into the molten layer.

Since the solidification of this alloyed layer occurs very rapidly as the beam is swept across the surface, a very fine microstructure resembling splat-cooled metal is produced.

1.5 Diffusion in the Pt-Al system and the Ni-Al System

The intermediate phase layers produced on aluminizing pure platinum or platinum coated-IN-738 superalloy correspond to the phases found in Pt-Al binary system (fig. 2). Normally only three intermediate phases are found in these types of coatings, these are $PtAl_2$, Pt_2Al_3 and PtAl. The prediction of diffusion rates in these multiphase systems is of importance when considering the formation and subsequent behaviour of aluminide coatings. This is normally done by simple mathematical analysis of layer growth data which will establish unambiguous $\tilde{D}$ values for the different phases at given temperature, this is not possible in such technique because of the presence of voids and the difficulty of defining 'zero' time in pack-aluminizing process. Other types of problems may arise with this technique, for example $\tilde{D}$ for some of the phases may be so low that they may not grow to detectable thicknesses. Thus, in the presence of $PtAl_2$, only Pt_2Al_3 grows to a finite thickness: all other phases assume infinitesimal thicknesses (Chatterji et al (13)).

Greater attention has been given to the diffusion in the Ni-Al system, in which normally the following phases are seen on aluminising : Ni_2Al_3, NiAl and Ni_3Al. In NiAl which is the principal component of the aluminide coating it has been shown that $\tilde{D}_{NiAl}$ varies strongly with composition (Gupta et al (28)). For Ni_3Al available data (Hancock (29) , Janssen (30), Swalin et al (31)), indicates that D varies less than a factor of two over its

composition range. In the case of Ni_2Al_3 no evidence has been found for a variable $\tilde{D}$ (Janssen and Rieck (4)), see table 3 . Ni_2Al_3 which is hexagonal has been found to obey a parabolic growth law after a certain transient period which indicates control of layer thickening by volume diffusion (Castleman and Seigle (32)). A very large interdiffusion coefficient has been found for Ni_2Al_3 (Janssen and Rieck (4)), Table (3).

NiAl is an ordered compound with CsCl (B2) structure. Bradley and Taylor (33) found that the density increased with nickel content across the phase field but that the lattice parameter exhibits a maximum near the stoichiometric position. The nickel-rich alloys were considered to be substitutional solid solutions of Ni in NiAl. In the aluminium rich alloys vacancies were thought to occupy some nickel sites causing a decrease in both density and lattice parameter.

Whilst it is now generally recognised that diffusion in pure metals and alloys occurs by random motion of vacancies, it is still not resolved how diffusion occurs in ordered alloys or intermetallic compounds. Because of the requirement that the material remains ordered, random vacancy motion is not possible and consequently a number of proposals have been made as to the mechanism of diffusion in CsCl type alloys (Elcock et al (34), Elcock (35), Flynn et al (36)). The two mechanisms for diffusion in NiAl are thought to be the six jump cycle for the Ni-rich side and next neighbours exchange for the aluminium-rich side.

1.6. Oxidation and scale adherence of Platinum-Aluminide Coatings

In developing oxidation materials for service at elevated temperatures, two requirements must be satisfied, diffusion through the oxide scales which are formed on the surfaces of such materials must occur at the slowest possible rates and oxides scales must be resistant as possible to spalling when subjected to growth and thermal stresses.

The formation of an external, protective scale on an alloy or coating during oxidation, however, is not the sole criterion for optimum performance. It was shown that Al_2O_3 and other types of oxide scales spall from most alloys and coatings in the presence of thermally induced stresses. It has been apparent that the performance of the alloys and coatings currently in service can be improved by developing adherence of their oxide scales.

Several mechanisms have been tentatively proposed to account for the influence of alloy additions, such as Yt,on enhancing oxide adherence. These mechanisms include (Giggins et al (37)):
1. The mechanical keying of the oxide scale through the protusions of oxide pegs into the alloy substrate, 2. the formation of an interlayer to act as a graded-seal between the oxide and the substrate. 3. accommodation of growth and thermal stresses through enhanced oxide plasticity due to the incorporation of the alloying elements in the oxide, and 4. precipitation of fine particles of alloying-element oxides in the substrate or the solution of such elements in the alloy which act as preferred condensation sites for excess vacancies and thereby improve adherence by preventing void formation at the oxide-substrate interface.

One of the requirements for satisfactory performance of an oxidation resistant alloy or coating is that reaction between the alloy or coating and the gas, produces a product which retards further reaction. Because of this demand for a system which retains adequate surface integrity for longer times at higher temperatures, the alloys and coatings which have evolved are those upon which protective scales such as Al_2O_3, Cr_2O_3, or SiO_2 are formed. It has become apprent from experience that the best performance of nickel and cobalt-base alloys and coatings in the hot sections of aircraft gas turbine engines is obtained when Al_2O_3 scales are formed.

During the past decade, numerous attempts have been made to improve the oxidation and hot corrosion resistance of diffusion aluminde coatings. A moderate increase in resistance to hot corrosion at intermediate (800 - 900^{o}C) temperatures can be achieved by increasing the chromium concentration over that normally derived from the superalloy substrate. This can be accomplished by a chromizing process, such as pack cementation or electroplating prior to aluminizing, because chromium has only limited solubility, about 6 - 8%, in NiAl, additional amounts of this element exist in such coatings as a second phase which can be deleterious to high temperature ($\geq$ 1000^{o}C) oxidation resistance (Goward (6)). Perhaps the most important improvements are those which have been achieved by incorporating noble metals, such as Pt, in diffusion aluminide coatings (Bungart (38)) (the effect of the phases formed on the oxidation resistance have been discussed in Section 4.7.). Detailed mechanisms to explain these

improvements have not been established but investigations by Felten and Pettit (39) on the development, growth and adhesion of α-Al_2O_3 scales on platinum-aluminium alloys containing between 0.5 and 6 wt.% aluminium studied at temperatures in the interval between 1000°C and 1450°C, the morphologies and microstructure of the α-Al_2O_3 scales were found to be influenced by the temperature, oxygen pressure and the microstructures of the alloys. The oxidation rates of the alloys appeared to be controlled by transport of oxygen along grain boundaries in the α-Al_2O_3 scales. This scale adheres to the platinum-aluminium substrate even after extensive periods of cyclic oxidation. It was suggested that the good adhesion of the Al_2O_3 may result from the mechanical keying of the oxide to the alloys due to the development of irregular oxide-alloy interfaces.

The kinetics for the growth of the Al_2O_3 scale at 1200°C could not be determined by using weight change vs time measurements, since concomitantly with the oxygen pick-up to form Al_2O_3, platinum was being lost to the gas phase due to the formation of gaseous PtO_2. The kinetics of the scale growth were determined by measuring th thickness of the scale as a function of time using the scanning electron microscope. Parabolic rate was observed for oxidation times up to about 100 hours at 1200°C, whereas for longer times the instantaneous parabolic rate constant gradually decreased with time.

Felten (40) in his study on the effects of precious metals on the adherence of Al_2O_3 to a Ni-8Cr-6Al alloy showed that the additions of platinum between 2.5 and 10 wt.% and rhodium (5 wt.%)

were found to improve oxide adherence at 1100°C and 1200°C during cyclic oxidation testing, but were less effective at 800 and 1000°C. It has been shown also that in addition to inhibiting spalling, the presence of platinum in sufficient amounts allows the Al_2O_3 scale to reform when modest spalling does occur.

Fountain et al (41) have shown that the presence of platinum as a piece of foil alongside flat specimens of various single-phase and duplex iron-base and nickel-base alloys α-Al_2O_3 formers in the furnace hot zone, postponed markedly the breakdown of the α-Al_2O_3 scale formed. Electron microprobe analysis showed that the platinum-stabilized α-Al_2O_3 scale formed after 24 hours at 1200°C contained approximately 1.2 wt.% Pt. Therefore, another kind of explanation involving the transfer of platinum in the gas phase has been suggested, in much the same way as would rare-earth additives to the alloy, except that in this case the additive comes from the gas phase.

Wood et al (42) in his study on the oxidation resistance of aluminized coatings on a directionally solidified Ni-Al-Cr_3C_2, eutectic alloy found that the α-Al_2O_3 scale produced when isothermally oxidising platinum-aluminized coatings (system LDC-2), the surface topography of the oxide was quite different from other aluminized coatings. The oxide was not convoluted but had a very nodular appearance. In addition, there were many whisker-like growths from the surface of the nodules. Although breakdown of the scale does occur during thermal cycling, rapid re-formation of α-Al_2O_3 prevents excessive oxidation of the

exposed coating.

Restall (43) in his review of various coating systems, showed interest in the performance of the platinum, rhodium aluminide coatings which will be used to protect superalloys (IN792, IN738 and MM509) in the hot section of FT4 engines to be installed on oil rigs in the North Sea, where these components will be operating in a highly sulphidating environment (44). The effectiveness of these coatings appears to depend on the initial cleanliness of the substrate surface, coupled with the quality of the previous metal deposit and the aluminising approach used.

Celland (45) claims that pack-aluminised IN-738C appears to be more resistant to hot corrosion than pack-aluminides on a less corrosion resistant wrought alloy. Further, the laboratory examination of solid rotor blades of a marine engine after 2269 hours of service have shown that the precious metal coating was the only coating which did not show parent metal attack.

Katz et al (46) gave a fairly comprehensive account of the results of a coating evaluation programme on both first stage nozzle guide vanes and first stage turbine blades carried out on the GTV Asia Freighter. During various stages of this test components were removed for metallurgical examination and after 2828 hours of engine operation, it was observed that a thick aluminide and rhodium-modified aluminide coatings were rated as nearly equal best in corrosion behaviour, relative to a number of development overlay coatings. At the same time there appears to be a concensus of opinion derived from corrosion rig and engine

experience of diffusion coatings, which favours the selection of precious-metal aluminides in preference to plain aluminides for marine and industrial gas turbines (45, 46, 47, 48) (structure of the coatings is given in Section 1.5). The JML-1 platinum aluminide coating system (21) (structure of the coating is given in Section 1.5), has undergone exhaustive assessment in burner rig trials. The result from these trials have shown the JML-1 system to considerably outperform the conventional aluminide coatings but at the same time, the coating performs as well as the commercial LDC-2 and RT-22 systems, since the outer thin layer of Pt_2Al_3 found in JML-1 coating will disappear after a short period of service life. The JML-2 system, a modification of the JML-1 system, designed to achieve a more even platinum distribution throughout the coating structure, clearly provides protection at higher temerature engine operation but has limitations as a system for lower temperature hot corrosion resistance.

One reason that may explain the improved performance of the JML-1 system is that its compositional difference from the commercial platinum aluminides results in the production of an inherently more corrosion resistant coating. However, it is possible that other factors such as erosion resistance or ductility play a significant role in resisting coating degradation. The authors finally concluded that platinum aluminide coatings in general may well have the potential for application in both hot corrosion and oxidation environments making them suitable as protective coatings for high strength alloys in industrial, marine and aerogas turbines.

CHAPTER 2

EXPERIMENTAL PROCEDURE

2.1. INTRODUCTION

In this chapter experimental techniques which provided microstructural, crystallographic and chemical information on as-coated, heat-treated and oxidised specimens, are described. Microstructural data was obtained from optical metallography and scanning and transmission electron microscopy. Electron and X-ray diffraction provided crystallographic data while probe micro-analysis and SEM analysis produced chemical information. The techniques that were used are explained separately, although the information obtained from them was quite often complementary. Following this is the description of experimental methods adopted to study the oxidation behaviour of some of the coating structures produced.

2.2. Materials and specimen preparation

Coupons of cast IN-738 LC of ∿ 12 x 10 x 2 mm size were sliced from a vaccum casted (4" x ½" x 2") ingot, (original ingot was supplied by Willans Ltd). Compositional analysis of this material is given in Table 1. Coupons were then ground on successively fine grades of SiC paper, finishing with 1000 grade, to provide a suitable surface finish. Prior to electroplating the specimens were degreased and rinsed in water and then a 2mm hole was drilled in the specimen using a spark drilling machine.

2.3. Platinum plating

Platinum-aluminide coatings were fabricated by first applying a thin layer of platinum, using fused salt electroplating method (49), (this process was kindly carried out by Johnson Matthey

using a fused salt platinum deposition method). The process uses a eutectic salt mixture, 53 percent sodium cyanide and 47 percent potassium cyanide, which has a melting temperature of about 520°C.

Normal control of plating thickness can be achieved by varying either the plating current or the speed of the specimen through the bath, a deposition rate of 20-25 microns per hour can be achieved using this method. After plating the specimens are subject to a vacuum heat treatment at 600°C for 30 minutes to ensure a good adhesion bond between the platinum and the substrate. The deposit obtained is ductile and has many other attractive features when compared to aqueous platinum plating, such as good adhesion, high purity and lack of porosity. Two different platinum thicknesses have been used, namely 5 and 15 μm.

2.4. Coating Conditions

The aluminising powders were made up from analar NH_4Cl dried and sieved (100 mesh), 99% aluminium powder(Hopkin and William Ltd.) and 99% alumina powder (Morgans furnace packing powder). The two powder packs were :-

Powder 1 — 0.5 wt.% NH_4Cl 5 wt.% Al, base Al_2O_3 (high activity pack)

Powder 2 — 0.5 wt.% NH_4Cl 25% Ni_2Al_3, base Al_2O_3 (low ")

Aluminising was carried out in a cylinder (3 cm. diameter, made of Ni-base high temperature resisting alloy), with one end welded with a stainless steel piece and the other end closed by refractory block. The cylinder had previously been aluminized inside using one of the powder packs. The specimens to be coated were immersed in the

aluminising powder contained in the cylinder and then covered with an alumina refractory cover. A maximum of two specimens were coated at one time after they were arranged inside the cylinder. Coating was carried out using a silica tube furnace containing argon at 2/3 atmospheric pressure (at R.T.). The coating was carried out at 1000^{o}C for a maximum of 3 hours.

2.5. Heat treatment of coatings

All the as-coated specimens were heat treated (see Section 3.7). This was performed in a silica tube furnace with a vacuum of $\sim 10^{-2}$ torr. The as-coated specimens were given heat treatments of the following temperature and times :-

1000^{o}C	5 hrs	50-55 hours	1000-1200 hours

2.6. Experimental assembly for oxidation experiments

The experimental assembly (details of which are given in Flatley's thesis (50)), is shown in Figure 4 the high temperature reaction tube 'A' and the gas admittance fitting 'B' are made of clear silica, the pyrex constriction unit 'C', through which silica suspension rod passes, prevents contamination of the reaction chamber by carefully balancing the flow rate of nitrogen passing through the balance chamber. The nitrogen flow rate is adjusted so that most of the waste gases are removed via the lower exit tube, although to completely avoide the contamination of the reaction chamber some gases should leave at the top exit tube. The oxygen from the purification unit was fed via the inlet tube 'D' attached to 'B' into the bottom of the reaction tube where it flowed up past the specimen. Silica rods of 1 mm diameter were

used to suspend the specimen which was positioned opposite to the head of Pt - Pt/13% Rh thermocouple contained in 'D'. The specimen and the thermocouple were positioned in the centre of the furnace's constant temperature zone.

All kinetic data was obtained using an automatic recording balance, modified from the original design of Beeton (51). The balance is shown complete with control unit and chart recorder in Figure 5, the use of a photo-electric sensing system allied with magnetic coupling serves to maintain the beam stationary during specimen oxidation keeping the same thermal condition. Assessment of gravimetric changes to an accuracy of $\pm$ 0.3 mgs, together with a continuous record provides a continuous assessment of any variations in the kinetic behaviour. The furnace employed throughout was nichrome wound and capable of attaining 1050^{o}C and was controlled by a West 'Guardsman' Controller via a chromel-alumel thermocouple. The furnace and its carriage were counter-balanced and mounted on vertical tracks which permitted easy and rapid movement in a vertical plane.

2.7. Operational procedure

Each oxidation run was prepared and progressed under as near identical conditions as possible. All the coated specimens were washed thoroughly in hot water to remove any presence of NH_4Cl on the coated layer. They were dried in a hot air blast. The specimen dimensions were measured and recorded. The specimen was suspended in position using a silica hook through the hole of the specimen. Oxygen was flushed through the apparatus at a higher flow rate. The furnace was turned on and set to the

desired temperature. The balance and recorder were switched on before starting the reaction by raising the furnace over the reaction tube. The recorder took 10 minutes to stabilize and become ready to respond immediately to change in the specimen weight. Oxidation experiments were terminated by lowering the furnace and leaving the specimen to cool in the reaction gas (oxygen). Cyclic oxidation experiments were carried out by lowering the furnace after a specified oxidation time, allowing the specimen to cool down then raising the furnace again for another period of oxidation cycle, and so on.

2.8. Calibration of the recording balance

After cleaning and re-assembling the recording balance, calibration was carried out by suspending progressively larger weights from the balance arm, noting the change in millivolts, thus produced. The calibration was linear and equal to 0.128 $mg.mv^{-1}$ (Figure 6). The calibration was checked periodically throughout the project but no variation was found.

2.9. Metallography and specimen preparation

2.9.1. Optical metallography

Specimens were mounted in conducting bakelite (for probe microanalysis) ground to 600 grade SiC paper and subsequently polished using 6 μm and finally 1 μm diamond wheels. They were then etched in the following freshly prepared solutions:

ETCHANT 1

3 parts lactic acid

3 parts acetic acid

2 parts conc. hydrochloric acid

1 part conc. nitric acid.

(Goward et al (52))

This was found very satisfactory in etching the βNiAl phase and the outer coating in general but not the diffusion zone, so a second freshly prepared solution consisting of :

ETCHANT 2

100 ml H_2O, 100 ml 5 pct NaoH solution and 5 gm $KMnO_4$ (Rideout et al) (53) was therefore used. This etchant selectively stains α phase Cr rich phase and M_6C phase. The matrix phases, MC and $M_{23}C_6$ phases remain unattacked (see figure 10). Several measurements of coating thicknesses were taken from optical micrograph negative plates to give an average with an estimated accuracy of $\pm$ 5%. It should be mentioned that the edge effect (rounding effect) has been the major problem in determining the accurate coating thickness of the coated specimens.

2.9.2. Scanning electron metallography

Scanning electron microscopy, using a Philips PSEM 500, was employed initially to examine the finer detail not resolvable in the optical microscope. Surface topography of the coated layer, coating/substrate interfaces were also examined. Specimens were ground and polished so that the coating was present around the edge of the sample. This made examination of the full coating layer possible. The above work was carried out on all the as-coated and heat-treated specimens.

2.9.3. Transmission electron metallography

Carbon replicas have been prepared by polishing the flat surface of the specimen up to 1 μm on a diamond wheel then slightly etching the specimen using Etchant 1. Once etched the specimen

was carbon coated by evaporating carbon onto the specimen from a carbon arc. Squares were then marked out on the surface and the specimen immersed in 10% nital solution to loosen the carbon layer. Finally the specimen was lowered at an angle into distilled water to lift off the carbon squares. These were picked up on a copper grid. Examination of replicas took place in a Philips STEM 401 Transmision Electron Microscope.

2.10 Electronprobe and SEM micro-analysis

2.10.1. EPMA

After optical examination the specimens were polished on ¼ µm diamond wheels to remove the etched layer. The specimen was then ready for micro-analysis which was carried out on a Microscan V made by Cambridge Instruments Ltd.

The microanalyser was first set up according to the optimum operating conditions for the particular elements present (see Table 4). A specimen was brought into focus under the optics. The EHT switched on and an accelerating voltage of 15 kv chosen. The electron beam was focussed onto this specimen. The probe current was a compromise reached by taking several factors into consideration. Firstly that the maximum count rate produced from a pure standard requires a dead time correction of approximately 2%. Secondly that a sufficient count rate was produced for those elements present in only small concentrations to produce a statistically significant number of counts within 100 secs. Thirdly that high probe currents implied a poor spatial resolution but this was often better than 2 µm. An electron image of the coating was obtained and a line scan perpendicular to the coating/

substrate interface was set up. The distribution of elements throughout the coating was determined by allowing the electron spot to scan across the coating along the electron line set up. The specimen was positioned in most cases, such that this scanning was in the y-direction, i.e. parallel to the spectrometer axis, to avoid defocussing of the spectrometers. The variation in X-ray counts with distance into the coating from the elements was then recorded on a chart. The scan was allowed to continue into the nickel-base substrate whose composition was known,thus providing an in-built standard. Conditions were set up for the remaining elements present and each in turn were recorded in a similar manner. The reference standards used were pure elements. Having obtained an X-ray count-distance scan the electron spot was positioned on the standard,peak counts were taken over a period of time so that a statistically significant number were obtained, i.e. 10^4 counts ≡ 1% error, this was repeated and an average taken; the background counts were then taken at $\pm 2^o$ of the peak value. The data obtained from line analysis which was in the form of peak and background ,c.p.s. for specimen and peak and background, c.p.s. for standard needed firstly to be corrected for the dead time of the counters, i.e. the time (τ) after each pulse when the counter is inactive and will not count another quantum. The number of pulses lost due to this effect is greater the greater counting rate, since then the statistical chance of two events occurring in the time interval of less than τ is greater. The relation between observed counting rate, N_o, and true counting rate is given by :-

$$N_t = N_o / (1 - N_o \tau)$$

provided the difference between N_t and N_o is less than 10%. Dead time corrections could be ignored for count rates <1000 c.p.s. (0.2% correction for τ = 2 μs). Once this correction had been made, the peak minus background for specimen I_A, and standard I_{std}, were determined. A k value represented by $\frac{I_A}{I_{std}}$ was then worked out.

There are several correction procedures which can be used to convert the intensity ratios to weight concentrations. By far the most popular in the so-called ZAF correction process which can be expected to give analysis accurate to about 5% of content and often rather better. The accuracy of any analysis does of course become worse at low concentrations. The correction processes generally applied are as follows :-

The atomic number correction (Z)

i. Back scattered electron correction

A certain fraction of the incident electrons are back scattered from the surface, so cannot produce X-rays in the sample. This fraction increases with atomic number of the specimen and is, therefore, a function of the mean composition.

ii. The stopping power correction

This is related to the efficiency of producing X-rays and again to the atomic number of the specimen. The mean electron range will be greater in a light element but the overall generation of X-rays is lower.

The absorption correction (A)

The X-rays are generated at various depths throughout the interaction volume. The intensity that escapes from the specimen is, therefore, dependent on the amount of absorption they experience on their passage to the surface This will depend on the size of the interaction volume and on the absorption of the material (thus varying with the mean composition) and on the wavelength of the X-rays that are being examined. The absorption path length will also depend on the take off angle of the spectrometer, hence the need for a high angle. This is usually the most important correction.

The Fluorescence correction (F)

X-rays are produced by other X-rays as well as by electrons. The emission of any characteristic line will be caused by the primary beam and by any of the characteristic lines from other elements in the specimen that have a sufficiently high energy. Again, the magnitude of this effect depends upon the composition of the specimen.

In this study a ZAF correction was used to obtain concentration values from measured intensity ratios. The correction is based on a direct translation into BASIC of programme FRAME 3 written in FORTRAN and described by Yakowitz et al (see Appendix 1). Sheffield Frame 3 is a version that can deal with intensity ratios measured relative to compound standards as well as pure standards. It can deal with up to 9 elements (including those in compound standards). It is written for use on a Hewlett-Packard 9830A computer and uses 7722 words of memory.

2.10.2. SEM X-ray analysis

A Philips SEM 500 with a Link EDS attachment was used for the quantitative analysis of precipitates, lamellae, inter lamellae, acicular phase and coating matrix phases in the as-coated, oxidised and heat treated coatings. Samples were prepared in the manner described in Section 2.2. Point analysis were made on the above-mentioned areas and the resulting energy spectra recorded (A typical example of computer output is shown in Figure 7). This information when combined with quantitative probe microanalysis, allowed rapid identification of the precipitates, matrix phases and their distribution. Table 5 gives a comparison result of EPMA and point analysis using EDS on the SEM made on the substrate of a coated specimen.

2.11. X-ray Diffraction

All as-coated, heat-treated and oxidised specimens were prepared for X-ray diffraction by mounting them on a piece of plasticine in the specimen holder of a Philips diffractometer using the rotating stage of the instrument. Once the specimen had been levelled, ensuring that no plasticine would be hit by the X-ray beam thus causing spurious peaks, a scan was commenced. Either Co K_α or Cu K_α was used. The change in X-ray intensity with 2θ was recorded on a chart. The conditions set up were as follows :-

Cu tube - 40 kv/24MA (tube - pw 2103/00)

Co tube - 40 kv/32MA (tube - pw 2236/20)

Scan speed 1^o 2θ/min

Scan range $15\text{-}100^o$ 2θ for Cu and Co

Time constant - 1 sec.

Chart f.s.d. - 2000 c.p.s.

In a few cases the layer-by-layer technique has been used to identify the inner layers, this was done by polishing the surface of the specimen until the layer to be identified is on the surface of the specimen (as can be seen by the optical microscope) then a second scan was performed.

2.12. Electron Diffraction

Two specimens only (5 and 15 μm pt-coated IN-738 aluminized with 25% Ni_2Al_3 then heat treated for 1000 hours at 1000^{o}C) were carefully prepared for electron diffraction study, replicas were extracted in the same way described in section 2.9.3, prior to examination of coatings eucentric tilt was obtained, single precipitates were selected and diffraction patterns obtained from them, in each case tilting, either single or double, being used to bring in other zones. After the session, a standard aluminium ring diffraction pattern was obtained in order to calculate the camera constant.

Given the camera constant, λL, the d values corresponding to the different spots on the diffraction patterns, obtained from various phases could be evaluated. Electron diffraction results can be found in Section 3.8.4.2.

2.13 Micro-Hardness Measurements

Micro-hardness measurements were made on the coatings using Ernst-Leitz Wetglar - 3106 micro-hardness tester (50 gm load used). Micro hardness data indicated the change in composition of the

coating at different depths from the surface of the coating to the substrate. Findings of different hardness values across the coating zone provided supporting evidence of the presence of different phases which were further verified by SEM, X-ray and EPMA. Micro-hardness results can be found in Section 3.6.

CHAPTER THREE

RESULTS

3.1. Introduction

The results of the investigation into platinum-aluminide coating structures on IN-738 superalloy and their oxidation behaviour are presented. The coating treatments which have been applied are coded as follows :-

				Code
1000°C	2 hrs.	Powder 1	5 μmPt	A
1000°C	3 hrs.	Powder 1	15 μmPt	B
1000°C	1 hr.	Powder 2	5 μmPt	C
1000°C	2 hrs.	Powder 2	15 μmPt	D
1000°C	2 hrs.	Powder 1	(After 50 hrs. pre-heat treatment at 1000°C)	E

Details of Powders 1 and 2 are given in Section 2.4.

In addition to the optical metallography describing the structure of the coating the major part of the work has been the identification of the phases present in the coating. X-ray diffraction, electron probe microanalysis to determine the compositional profile (using WDS), point analysis using EDS

on the SEM, and electron diffraction have been used. The results which provided this information are presented. In addition to this, results relating to the study of segregation of elements in the sub coating region and the effect of heat treatment at 1000°C for a range of times, on the coating structure are presented. Finally, the oxidation behaviour of some of the coated specimens in pure oxygen at one atmosphere pressure in the temperature range (800 - 1000°C) are reported.

3.2. Aluminization of Bulk platinum

The aluminization of platinum was studied to provide supplemental data. A series of intermetallic Pt-Al compounds form and is the subject of the following section.

Figure 8 shows the distinct layers formed on Pt at 1000°C in a high activity pack. The outermost layer, occupying the larger part of the aluminided zone was identified by X-ray diffraction as Pt_2Al_3 (see table 10 for similar results). The identity of the inner layers could not be determined by layer-by-layer X-rays because these layers were generally very thin and characterized by irregular interfaces. However, these layers were identified by means of careful point analysis using EDS on the SEM microscope (see Figure 7 for Link settings). The second layer was identified as PtAl containing about 45 at pct Al (Figure 8), this was followed by another thin layer, containing about 25 at pct Al. This layer is believed to be Pt_3Al according to this analysis. The diffusion layers developed in this pack were relatively free from any void formation. It should be also mentioned that, the microstructural

features remained unchanged at higher and lower aluminization temperatures (from 800°C to 1000°C), using the same pack mixture, although for any given aluminiding time, all layer thicknesses were greater for higher temperatures. The observed phase growth requires a diffusion coefficient of $\sim 0.58 \times 10^{-4}$ $cm^2/sec.$ at 1000°C. Figure 9 shows a graph of Log D in cm^2/sec versus $1/T\ k^{-1}$ obtained by analysing the results after aluminizing platinum foils for different periods of time at different temperatures. Approximate average diffusion coefficients for Al were calculated based upon the penetration depth of Al assuming an initial layer of Al for each processing time.

3.3. Simple Aluminide Coatings on IN-738

Coatings produced by a pack-aluminising process on IN-738 have been studied. Chemical composition and the distribution of precipitates in the aluminide as well as the effect of heat-treatment as it affects the structure of the coating are presented.

3.3.1. As-coated IN-738

The microstructures of the as-coated conditions were generally similar. Coating thickness obeyed, generally, a parabolic law with time, but it is also commonly found that a diffusion process occurs in the pack as well as in the component and a zone of Al denudation is found around each component after the process is complete. The microstructure formed in this study using powder 1 (high activity), resulted from primarily inward diffusion of aluminium. These conclusions were based on analysis of microstructures formed during several hours of processing (aluminide contains more than 50 at.% Al). In this study, a brief review of the aluminization

of IN-738 will serve as an introduction to the present studies. When packs reach furnace temperature in about 15 minutes, initially aluminium supply is rapid, Al diffuses into the surface of the superalloy, and Ni_2Al_3/NiAl phases are formed, in most cases the limited solubility of several of the alloying elements in the coating results in the formation of precipitates at the coating-substrate interface and throughout the bulk of the coating (figure 10), Ni_3Al may form, but in many cases this layer is very thin.

However, for many of the alloying elements the concentration produced by a simple dilution with aluminium will exceed the solubility limit in the aluminide, in which case the element will be rejected from the coating and build up as shown in figure 10, where Cr and W are shown segregating in this way. This leads to such a build-up in the substrate at the substrate-coating interface that the solubility limit in the Ni-base superalloy substrate may be exceeded, when precipitation will occur. The interface is frequently of lamellae form, with one set of lamellar enriched in Cr, Mo or other alloying elements (Table 6). The other set believed to be a mixture of NiAl + Ni_3Al, as suggested by X-ray diffraction study. These lamellae persist across the interface into the aluminide where spheroidisation takes place and further diffusion of aluminium and often other alloying elements to precipitate particles occurs, generally causing a change of phase.

At least two types of precipitates have been found in the outer coating region. Using etchant 2 (see section 2.9) the first type stains in a light blue colour and found normally in the outermost part of the coating, is characterized by its high aluminium,

tungsten, molybdenum and niobium content (Table 6), X-ray diffraction study could not confirm its structure, but previous study (Bowker, (57)) suggests that this phase could be of Al_3Ti type. The second type stains brown in the same etchant, SEM (EDS) analysis suggests Al_9Cr_4/Al_8Cr_5 phase (table 6) structure type Cu_5Zn_8 as shown by Bowker (57).

3.3.2. Heat-treated condition

Several coated specimens had been heat treated at 950°C and 1000°C in vacuum for a total period of 1000 hours. The result is a reduction in the aluminium content of the bulk of the coating (figure 11). This must come about by diffusion through the aluminide and in general will involve diffusion of aluminium inwards and of nickel and other elements soluble in the aluminide outwards. The bulk of the coating may show a coarsening of the precipitate and a different phase may replace the original precipitated phase, thus a globular phase in the outer coating region has been observed (figure 11) in few cases; this phase is in equilibrium with a Ni-rich NiAl. The composition of this phase as determined by SEM (EDS) analysis shows a high concentration of Cr, W and Mo (Table 7). The exact structure of this phase could not be determined, however, the composition suggests that this phase could be a kind of σ phase.

No evident extensive inward aluminium diffusion into the base metal was seen, however, a platelet phase is formed beneath the diffusion zone after several hours of heat treatment. This phase is to some degree associated with globular particles in the diffusion zone. X-ray diffraction study taken from a region containing this phase gave a diffraction pattern and d spacings which closely resembled those reported for the Cr-Ni-Mo, Cr-Co-Mo and Co-Cr-Ni-Mo σ phases (table 8). EPMA (WDS) and point anal-

ysis using EDS attachment on SEM showed that it contained both chromium and molybdenum in high concentrations (Table 7). Also a build-up of Cr,Mo and Co with an accompanying decrease in nickel was found in the layer containing this phase; these compositional changes would favour α phase formation.

3.4. Aluminization of Pt-coated IN-738 using Powder 1

3.4.1. As coated 5 μm pt-coated IN-738

Figure 12 presents an optical micrograph of coating formed after 2 hours aluminizing at 1000°C using the high activity pack (Treatment A). This structure is a typical structure formed when aluminizing a thin Pt-coated IN-738 (5 μm Pt-thick), and is characterized by an outer $PtAl_2$ (golden yellow) layer, as determined by X-ray diffraction (see Table 9), about 10 μm thick. Line scans were performed across the coating and slightly into the substrate perpendicular to the coating/substrate interface. The weight pct-distance profile for Pt, Ni, Al, Cr, Co and W are shown in figure 12. Pt concentration is about 60 wt.% (25 at %), while aluminium concentration averages about 20 wt.% (53 at %) and Ni is only 9 wt.% (22 at %) in this outer layer.

The second layer, stained dark when etched with etchant 1 (see Section 2.9), occupying about 10 μm of the total coating thickness, is believed to be a β(Ni,Pt)Al layer. A sharp increase in Ni concentration and a sharp decrease in pt concentration can be seen (figure 12) when moving toward this layer, where Pt concentration drops to zero within 10 microns while Al concentration increases steadily.

A third layer etching brighter than the previous layer when using the same etchant is normally found before the diffusion zone and is believed to be of pure β(NiAl) free of platinum, the structure of these β phases has been determined by layer-by-layer X-ray diffraction technique. Aluminium concentration has been found to be constant in this layer ($\sim$ 56 at %). A low volume fraction of precipitates has been found in this layer, these precipitates are believed to be similar to those found in the simple aluminide coatings (see Section 3.3). Porosity between the $PtAl_2$ layer and the β(Ni,Pt)Al layer has been observed. This porosity may be extensive in some coatings and leads to separation along phase boundaries in the outer coating region. Finally a diffusion zone of a few microns thickness has been observed where the peak in refractory elements (Cr, W, (Ti and Mo not shown)) seen in figure 12 coincides with this zone, which is believed to be structurally similar to the diffusion zone found in simple aluminide coatings, i.e. similar to the case for aluminizing bare IN-738.

Point analysis using the analysing facilities (EDS) on the SEM had confirmed the above results obtained from EPMA and had supplied more information about the distribution of elements across the coating.

Figure 13 shows a SEM micrograph of the coating surface where the rough, porous surface is a common factor in this type of coating.

3.4.2. As-coated 15 μm Pt-coated IN-738

Figure 14 shows an optical micrograph of the as-coated treatment B, the structure formed shows an outermost Pt_2Al_3 layer of blue-violet surface colour containing about 2/3 of the coating thickness (∿ 50 μm), line scan analysis using EPMA (WDS) across the coating shows that platinum content of this layer is about 85 wt.% (∿44 at %); this layer was shown to be Pt_2Al_3 using X-ray diffraction studies as shown in Table 10. It was not possible to use X-ray diffraction to identify the thinner layers (these can be seen having a thickness of 1-2 μm) because of their irregularities and thicknesses. Point analysis using EDS on SEM was useful in determining the composition of the inner thin layers (Table 11), where a thin layer (∿1 μm thick) was revealed next to the outer Pt_2Al_3 layer in which part of the platinum has been replaced by nickel to give a layer of $(Pt,Ni)_2Al_3$ having a nickel content of ∿15 at %). The following two thin layers are believed to be PtAl layers having different amounts of nickel and etching differently. Nickel concentration mounts up to ∿24 At % in the inner-most PtAl layer.

The remaining (∿15 μm) of the total thickness would indicate a dilution of the substrate elements by platinum, giving a single phase layer, which we could not identify. No refractory elements build-up has been seen at the coating/substrate interface.

3.5. Aluminization of Pt-coated IN-738 using Powder 2

3.5.1. As-coated 5 μm Pt-coated IN-738

Figure 15 shows the optical micrograph of a coating formed

after one hour of aluminization at 1000°C (Code C). The structure shows that within the total coating thickness of about 30 microns, the first twenty microns of surface structure consists of a continuous golden yellow colour of $PtAl_2$ (as identified by XRD,(See Table 9) for $PtAl_2$ d values). This layer is followed by ∿ 10 microns of a duplex ($PtAl_2$ + NiAl) structure zone. The composition of this duplex layer was revealed using EDS point analysis on SEM (Table 12) which showed that platinum is incorporated as a solid solution component substituting for nickel in the β(NiAl) phase (dark etched) and nickel as a solid solution component substituting for platinum in the $PtAl_2$ phase (not etched).

The diffusion zone (finger-like structure) was found to be rich in chromium and other refractory elements, having a duplex structure similar in appearance to the diffusion zone normally found in the simple aluminide structures and containing carbides and intermetallics in a matrix of β(NiAl). The coating finally terminates with the alloy microstructure. It should be noted also that porosity has been found between the duplex layer and the diffusion zone.

3.5.2. As-coated 15 μm Pt-coated IN-738 using Powder 2

Figure 16 shows the microstructure of coating treatment D where the first 15 microns of surface structure has a violet blue colour (Pt_2Al_3). Next is another 10-15 microns of un-etched golden layer ($PtAl_2$) which have a duplex nature in the last few microns of this layer. The density of the dark etching phase (βNiAl) increases as we reach the diffusion zone, which

itself contains thin lamellae extending into the substrate. Porosity has been observed between the outer coating and the diffusion zone.

Line scans across the coating were performed and the elemental profile is shown in figure 16. It is clear that the outer coating layer of Pt_2Al_3 contains very little nickel, while the diffused nickel is concentrated in the next $PtAl_2$ layer and the duplex $PtAl_2$ + NiAl layer, where Ni and Pt are substituting each other, the βNiAl phase appears to have a solubility of about 10 at.pct Pt, with platinum apparently substituting for up to one-fourth of the Ni, while the $PtAl_2$ phase appears to have a solubility of about 40 at. pct. Ni.

SEM was useful in revealing a thin layer (∿ 1 μm) just after the outer layer of Pt_2Al_3. This layer is believed to be another layer of Pt_2Al_3 but having a higher concentration of nickel, as determined using EDS point analysis on the SEM microscrope.

3.5.3 Coating with duplex structure (coating treatment E)

Several attempts have been made to synthesis a coating having a duplex ($PtAl_2$ + NiAl) structure in the outer coating region which resembles the commercial coating named RT-22. This was achieved by adopting the following idea: if a Pt-coated IN-738 is annealed for some time, a Pt-Ni solid solution will be established in the outer surface. Furthermore, if Ni concentration exceeds its solubility limit in $PtAl_2$ phase (fuller explanation is given on ternary isotherm, section 3.7), a duplex ($PtAl_2$ + NiAl) structure will be established in the outer coating if an aluminizing treatment is carried out.

Figure 17 shows an example of this type of coating which was produced by annealing a 15 μm Pt-coated IN-738 for 50 hours at 1000°C. In this treatment a Pt-Ni solid solution containing about 67 at % Ni has been established in the outer coating region. After that an aluminizing treatment using powder 1 was carried out for 2 hours at 1000°C. The final coating presented in Figure 17 clearly shows an outer duplex layer (fine precipitates of dark etched β(NiAl) in a matrix of $PtAl_2$) (see Table 13 for XRD results). Point analysis using EDS on the SEM has been performed, the elemental concentration is shown in Figure 17. Separate phases could not be resolved or analysed separately because of the fine dispersion of the β(NiAl) phase in the $PtAl_2$ matrix. However, a mean value for the different elements is given. A high concentration of chromium and cobalt across the duplex structure has been noticed (8 wt.% and 4 wt.% respectively).

A second, β(Ni,Pt)Al layer can be observed next to the duplex layer extending for about 35 μm of the total coating thickness (∿ 80 μm): an average analysis is given in figure 17. A fine precipitate has been observed in the inner-most part of this layer. Finally a thin diffusion zone can be seen between the coating and the substrate, point analysis using EDS on the SEM revealed that no Cr or other refractory elements build-up has taken place in this zone.

3.6. Microhardness results

Figure 18 presents a typical microhardness gradient across coating treatment A, a hardness value of about 1025 Hv is up to 10 μm from the surface ($PtAl_2$), a lower hardness value was obtained

for the NiAl type structure in the inner coating region. The microhardness value for the $PtAl_2$ layer is in accordance with the results found in literature (Chatterji et al (13)) where $PtAl_2$ was found to be very hard and brittle.

The same figure shows a typical microhardness gradient across coating Treatment B, a hardness value of about 1000 Hv has been obtained for the outer Pt_2Al_3 layer. The microhardness value decreased as we move from a Pt_2Al_3 layer to PtAl layer.

Figure 19 shows a microhardness profile across Coating C, the outer $PtAl_2$ has a microhardness value of 1025 Hv, while the inner duplex layer has a microhardness value of ∿1000 Hv. The hardness decreases sharply as we approach the diffusion zone. The same figure shows the microhardness gradient across Coating D, a hardness of ∿1000 Hv has been obtained for the outer Pt_2Al_3 layer, while the inner layers have a lower hardness value. The data reported are the average value of different tests done on a similar coating.

3.7. Diffusion paths

The microstructure developed in aluminizing Pt. coated IN-738 follows a general pattern that can be mapped on the appropriate phase diagram. In Figure 20 is shown a schematic isothermal phase diagram for Ni-Pt-Al at 1000°C. This diagram is hypothetical but is based on available data and on microstructural observations made in this study (see section 4.4. for more details).

The path marked A is for the case of thin pt coating aluminized with a high activity pack (coating treatment A) for this case the path starts in the $PtAl_2$ region but quickly moves into the (Ni,Pt)Al region. The Pt content reaches zero in the last few microns of this zone. So this path is expected to be entirely in the Ni-Cr-Al ternary isotherm from that point on. Path B is for the case of thick Pt coating when aluminized with a high activity pack (coating Treatment B), for this case, aluminization occurs only in the Pt, so the initial part of the path is the same as would be seen for aluminization of bulk Pt. However, the path departs from that of bulk Pt below the ptAl layer. At this point, the path enters the Pt-rich γ , and finally to the γ + γ' substrate

Path C is for the case of thin Pt coating when aluminized with the low activity pack (coating treatment C). The path starts in the $PtAl_2$ region, because of the outward diffusion of Ni from the substrate, the path moves to the two phase ($PtAl_2$ + NiAl) region before ending in the β phase.

Path D (thick Pt, low activity pack, coating treatment D) can be regarded as a diffusion heat treatment for path C, where

part of the outer $PtAl_2$ region has been replaced by a Pt_2Al_3 layer. Hence path D starts in the Pt_2Al_3 region, it moves quickly to the $PtAl_2$ region and from that point on, the path is similar to path C.

Path E is for the duplex coating. The path starts from the Pt-Ni binary region and move quickly to the two phase ($PtAl_2$ + NiAl) after pack aluminizing and might end in the single phase β(Ni,Pt)Al.

3.8. Heat-treated coatings

All the coatings given the treatments A, B, C, D and E were heat treated in a vacuum furnace at a pressure of $\sim 10^{-2}$ torr. thus enabling study of coating phase changes. The heat treatment conditions used were : $1000^{o}C$ for 5 hours, 50 hours and 1000 or 1200 hours.

3.8.1. Heat-treated coating - treatment A

Heat treated coatings given treatment A were examined using optical metallography and subsequently analysed by EDS on the SEM, using point by point analysis technique. In addition to this, EPMA (WDS) have been used to determine the composition of the coating heat treated for 1200 hours, whereas X-ray diffraction studies determined their structure. The results from these techniques are presented :

Optical micrographs of specimens heat treated for 5 hours, 55 hours, are presented in figure 21, the total coating thicknesses are 40 ± 5 μm, 60 ± 5 μm respectively. It can be seen in figure 21(a) (5 hour heat treatment) that no dramatic changes have

occurred during this short heat treatment and the same sequence of layers prevailed in the outer coating region, i.e. $PtAl_2$ followed by βNiAl as determined by XRD (similar results are given in Table 9).

Ananlysis of the outermost $PtAl_2$ layer showed that nickel concentration is ∿10 wt.% (∿12.3 At%) (see Table 14 for point analysis). Fine cracks and porosity have been observed in this layer. Next to the $PtAl_2$ layer is a β(Ni,Pt)Al layer containing an average concentration of about 3.4 at.% Pt. A third layer believed to be pure β(NiAl), almost free of Pt, can be seen before the diffusion zone and containing fine precipitates similar to those found in the simple aluminide coatings, but larger volume fraction of these precipitates than in the as-coated condition as well as thicker diffusion zone has been observed.

The structure of the coating heat treated for 50 hours (figure 21 (b)), has been proved by the same procedure to be similar to the previous coating structure except that the outermost layer is PtAl (as determined by XRD) containing about 24 at.% Ni (see Table 15 for point analysis), high density of porosity and fine cracks have been observed in this layer. Next is the β(Ni,Pt)Al layer containing about 2.2 wt.% Pt, then a third layer of pure β-(NiAl) containing fine precipitates before reaching the diffusion zone where chromium and other refractory elements build-up has been proved.

In figure 22, optical micrograph of the same coating after 1200 hours heat treatment at 1000°C is given, the coating thickness is 70 $\pm$ 5 μm, a layer of dark etching grains of β(NiAl) can be

seen extending throughout the outer coating, whereas the inner coating is characterized by the presence of massive plate-like acicular α phase extending into the substrate. This phase seems to be associated with a globular phase in the diffusion zone. Porosity was found in the outermost part of the coating. Elemental profiles across the coating heat treated for 1200 hours are presented in Figure 22. It can be seen that nickel has diffused through the outer coating region to almost its level in the substrate. X-ray diffraction studies resulted in the identification of the outer coating as NiAl structure (see Table 16 for XRD results). It is worth noting that the concentration of cobalt in the outer coating is about 8wt.pct while that of chromium is only 6 wt. pct. A very high level of chromium and refractory elements W and Mo has been found in the diffusion zone where it was possible to analyse the globular phase found in the diffusion zone using the EDS attachment on the SEM. This phase was in equilibrium with a matrix rich in Ni and Pt, containing up to 6 wt. pct. Al. Finally no precipitates were found in the outer coating region.

3.8.2. Heat Treated Coating Treatment B

The same techniques employed in the examination of heat treated coating treatment A were applied to heat treated coating treatment B (high activity 15 μm Pt. thick). The results obtained from these techniques are presented :

Figure 23 presents optical micrographs of specimens heat treated for 5 and 50 hours, the total thickness of the coatings are 55 ± 5 microns respectively. It can be noticed that no dramatic

changes have occurred during short time heat treatment (figure 23 (a)), where an outer Pt_2Al_3 layer (as determined by XRD, (see Table 10 for d spacings of Pt_2Al_3) extending for about 20 μm, persists in the outer coating region. Point analysis using EDS on the SEM showed that this layer contains traces of nickel (see Table 17, for complete point analysis). This layer is followed by a brighter layer, about 15 μm thick, of PtAl containing about 5 at.% Ni, then a second PtAl layer etching differently and containing about 25 at.% Ni (different layers having different colours can be the same phase, this is due to the change in diffusion values (98)). Finally a diffusion zone of very fine lamellae and precitates. The microstructure of the same coating heat treated for 50 hours can be seen in figure 23 (b) where the outer coating has been transformed to a bright etching PtAl of about 30 μm thickness and containing about 1 at.% Ni (see Table 18 for complete analysis). SEM analysis revealed what is believed to be another PtAl layer of few microns thickness containing about 11 at%.Ni next to the outer layer. The next 20 μm appears to be a fine duplex structure of (Pt,Ni)Al and (Ni,Pt)Al where the dark etching β(Ni,Pt)Al appears to be more concentrated in the inner part of this layer, the matrix in the duplex layer is still PtAl type structure containing up to 40 at.%Ni. Finally, a well developed diffusion zone containing fine precipitates and a fine acicular phase extending through the substrate can be noticed.

The coating structure after 1200 hours heat treatment can be seen in figure 24, where a light etching PtAl layer of about

60 microns thickness extends through the whole outer coating region, X-ray diffraction studies showed that the structure in the outer coating region is mainly PtAl (see Table 19 for XRD results). Line scans for six elements are shown in figure 24, it can be seen that Ni,Pt and Al concentrations remain fairly constant in the outer region of the coating. The outer PtAl layer is followed by a darker etching diffusion zone ($\sim$20 μm thick) containing finger-like phases. The elemental profile shows that Pt and Al drop in this zone while Ni and Cr increases in concentration, together with other refractory elements. The structural appearance of this zone is quite different from other diffusion zones seen so far in heat treated coatings, the absence of acicular phase, together with the low concentration of Al ($\sim$4 at.%) in the matrix suggests that the matrix could be of γ' plus γ, but this cannot be confirmed because of the lack of structural evidence.

3.8.3. Heat treated coating Treatment C

The same techniques used in the examination of heat treated coatings A and B were used in the examination of heat treated coating C (low activity pack, 5 μm thick platinum). Results are presented for the different techniques:

Optical micrographs of specimens heat treated for 5 hours and 55 hours are presented in figure 25, the total coating thicknesses are 35 $\pm$ 5 μm, 40 $\pm$ 5 μm respectively. It can be seen in figure 25 (a) (5 hours at 1000^{o}C) that we have an outer unetched layer of Pt_2Al_3, as determined by XRD, about 15 μm thick. Nickel concentration in this layer is about 8 at.% (see Table 20 for complete

analysis) This was followed by a dark etching β(Ni,Pt)Al layer extending for about 8 μm, containing about 1.5 at.% Pt and having very fine precipitates which cannot be seen optically. Finally, a diffusion zone containing precipitate rich in chromium, tungsten and other refractory elements in a matrix of β(NiAl) can be seen.

The same specimen heat treated for 55 hours at 1000°C can be seen in figure 25(b) where an outer slightly etched (Pt,Ni)Al layer extending through the outer coating region is clear. This layer contains an average concentration of 45 at.%Ni (see Table 21 for complete analysis), a very fine porosity in the outer coating region and bigger porosity at the interface between the outer coating region and the diffusion zone has been observed. A very fine acicular phase starts to form in the diffusion zone. This phase is associated with a globular phase having similar analysis to those globular phases described earlier.

Figure 26 shows the coating structure and elemental profile for the same coating after 1000 hours of heat treatment at 1000°C, where the first 30 μm is a continuous layer of slightly etched grains of a mixture of NiAl and PtAl phases, as determined by XRD (Table 22) with NiAl lines stronger than PtAl lines. The elemental profile across the coating shows that Al,Ni,Pt,Cr,Co and W profiles in the outer coating region is fairly constant (Pt: 11, Ni: 56, Al: 32, at.%). The absence of segregation of these elements in this layer suggests that NiAl and PtAl could be in solution or the segregation is in a very fine state.

The outer coating layer is followed by an unetched layer (diffusion zone) of about 20 μm thick, except for the upper zone of this region where a duplex ($\alpha + \beta$) structure can be seen, a chromium peak coincides with this zone similarly Mo, Ti (not shown) and W. An acicular phase extending into the substrate can be seen in this zone also, but no porosity has been observed in this type of structure. The change in lattice parameter with Ni content of PtAl is shown in figure 27. The method used in determining the lattice parameters involved measuring the angular displacement between individual X-ray diffractions, indexed according to PtAl unit cell and subsequent computation of lattice parameter. It can be seen that the lattice spacing of PtAl phase falls as Ni content is increased.

3.8.4. Heat treated Coating D

The same techniques used in determining the compositions and structures of the heat treated coating A, B and C were employed in the examination of the heat treated coating D. In addition to these techniques, replicas extracted from the surface of the heat treated coating D for 1000 hours at 1000°C, were examined using electron diffraction analysis. Results of the different techniques employed are presented in the following sections.

3.8.4.1. Optical Metallography, EPMA, SEM and X-ray diffraction Results

Figure 28 presents an optical micrograph of specimens heat treated for 5 hours and 55 hours at 1000°C, the total thicknesses of the coatings are 50 ± 5 μm and 60 ± 5 μm respectively, compared with the as-coated optical micrograph (see Figure 16), the coating

structure after 5 hours heat treatment (figure 28 (a)) has an outer continuous unetched Pt_2Al_3 layer containing about 3.4 at. pct.Ni and covering about 30 μm of the total coating, followed by a duplex (PtAl + NiAl) layer, about 10 μm thick, where both Ni and Pt substitute each other in these phases (see Table 23 for the composition of these phases); the duplex phase ends with a dark etched (Ni,Pt)Al layer of about 15 μm thick. Finally a diffusion zone can be seen with very fine precipitates rich in chromium and other refractory elements.

The analysis of the above phases has been made using point analysis using EDS on the SEM, where this technique has been proved useful in such structures. Additional heat treatment ie. 50 hours at 1000°C (figure 28(b)) changes the outer region of the coating to PtAl structure in which two distinct PtAl layers can be identified, the first (∿3 μm thick) of this layer is unetched and contains about 10 at.pct. Ni, the remaining PtAl (∿40 μm) is slightly etched with an average Ni content of 42 at. pct. (Table 24). These layers are followed by a well developed diffusion zone of a duplex structure composed of a dark etching phase believed to be either β(Ni,Pt)Al or γ' $(Ni,Pt)_3Al$ or maybe a mixture of both and an unetched α phase. A fine acicular phase extending into the substrate can be seen in this zone also. Porosity has been noticed at the interface between the outer coating and the diffusion zone.

Further heat treatment of the same coating, i.e. 1000 hours at 1000°C produced an inner duplex structure (figure 29) which has spread to cover the outer (∿ 55 μm) of the coating. XRD

revealed a mixture of PtAl and NiAl (Table 25) with PtAl lines stronger than NiAl lines. Line scans through the coating were performed (figure 29). It can be seen that the profile of the six elements analysed are fairly constant in the outer coating region, whereas the peaks in chromium, tungsten and other refractory elements (not shown) coincide with the diffusion zone.

SEM technique revealed a duplex structure of very fine nature in the outer coating region, but due to the lack of resolution of the X-ray analysis in the microscope was not able to determine the exact composition of each phase, however, it seems reasonable to attribute the dark etching lines in the outer coating region to be NiAl type.

3.8.4.2. Electron diffraction

Extraction replicas were prepared from the coating (D), heat treated for 1000 hours with the intention of gaining more information about the structure of the coating by using the electron diffraction analysis. These replicas were obtained after carefully polishing away about half of the outer coating ($\sim$ 20 μm). Figure 30 shows a transmission electron micrograph of this replica (taken on a Philips STEM 401 Electron Microscope). It can be seen that a spherical shaped precipitate covers most of the outer coating region· these precipitates are not extracted. Few particles extracted were of a shape that suggested they had been formed by impingement of spheres. Three diffraction patterns taken from these (dark area in figure 30 a) are presented in figure 30 b, c and d. These diffraction patterns have been indexed as shown to identify this phase as γNiCr.

The same replica was used for EDS analysis on STEM. This analysis indicates at least two types of precipitates having different compositions, the average compositions of these precipitates (in wt.%) are as follows :-

High Cr content precipitate (average analysis of two particles)

Ni : 58, Cr : 25, Co : 7, Al : 1.2, Mo : 3, Fe : 2.

Low Cr content precipitate (average analysis of two particles)

Ni : 70, Cr : 14, Co : 12, Fe : 2 (other elements are less than 0.5 wt.%).

Both types of precipitates showed similar diffraction patterns.

These results suggest that during long term heat treatment Cr, Co and other refractory elements are being rejected from PtAl phase to form γ phase with the diffusing Ni from the substrate. It is difficult to know whether there are only two types of precipitates or a complete γNiCr composition range. However, these results are in agreement with our suggestion since it indicates that as the spheres are growing, a continuous process of rejection is taking place.

3.8.5. Heat treated(duplex structure)coatings (Code E)

Duplex coating obtained by special treatment (see section 3.5) has been heat treated for 156 hours and 516 hours at 1000^{o}C in vacuum. These heat treated coatings were examined using optical metallography and subsequently analysed using EDS on the SEM. X-ray diffraction technique has been used to determined their structure, the results are presented.

Optical metallography and SEM study of the heat treated coating (after 156 hours at 1000°C) (figure 31(a)) shows that the outer coating layer has completely transformed to β(NiAl) type structure, containing very fine precipitates dispersed throught the outer coating layer. The average analysis of the outer coating layers is given in Table 26. The analysis showed also that the concentra tion of Pt decreases as we approach the diffusion zone while Ni increases as we approach this zone, which itself is composed of α phase in a matrix of β (NiAl). Figure 31(b) shows the microstructure of the coating after 516 hours heat treatment at 1000°C where an outer β(NiAl) layer can be seen covering about two-thirds of the whole coating thickness (∿110 μm), the composition of this layer is given in Table 27.

Bright etching precipitates can be seen in the outer coating layer. These are believed to be similar to those found in the oxidised specimen (figure 43), the analysis of this phase suggests a γ' $(Ni,Pt)_3Al$ phase (see Section 3.9). Table 28 summarises the results of heat treatments for all types of coatings.

3.9. Oxidation of Platinum-Aluminide Coatings

The oxidation behaviour of platinum-aluminide structures on IN-738 superalloy was studied at temperatures (800°C to 1000°C) in an atmosphere of pure oxygen at 1 atmosphere pressure for different periods. The rates of oxidation were measured by continuous recording chart attached to the micro-balance, details of which have been presented in Chapter 2.

Firstly, the rates of oxidation of bare and simple aluminized IN-738 were evaluated in the temperature range (800°C - 1000°C) so that a comparison can be made between the bare, simple aluminide and the platinum-aluminide coatings. The weight gain versus time curves for the uncoated specimens shows that the weight gain obtained at 950°C in five hours was slightly more than 1 mg/cm^2 (figure 32). Most of the oxidation took place in the first hour of oxidation and thereafter the oxidation rate slowed down. The weight gain versus time curves for the simple aluminide coated specimens shows that the weight gain obtained in five hours at 1000°C was 0.5 mg/cm^2 (figure 33). The oxidation kinetic obeyed parabolic rate law in the first few hours of oxidation then deviated from the parabolic behaviour as can be seen in figure 34. Measurements taken of weight changes are by themselves not a reliable criterion, regarding the behaviour shown by a protective coating in the oxidation test. Additional tests were carried out by way of metallographic examination of the test specimens after a given test period. Figure 35 illustrates a micro-section of the coating after 200 hours of oxidation at 1000°C, where a thin oxide layer (Al_2O_3) is covering the surface while the precipitate in the outer coating region has dissolved and a new phase, believed to be blocky α phase, nucleates in the outer coating region as well as the diffusion zone.

Some simple aluminide coatings were also thermally-shocked between 1000°C and room temperature in a two hours cycle. The protective Al_2O_3 layer which is initially formed tends to spall after some time. The spalling tendency persists with time and

Al_2O_3 forms immediately on the depleted oxide area (up to 200 hours of cyclic oxidation). Oxidation studies on the platinum-aluminide coatings have been divided into three categories :-

1. those which have PtAl type structure in the outer coating,
2. those which have a mixture of PtAl and NiAl in the outer coating and
3. those which have NiAl structure in the outer coating.

These types of coatings have been obtained by a suitable heat treatment of the as-coated specimens having either a 5 μm pt-thick coating or a 15 μm pt-thick coating followed by subsequent aluminization using a high activity pack. Finally a heat treatment at 1000°C was carried out until the structure required on the outer coating region had been obtained as indicated by X-ray diffraction results. In addition to this, specimens having a $PtAl_2$ or Pt_2Al_3 structures in the outer coating regior has been oxidized and their weight gain versus time has been recorded. In all these cases, the oxidation studies were carried out between 800°C - 1000°C.

The results shown in Figures 36, 37, 38 and Table 29, for the isothermal oxidation studies of different platinum aluminide structures indicate a better oxidation resistant in all cases compared to the simple aluminides. A parabolic growth rate can be observed in all cases (figures 39, 40 and 41). No spalling occured even after 427 hours of oxidation at 1000°C. The scale formed seems to be very adhesive to the coating even during cyclic oxidiation experiments. The maximum weight gained was 0.25 mg/cm^2 in 48 hours obtained when oxidising a specimen from the first

category. α-Al_2O_3 was the only oxide formed in all the oxidation tests studied, this was confirmed by SEM analysis which showed that a continuous layer of Al_2O_3 develops on all the specimens oxidised in pure oxygen at any of the temperatures in the interval between 800°C and 1000°C. As the oxidation time was increased, the morphological features of the oxide at the oxide-gas interface did not change significantly. Only the oxide thickness increases by time. Figure 42 (a) shows a scanning electron micrograph featuring the oxide protrusions penetrating the outer coating layer of coating treatment A, after 427 hours of oxidation, including cyclic oxidation, in pure oxygen at 1000°C. The oxide is multi-layered and the scale was tightly adherent to the coating. Figure 42 (b) shows a scanning electron micrograph of the oxidised surface of the same specimen showing the oxide protrusions. Point analysis using EDS on the SEM showed that the outermost layer of α-Al_2O_3 contains traces of Ni, Pt, Cr and Co. The concentration of Ni and Pt in the oxide scale increases as we move inward and amounts to 4 wt. pct. Ni, 1.5 wt. pct. Pt in the innermost oxide. Fine porosity has been found in the outer region of the coating and within the oxide scale. The scanning electron study of the surface scale of the same specimen shows that alloy-scale interface is highly convoluted with Al_2O_3 particulates covering the surface (figure 42 (a)).

The phase changes in the structure of the coating during oxidation were very similiar to those changes normally observed during heat treatments of similar specimens except that the rate is faster during oxidation.

3.10. Coating degradation

Figure 43 summarizes typical structure and composition information of coating treatment A ; degradation after extended oxidation and heat treatment at 1000°C. The first step towards coating degradation is manifested by the formation of white islands of γ' at the grain boundaries of dark etching β(figure 43 (b)), the former increasing and the latter decreasing in amount with time at temperature (figure 43 (c)). Evidence of γ' in the outer cating region of the structure shown in figure 43 (c), has been confirmed using XRD (Table 30).Point analysis using EDS on the SEM of this phase has given the following analysis :

Pt : 4.2, Ni : 67.5, Al : 11.8, Cr : 2.6, Co : 5.9, Ti : 5.5,

W : 1.3, Nb : 1 at.%.

The high partition of Ti, W and Nb to this phase with respect to β phase is worthy of note, however further study on this subject is needed.

CHAPTEP FOUR

DISCUSSION

4.1. INTRODUCTION

Aluminization of Pt-coated IN-738 superalloy can produce a wide range of structures which are highly dependent upon the thickness of platinum layer deposited and the coating conditions used. In this study, the structure of the platinum aluminide coatings on IN-738 superalloy have been identified. No comprehensive description for the phase constitution of platinum-aluminide coatings has previously been made. It is, however, possible to do this by an understanding of the phase distribution established between the coating and substrate, and how that distribution changes in service as the system tries to move towards equilibrium. This can be achieved in terms of the relevant phase diagram, when the diagrams are available, and diffusion path taken by the coating/substrate system can be considered directly. When the diagrams are unavailable, a study of the diffusion path taken can be used to gain phase diagram information. This understanding can be useful in developing improved coating compositions. Some progress can be made by considering Cr as a solid solution constituent associated with one or more of the Ni-Al, Al-Pt or Ni-Al-Pt intermetallics. Section 4.2 gives details of the theory of diffusion paths in ternary systems. A later Section (4.4) discusses the way in which pseudo-ternary phase diagrams can be used to describe the coating and matrix phases in both as-coated and subsequently heat treated coatings, although a more ideal system would be Ni-Cr-Pt-Al or higher order system.

Rules governing the description of diffusion paths in multi-component systems have been discussed in the literature. It should be noted that for diffusion paths plotted on a phase diagram, dashed lines do not represent distance in the actual diffusion couple, but represent an interface. In a ternary system, a three phase field will have no width in a diffusion couple because of the constant chemical potentials within that field (i.e. no kinetic data can be drawn from diffusion paths).

Since the Pt-Al phase diagram has not been characterized fully, it will be more diffult to consider platinum aluminide coatings on nickel-base superalloys in terms of the Ni-Al-Pt phase diagram or the more relevant Ni-Cr-Pt-Al phase diagram. However, the diagrams of Chatterji, et al (13) appear to give the best definition of the binary system. We have performed microstructural and microchemical analysis of coated and heat treated IN-738, and as a result we now have a limited picture of the appropriate phase diagram. Information about the solubility and diffusion in different Ni-Pt-Al intermetallics in the as-coated and heat treated conditions are discussed with a possible explanation given to account for the mechanisms of formation and degradation of the coatings. Diffusion paths representing the different types of coatings described in Section 3.4 and 3.5 are also presented.

There is a lamella layer at the coating/substrate interface in most of the coatings produced in this work. This has evidently formed as a result of the breakdown of a planar interface. A stability criterion based on the concept of constitutional supersaturation derived by Coates and Kirkaldy (58) in which local

equilibrium (defined by the ternary phase diagram) is maintained at all phase interfaces is used to describe the breakdown of a planar interface to a non-planar one.

In addition to this, the mechanisms that help to key the surface scale to the substrate and improve the scale-metal adhesion in both isothermal and cyclic oxidation tests have been discussed.

4.2. Theory of diffusion paths in Ternary Systems

Consider the meaning of a diffusion or composition path and how it can be represented. If we have a ternary system A-B-C, shown schematically in figure 44(a) and a two-phase diffusion couple of terminal compositions designated by points P and Q is annealed for a time t, concentration profiles for the arbitrarily chosen independent components A and C might be shown in figures 44 (b) and (c). The corresponding interface concentrations are designated by points R and S. One can calculate the concentration profiles (Kirkadldy (59)) by solving (subject to the appropriate mass balances and boundary conditions) Fick's second law for a planar interface at which local equilibrium is maintained. As in the corresponding binary problem the solution can be expressed as a function of one independent parameter λ, (λ = distance/(time)$^{\frac{1}{2}}$) i.e. $C_A^\alpha(\lambda)$, $C_C^\alpha(\lambda)$, $C_A^\gamma(\lambda)$, $C_C^\gamma(\lambda)$. The interface compositions are not known from the start and their determination forms part of the solution. For each phase one can eliminate λ between the solutions for the concentration distributions to give $C_A^\alpha = C_A^\alpha(C_C^\alpha)$ and $C_A^\gamma = C_A^\gamma(C_C^\gamma)$. The choice of component C as the independent variable is completely arbitrary. It should be noted that these expressions are distance and time independent

and, therefore, can be plotted on the ternary phase diagram. In conjunction with the appropriate (unique) tie-line, they define the composition or diffusion path (solid line joining P and Q in figure 44(a) for the given diffusion couple. Note that such diffusion paths give no distance information. In cases where we have a non-planar interface at the coating/substrate boundary, some attention should be focussed on the phase interface stability of diffusion couples within ternary systems. However, the system considered in this work (i.e. IN-738-Pt) is more complex than those which have been dealt with so far. Kirkaldy and Fedak (60) have experimentally studied the non-planar interfaces which occur in two phase infinite diffusion couples within the Cu-Zn-Sn system. They noted the close analogy between this phenomena (which involves two diffusion fields in each phase) and the problem of solid-liquid interface stability during steady-state solidification of dilute binary alloys (which involves a thermal field and single diffusion field in each phase). In the latter case, the breakdown of a planar interface is associated with the onset of constitutional supercooling in the liquid layer ahead of the moving interface (Rutter and Chalmers (61). In keeping with this analogy Coates and Kirkaldy (58) have proposed that the transition from a planar to a non-planar interface morphology in ternary diffusion couples is associated with the production of a layer, directly ahead or behind the planar interface, which is constitutionally supersaturated. In other words, the calculated diffusion path for a couple assumed to have a planar interface defines points on the ternary phase diagram which lie within the two phase field even though local equilibrium is maintained at the interface (see figure 44(d).

It was noted by Mullins and Skerka (62) and confirmed by Coates and Kirkaldy (58) that it appears possible to have instability without constitutional supercooling and constitutional supercooling without instability. Coates and Kirkaldy demonstrated the possibility of analogeous situations in isothermal ternary systems. The proposals by these authors are not conclusive but from a thermodynamic view point there appears no objection to constitutional supercooling or supersaturation without instability. However, instability without supercooling or supersaturation is more difficult to understand, although this was suggested by Kirkaldy and Fedak (60). Under these conditions an internal source of free energy is required, which can contribute to the internal free energy stored via the solute segregation reaction which accompanies instability.

4.3. Solubility and diffusion in $PtAl_2$, $PtAl_3$, PtAl and β (Ni,Pt)Al

An early understanding of the formation of aluminide coatings was due to Goward and Boone (63). Further developments have been reviewed by Pichoir (27). An attempt has been made in the following lines to describe the as-coated structure. as well as the effect of heat-treatment in terms of the diffusional processes involved. During the formation of the coating on the highly alloyed nickel substrate (IN-738), used in this work (inward diffusion of Al, high activity pack), a relatively high density of secondary phases is formed because of the insolubility of these phasesin the

(Ni_2Al_3) and aluminium-rich β(NiAl) phases. These secondary phases must effectively decrease the cross sectional area

available for the diffusion of aluminium through the coating and thereby contribute to the establishment of the aluminium concentration gradient (figure 10) which corresponds to the presence of aluminium-rich β(NiAl) in the coating.

The absence of a distinct layer of γ' (Ni_3Al) phase below the aluminium-rich β(NiAl) layer adjacent to the substrate is as expected; diffusion rates in the γ' (Ni_3Al) phase are three to four orders of magnitude lower than in the aluminium-rich phases (Goward et al (63)). The secondary phases precipitated in the various layers during coating formation, while rich in chromium and molybdenum, exist in a fcc rather than the expected bcc structures. Variations in the types of precipitates formed through the thickness of the coating come about either by the diffusion controlled process described earlier, or by change in the equilibrium as a consequence of change of concentration of aluminium (Haworth (64)). Subsequent heat treatment converts the outer layers of aluminium-rich phase (s) to nickel-rich β(NiAl). This must involve an outward nickel diffusion through β(NiAl) (figure 11) and subsequent aluminium motion through the residual aluminium-rich phase (s). The nickel-rich β(NiAl) phase formed by this process contains secondary phases derived from these precipitates which formed during the original coating formation process but these phases now revert to their equilibrium state. It must be mentioned that this process is a slow process (more than 200 hours of H.T. at 1000°C was required in order to obtain the structure shown in figure 11). Because the substrate alloy, IN-738, consisting of γ' (Ni_3Al, Ti) in a γ (Ni solid solution)

matrix, removal of nickel, with the consequent enrichment of aluminium, must cause the formation of another layer of the β(NiAl) phase or γ' (Ni_3Al) phase or both. This layer must be free of precipitate, below which the lamellae structure develops because of increase in relative concentration of alloying elements. This layer must increase in thickness by advancement of its internal front into the substrate alloy as long as nickel is being removed to react with aluminium in the outer coating zones. Because of the high Mo and W content of the substrate, a topologically close packed phase ($\sim$) intervenes between γ and Cr rich phase, therefore ($\beta + \gamma'$) $+\sim$ is normally observed.

The composition and structure of $\sim$ phase precipitated in this zone and the matrix associated with it is given in Tables 6 and 7.

The pack aluminizing process is itself a complex process including two important steps that are occurring simultaneously; Al is being deposited onto the substrate primarily by a gaseous reaction and the Al that has been deposited is alloying with the substrate by diffusion (see Section 1.6.2. for more details). A recent study by Rairden et al (65) on the aluminization kinetics of the early stages (first few minutes) on the superalloy Rene 80 have shown that the Al surface concentration decreases with pack cementation time (most of the deposition occurs during the first few minutes of processing) and the surface concentration to be nearly independent of pack activity. These results might be supposed true for the deposition of Al on Pt.

The results of the study of Jackson et al (16) on the aluminization kinetics of Pt reporting an initial very rapid deposition of Al and in particular the fact that almost twice as much as Al is deposited on pt as on IN-738, can be attributed to the build-up of Cr and other refractory elements beneath the coating layer, when aluminizing bare IN-738, hence there is less Ni available. Thus NiAl forms more slowly on IN-738 than the Pt-Al intermetallics formed on pure Pt. These results indicate also that the limiting step in the aluminization of IN-738 using the given processing conditions is the assimilation of Al in the substrate rather than the transfer of Al from the pack. Aluminium deposition will cease whenever its activity on the substrate surface is equal to its activity in the vapour. By this reasoning, Pt has a larger capacity than IN-738 for aluminium assimilation, i.e. Al from the pack controls the phases when aluminizing pure Pt. Within the platinum-aluminium binary system (figure 2) there are a number of intermetallic compounds. Due to the kinetics of the aluminizing process, only the intermetallics $PtAl_2$, Pt_2Al_3 and PtAl are generally found in aluminized structures, keeping in mind that the absence of any other phase does not, by itself, suggest its absence in the phase diagram.

$PtAl_2$ is fcc having CaF_2 structure is reported to exist in narrow range of composition (32-33 at.%Pt). However, evidence for Pt-rich nonstoichiometry of this phase has been observed (Chatterji et al (13)). No such evidence has been observed in this work. Information on solubilities in this phase does not exist, however, results obtained from this study show that the

interdiffusion of Al and Pt is quite rapid (absence of $PtAl_2$ during the aluminization of bulk platinum even after short time aluminization). This is probably due to (1) the apparent fast diffusion rate of Al into Pt and (Pt,Al) compounds, and (2) the high atom fraction of Al in $PtAl_2$ as compared to Ni_2Al_3 or NiAl.

In the present work, other elemental solubilities, e.g. Ni in $PtAl_2$ have been found equal to about 25 at. pct. Cr - 7 at. pct., Co - 4 at. pct. However, we must say that the solubility limit measured could be the diffusion controlled solubility.

Aluminium-rich intermetallics form with considerable expansion; the platinum-rich with a contraction (relative to pure Pt). In the ideal cases (no volume change, voids formation, etc.) a simple mathematical analysis of layer-growth data, in the form of time vs. layer thickness, will establish unambiguous D values for the different phases at a given temperature. Important equilibrium, as well as kinetic information may then be obtained from a single experiment. In our experiments this was not possible because of the difficulty in determining the boundary conditions and because of the presence of voids and the difficulty of defining 'zero' time in the pack aluminiding process. In addition to this, coatings based upon the platinum-aluminium binary and which specifically generate $PtAl_2$ at the surface constituting a significant portion of the platinum aluminide layer, will undergo as much as 19 percent volume contraction during service as a result of degenerating from $PtAl_2$ to PtAl. It is

unlikely that such a volume change within an inherently brittle matrix could be accommodated without void formation or cracking. Only the molecular volume of Pt_2Al_3 shows any resemblance to the 'ideal' volume predicted by linear correlation between volume and composition (Table 31). Pt_2Al_3 is hexagonal having Ni_2Al_3 structure, the lattice parameter of the two pure aluminides are similar enough to suggest isomorphic behaviour and in addition to this, there is about 15% difference in atomic sizes between Pt and Ni.

It is known that the Ni_2Al_3 structure is highly defective (Bradley and Taylor (33)) with a very high interdiffusion coefficient e.g. $D_{Ni_2Al_3}$ at 1000°C $\approx 10^{-7}$ cm^2 sec^{-1}. However this research shows that the intermetallic Pt_2Al_3 behaves as an effective diffusion barrier restricting the movement of nickel to the surface, because the maximum solubility of Ni in Pt_2Al_3 was found to be equal to 17 at. pct. at 1000°C (compared with about 52 at.% for PtAl and 25 at.% for $PtAl_2$). Other elemental (Cr, Co,Ti, etc.) solubilities were found to be practically nil in this phase, which could be due to the lack of diffusion in this phase.

PtAl has an ordered bcc structure similar to NiAl, both intermetallics exist over a wide range of composition (41-51 at pct. Pt for PtAl at 1000°C and 42-65 at. pct. Ni for NiAl at 900°C). It is interesting to note that both structures are the main structures found in the coating after long time heat treatment.

Figure 27 shows the change in lattice parameter with Ni content of PtAl, the scatter of points is believed to be due in

part to the method of calculation of lattice parameters (a particular plane (211) had been chosen from the indexed X-ray diffractions, then the lattic parameters were subsequently computed) and, in part to the type of specimens used (flat specimens instead of powder ones).

Ni has been found to be soluble in PtAl up to 52 at.pct, Cr up to 10 at.pct. and Co up to 4 at. pct., other elements are soluble up to 1 at. pct. β(Ni,Pt)Al appears to have a solubility limit of about 12 at pct. Pt, with Pt apparently substituting for up to one-fourth of the Ni. Cobalt and Ti has great diffusivity through β(Ni,Pt)Al phase than Cr and other refractory elements (cobalt solubility is up to 5 at. pct. while Cr is $\sim$ 4 at. pct.). We must say that these figures may be lower than the true values due to the diffusion process and/or the boundary conditions imposed by the process. However, the same observations have been reported earlier by Taylor (66) and Schramm (67) for a pure β NiAl phase.

The ability of Co and Ti to establish a relatively high composition profile throughout the coating structure after long-term high temperature stability tests, is undoubtedly beneficial to coating performance. Refractory elements such as tungsten and molybdenum, although essential solid solution strengtheners, may have an adverse effect upon resistance to hot corrosion. Peters et al (68) have indicated that Mo is harmful. However, it should be noted that other workers (69, 70) have shown that Mo, W and Ta can be beneficial to the hot corrosion resistance of Ni-base superalloys.

Sarkel and Seigle (71) gave data for the interdiffusion cofficient, together with the tracer diffusion coefficient D^*_{Ni} (Hancock and McDonnel (72)) as a function of Ni content for NiAl at 1100°C. They showed that D^*_{Ni} becomes greater than $\tilde{D}_{NiAl}$ and hence $D^*_{Ni} > D^*_{Al}$, as the Ni content is increased. Moreover, the work by Janssen and Rieck (4) does agree with the argument of D_{Ni} being greater than D_{Al} in Ni-rich NiAl.

4.4. Diffusion paths and equilibrium

Phase equilibria in ternary and high order systems can be extremely useful in correlating coating/substrate composition, microstructures and behaviour. For example, the time/temperature change in formation and degradation of coatings on superalloy surfaces can be described in terms of multi-element diffusion between the elements added (e.g. Al from the pack) and the elements in the substrate by mapping the diffusion paths through the appropriate phase diagram.

If a diffusion couple consisting of two alloys of different compositions containing elements A, B and C is heat treated, it is possible to express the resulting composition profile in terms of a diffusion path on an isothermal section of the ternary phase diagram A-B-C. An example is described in Section 4.2. Consider now the application of these diffusion paths to represent the phase constitution of platinum aluminide coatings on IN-738 superalloy. Since the Pt-Al diagram has not been characterized fully, and the lack of knowledge of higher order phase diagrams, it is difficult to consider platinum aluminide coatings on IN-738 superalloy in terms of the Ni-Cr-Al-Pt phase diagram. However,

Jackson et al (16) did use a quaternary diagram to explain their coating structures. This diagram (figure 3) is hypothetical (especially in the Al-rich phase fields of the ternary NiCrAl and NiCrPt). Moreover, we think that the ternary NiAlPt is perhaps the best that we can do at the present time, since the quaternary diagram is of limited usefulness for any extension to more than four components. In addition to this, most paths observed needed only ternary faces or just below the faces to be drawn.

Approximate diffusion paths, as observed from metallography and microanalysis, have been mapped onto pseudo ternary diagram (figure 20). Each path represents the compositional profile from coating surface into the substrate, dashed lines represent zero distance in the microstructure. The lines shown in Figure 20 in various phase fields are simple diffusion paths and consequently it is only the last point (where full line becomes dotted) that is expected to show limiting solubility. However, most of the coating structures are very fine and hence difficulty arises in determining the solubility limit of various phases because of the lack of spatial resolution in the EPMA and SEM.

One must keep in mind, however, that because the diagrams are not strictly ternaries there may be coexistence of phases over a range of the matrix aluminide phase field, e.g. there is possibly considerable overlap between carbides and Al_9Cr_4/Al_8Cr_5 in equilibrium with β(Ni,Pt)Al and beyond this phase, where the lack of consideration of Cr in a proper manner becomes more important.

The following structures are expected to give reliable data for the limiting solubilities in different phases: the as-coated structure of coating treatment E is expected to give limiting solubility in $PtAl_2$ and NiAl phase (figure 17). However, accurate data could not be obtained because of the finess of the structure, whereas the as-coated structure of coating treatment D (figure 16) is supposed to give limiting solubility in the outer Pt_2Al_3 phase and the following $PtAl_2$ layer. In the same way, the heat treated coating treatment C (Heat Treated for 5 houres at 1000°C, (figure 25a)) is believed to give limiting solubility in Pt_2Al_3 and (Ni,Pt)Al,and finally the heat treated coating treatment B (Heat Treated for 5 hours at 1000°C (figure 23a)) is supposed to give limiting solubility in Pt_2Al_3 and PtAl phase.

This assessment is based on the experimental results obtained in this study. However, one should keep in mind that these solubilities are diffusion controlled.

4.5. Pt-Aluminide Coating Structures

4.5.1. As-coated

The as-coated structures encountered in this research can be divided into three classes :-

i. Those which form $PtAl_2$ layer on the outer coating region i.e. coatings obtained by treatments A and C (figures 12 and 15). Consider coating by treatment A (5 μm Pt, high activity pack), the deposition rate of Al is high enough for the formation of $PtAl_2$ in the initial stages of coating, since the amount of platinum

available is limited, the excess Al will cross the initially formed layer to form another layer of simple aluminide. The segregation of certain elements e.g. Cr and other refractory elements at the coating/substrate interface and in the simple aluminide layer is due to their limited solubility in the matrix aluminide. However, some interdiffusion of Ni and Pt has occurred during the coating treatment giving the simple aluminide layer two etching characteristic . When the first few microns of the simple aluminide zone stain dark, because of the presence of platinum in this layer (Ni, Pt)Al, while the Pt free layer stains slightly brighter than the previous layer.

Substantial amounts of porosity is evident in this group of coatings; this porosity is normally located between the outer $PtAl_2$ and NiAl layers. The appearance of porosity in diffusion couples is usually associated with the Kirkendall effect. This explanation would require that Ni diffuses out faster than Al diffusion in although, this does not fit with normal Kirkendall behaviour but can be explained in terms of the various diffusion rates in PtAl and NiAl phases. In some cases partial coating delamination occurred, indicating failure because of large differences in thermal expansion (16) or because of poor initial bond between Pt and IN-738. However, the situation is not altogether clear. Consider now coating C (5 μm Pt, low activity pack); the same coating formation mechanism can be proposed for this type

of coating, bearing in mind that the rate of deposition of Al is slower in this case. This will lead to a slower consumption rate of the Pt layer. Moreover, because of the processing time (1 hour compared to 2 hours for coating treatment A), a thicker $PtAl_2$ layer is normally found in the outer coating region. A duplex (βNiAl + $PtAl_2$) can be seen between the outer $PtAl_2$ and the innermost β(NiAl) layer indicating the regions where the solubility of Ni in $PtAl_2$ has exceeded its limits due to the outward diffusion of Ni where the conditions favour the formation of β(NiAl).

ii. Those coatings which form a Pt_2Al_3 layer in the outer coating region i.e.coating obtained by treatment B and D (figures 14 and 16). Consider Coating B (15 μm Pt. high activity pack), in which the system behaves as two unconnected couples, IN-738/Pt and Pt/Al (Jackson et al (16)). As the Pt layer becomes thinner relative to diffusion distance, the two couples begin to interact through the common Pt terminus. In this case aluminization occurs only in the Pt so the initial path is the same (more or less) as would be seen for aluminization of bulk Pt. The remainder of the coating structure is for diffusion that occurs between bulk Pt and IN-738. Notice the absence of elemental segregation in the innermost part of the coating which is due to the fact that not so much Al has arrived at a high activity at the substrate. Adding to this, the high solubility of Cr, Co

and other refractory elements in the Pt-Ni structure. In this class must also be included the structure produced by coating Treatment D (15 μm Pt, low activity pack). This coating appears unique in its structure (Pt_2Al_3 on top of $PtAl_2$), i.e. part of the $PtAl_2$ initially formed in the outer coating has transformed to Pt_2Al_3, the remainder of the coating appears to be similar to coating Treatment C. The description of the aluminization mechanism of 15 μm Pt thick coated IN-738 using the low activity pack is; after the initial Al deposition and $PtAl_2$ formation on the surface, because of the slow deposition rate of Al after some time and the rapid inward diffusion of Al there is insufficient Al at the surface to maintain $PtAl_2$, and Pt_2Al_3 is now formed at the outer surface (figure 16). In addition, because of the initial Pt thickness, thereare insufficient substrate elements (especially Ni) at the outermost part of the coating to stabilise the $PtAl_2$ formed initially (there was no Pt_2Al_3 layer in ther outer coating region after aluminizing a thin Pt-coated IN-738 under the same conditions, because Ni had stabilized the $PtAl_2$).

iii. Those coatings which form a duplex structure ($PtAl_2$ + β(NiAl)) in the outer coating region.

The limited duplex ($PtAl_2$ + NiAl) layers seen in the inner coating region (figures 15 and 16), obtained when aluminizing with the low activity pack, formed because of the outward diffusion of nickel from the substrate during the aluminization process, where Ni concentration

has exceeded its solubility limit in $PtAl_2$ phase in that region, hence a duplex structure of $PtAl_2$ + NiAl is formed. Based on these observations, we decided to pre-anneal a Pt-coated IN-738 to give interdiffusion with the substrate so that the Ni level (figure 20) in the outercoating region exceeds its solubility limit in $PtAl_2$. Diffusion of Ni in Pt has been studied by Hauffe (73) at different temperatures, and the following values have been obtained for an alloy containing 14.9 at.%Ni.

D cm^2/sec	Do $cm^2/sec.T$	T^oC
5.2×10^{-11}	7.75×10^{-4}	1043
4.8×10^{-10}	"	1241
1.5×10^{-4}	"	1401

we have obtained a diffusion coefficient equal to 6.94×10^{-11} cm^2/sec at 1000^oC for the diffusion of Ni (from IN-738) in the platinum layer, assuming that the diffusion process obeys the parabolic relation $x^2 = 4Dt$. A layer of β(Ni,Pt) Al has been observed beneath the duplex layer in most of the cases. This is due to the fact that Al had diffused into the substrate before Ni had time to diffuse into Pt. One can imagine that by studying the diffusion of Al through Pt and $PtAl_2$, and that of Ni into Pt, one might succeed in choosing a temperature to give in one-step process the desired duplex coating structure.

4.5.2. Heat treated

The heat treatment of coatings A, B, C, D and E results in coating structure which can be classified according to three categories :-

i. in the first category, an outer β(Ni,Pt)Al layer develops after long term heat treatment, the following coatings fit in this group :-

	Optical micrograph and line scans
Coating A 1000°C t >>1200 hrs.	Fig. 22
Duplex coating E 1000°C t>>516 hrs	Fig. 31

in all the above coatings a well developed diffusion zone containing acicular sigma phase extending into the substrate can be seen. It should be noticed that in order to obtain such a layer in the outer coating region, a high Al concentration at the surface is required in the as-coated structure, i.e. $PtAl_2$ or ($PtAl_2$ + βNiAl) in the outer surface. The development of the coating structure during heat treatment is shown in figure 21, from which it can be noticed that the transformation sequence is according to the predicted PtAl phase diagram. It should be noted also that nickel seems to stabilise the $PtAl_2$ layer during short term heat treatment. A Cr rich precipitate similar to those found in the simple aluminide coatings appeared in the inner coating region at some stage during heat treatment. These precipitates dissolve in the coating at later stages of heat treatment.

ii. The second category of the heat treated coating developed a (Pt,Ni)Al structure in the outer coating region after long term heat treatment. One heat treated coating displayed this structure :

Coating B	1000°C	t >>1200 hrs	see Fig. 24 for optical micrograph and line scans

This type of heat-treated coating is normally formed from the as-coated structure which exhibits Pt_2Al_3 in the outer coating region (thick Pt-coating aluminized with the high activity pack to start with). No acicular phase has been found in the diffusion zone, even after 1200 hours of heat treatment at 1000°C, but rather a lamellar phase in a matrix of γ' $(Ni,Pt)_3Al$, despite the fact that acicular α phase had been observed in earlier stages of heat treatment (factors effecting the formation of a phase will be discussed in Section 4.6).

iii. The third category of heat treated coatings include those coatings which form a mixture of (Pt,Ni)Al and (Ni,Pt)Al in the outer coating region after long term heat treatment t > 1000 hrs, the following heat treated coating display this structure :-

			Optical micrographs and line scans
Coating C	1000°C	t >>1000 hrs	Figure 26
Coating D	1000°C	t >>1000 hrs	Figure 29

Note that this category of heat treated coatings are normally formed from as-coated structure aluminized using the low activity pack, the relative amounts of (Pt,Ni)Al or (Ni,Pt)Al in the mixture depends on the Pt-thickness started with, the general trend

in microstructure during heat treatment is similar to that described in the first two categories.

The inward growth of the lamella layer during heat treatment can be explained in terms of Al diffusing down the β layer, found in the diffusion zone between the lamellae, to the substrate since its depth was found to increase with time and temperature.

4.6. The sigma phase

Sigma phase is an electron compound with thirty atoms per unit cell in a complex tetragonal lattice. It is generally found in systems involving the transition elements. Significant features of this phase are broad homogeneity ranges and the composition and temperature range of stability are not the same in the different alloy systems. σ, μ and Laves phases have been termed 'Tcp' compounds by Beattie and Hagel (74), the designation standing for topologically close packed. It appears that both the atomic size factor and the electronic factor contribute to the formation and stability of the σ-phase, while μ, Laves and σ precipitate at higher electron densities in superalloys (lower electron vacancy number) when molybdenum is added, only σ is prominent with chromium because of atom size effects. Boesch and Slaney (75) realized the great importance of the fundamental nature of TCP compounds utilizing data from studies by Beck et al (76). Meanwhile Woodyatt, Sims and Beattie (77) calculated electron vacancy tendancies. These calculations were developed and refined further into a system called phacomp, for phase computation. The matrix elements are converted to atomic percent composition and scaled to 100%, then the matrix composition is used to cal-

culate the mean electron-vacancy number by summation:

$$\bar{N}_v = \sum_{i=1}^{n} m_i (N_v)_i$$

where $\bar{N}_v$ = average electron-vacancy number

m_i = the atomic fraction of particular element

n = number of elements in matrix

N_v = individual electron-vacancy number of particular element.

If (Cr + Mo), (Co), (Ni) are matrix compositions in atomic percent then the electron-vacancy number is calculated from the matrix atomic percent as follows : $\bar{N}_v = 4.66\ (Cr + Mo) + 1.71(Co) + 0.66(Ni)$. Alloys having electron-vacancy number less than 2.52 are expected to be σ free others having electron-vacancy number more than 2.52 are σ prone. We have calculated the electron-vacancy number for the matrix from which σ phase develops in a number of coatings and found that the electron vacancy-number is less than 2.52 for the matrix in the case of platinum-aluminide coatings (after adding Pt concentration to Ni), but the number was higher than 2.52 for the simple aluminide coatings despite the fact that both matrices are σ prone.

These reults may suggest that Pt is not equal to Ni when calculating $\bar{N}_v$, or it could be that the size factor is the determining factor in this case or there may be some other factors affecting the σ phase formation which are still unknown.

The presence of σ in the form of widmanstatten needles at the coating substrate interface in nickel based superalloys has

previously been reported by Fleetwood, Redden and Goward and Boone (78, 79, 80). Wells and Sullivan (81) have demonstrated the presence of a needle-like α phase extending below the fusion layer and into the substrate of aluminised U700 tested under low cycle fatigue conditions at 927°C. They concluded also that the presence of this phase is clearly due to interaction between the coating and the substrate. Strang (82) in his work on the mechanical properties of some aluminized nickel based superalloys suggested that the formation of needle-like α-phase below the coating diffusion layer is not detrimental to the base material properties, but at the same time raised a number of areas of concern especially the fact that needle-like α offers an easy path for crack propagation.

Brandis et al (83) had studied the mechanical properties of diffusion coating on Ni-base superalloys (IN-738 LC and IN100) including platinum-aluminium diffusion coating LDC-2 and compared to a nickel aluminide diffusion coating and chromium diffusion coating in the termpature range up to 850°C. They concluded that the DBTT (ductile brittle transition temperature) of an LDC-2 coating on IN-738 LC is dependent on the coating layer ($PtAl_2$ + NiAl) interactions more than the effect of different base materials. According to Lowrie (84) the DBTT $\simeq$ 0.6 - 0.7 T_m(K) so that for $PtAl_2$ DBTT ~730°C ...900°C and for NiAl DBTT ~ 870°C ... 1070°C. The results of the investigation showed that this empirical relation is valid. In all these studies α phases appears to be mostly not detrimental by exhausting the remaining alloy in chromium as these phases dissolve again when the level of Cr near the surface drops, but they can be very brittle even at high temperatures and lead to cracks. It should

nevertheless, be mentioned that sigma phases of different compositions vary widely in their higher temperature properties.

4.7. Oxidation and Scale adherence of Platinum-aluminide coatings

The results of the isothermal oxidation in oxygen obtained in this study (weight gain vs time curves described in Section 3.9) of the platinum-aluminide coatings showed that at temperatures between 800°C - 1000°C platinum-aluminide coatings have excellent oxidation resistance and remain protective throughout the oxidsation runs. Cyclic oxidation experiments showed a remarkable improvement in oxide adherence over the simple aluminide coatings. Table 29 shows a comparison of the rates of oxidation at different temperatures for the different aluminide structures.

One method which is commonly used to improve the oxidation resistance of metals is to add an alloying element which is subsequently selectively oxidized to produce a protective oxide layer, such as α -Al_2O_3. However, the production of such protective oxide layer is not necessarily sufficient to confer good oxidation resistance, since components frequently have to undergo severe thermal cycling during which spalling of the oxide may occur. Repeated reoxidation and spalling may then cause depletion of the selectively oxidizing component to such an extent that less protective scales are formed. The probability of oxide layers spalling is often increased by the formation of voids at the metal/oxide interface, a phenomenon which may be associated with one of the following :- the injection of vacancies into the metal (85), unequal diffusion of the alloying elements (86) or stresses (87). Vacancy injection occurs in cation-defective

oxides when a metal atom transfers from the metal substrate to the oxide, in order to diffuse to the oxide/gas interface. Such a jump leaves a vacant site in the metal, if no alternative sink is available. Vacancies injected in this way may coalesce at the metal/oxide interface producing voids.

Interfacial voids have been observed during the high temperature oxidation of Fe-Cr alloys and a wide range of alumina-forming alloys (85, 86, 87, 88). In the case of Fe-Cr alloys, the vacancies are believed to occur as a result of oxide growth by outward diffusion of cations. However, Al_2O_3 is thought to grow by the inward diffusion of oxygen along the grain boundaries (89) and if so it cannot act as a vacancy injector. In view of this, other mechanisms, including Kirkendall effect (86) is a further possibility for the origin of vacancy defects. Since Al is preferentially oxidized for all compositions, Al must be diffusing towards the oxide/metal interface and Ni must be diffusing away from the interface, thus producing a vacancy flux to compensate for different diffusion rates of Ni and Al. However, it is by no means certain that Kirkendall voids have to be produced in this way (Hutchings et al (90)). The work of Hutchings et al (90) together with that of Fraser (91) has conclusively shown that vacancies are introduced during the oxidation of NiAl. These vacancies inject into NiAl during surface oxidation and lead to the formation of voids at the metal/oxide interface, these voids being responsible for spalling of the oxide layer. Another mechanism proposed to explain the occurrence of voids at metal alumina interfaces is the production of stresses by the growing oxide. In this study spalling of the α-Al_2O_3 formed on simple aluminide coatings has

been observed during cyclic oxidation experiments even after short time oxidation. At present none of the proposed mechanisms can be considered to be generally valid and much remains to be learned about the nature of the oxide-substrate interface. However, the results obtained during the oxidation study on NiCrAl alloys indicate that spalling of Al_2O_3 scales occurs because of the effect produced by thermally induced stresses (92).

It can be seen also that α -Al_2O_3 scale formed on platinum-aluminde coatings is highly convoluted (figure 42) and there are whisker-like protrusions from the surface of the oxide. Protrusions of this type have been observed previously (93) on α -Al_2O_3 and have been explained in terms of dislocation pipe mechanism (94). Although the mechanism by which platinum improves the adhesion of α -Al_2O_3 on alloys has not been determined, mechanical keying of oxides to alloys appears to be an effective means of improving the adhesion of Al_2O_3 on alloys (39). Another possible effect of the platinum appears to be it either influences the stress relief mechanism at temperature via an enhanced diffusional creep process or enhanced grain boundary sliding, or alternatively, that it reduces oxidation growth stress generation. Finally, the improved adhesion, slow growth rate and stability of the oxide may arise by a mechanism similar to that proposed to explain the effect of Yttrium (95) on the alloys behaviour in cyclic oxidation conditions (i.e. that Yt prevents the lateral growth of the oxide which gives rise to the convoluted scale morphology). Certainly, the configuration of the oxide is quite different from that observed for the simple aluminized coating system (figure 42). Moreover, in the present work, a number of oxide intrusions

at the scale-alloy interface has been observed, when oxidising a platinum-aluminide coating. Both these factors assist in maintaining scale-alloy adhesion.

4.8. Coating degradation

Once the supply of aluminium that exists at the surface during aluminising is removed, all futher heat treatment tends to degrade the platinum-aluminide layer either by interdiffusion of aluminium and elements from the base alloy or by removal of aluminium at the surface by oxidation and corrosion. The mechanism by which a simple aluminide coating degrades during oxidation or corrosion has been reviewed by Goward (96) & Llewelyn (97), where it has been found that under realistic dynamic-cyclic oxidation conditions, by far the greatest loss of aluminium is by the oxide spalling process with only a relatively small amount being lost to the substrate during oxidation (in the temperature range 850 - 1000^{o}C).

The effects of withdrawal of nickel from the substrate are manifested by the presence of a layer of significant enrichment of substrate alloying elements, particularly chromium. molybdenum and tungsten, in the substrate underlying the coating proper (sigma phase). The zone would be expected to increase in thickness with total coating thickness because of the corresponding increase in nickel denudation.

No mechanism has been proposed for the degradation of platinum-aluminide coating, but one can assume that the only mechanism for aluminium loss would be through interdiffusion since the oxide formed is quite stable and does not spall even after long time oxidation. Evidence of γ' $(Ni,Pt)_3Al$ type phase (as determined

by XRD, Table 30)), in the oxidised and in some heat-treated specimens at the grain boundaries of β(Ni,Pt)Al matrix has been observed (figure 43). The mechanism of nucleation and growth of the γ' phase in the β phase during degradation is obscure. However, it has been suggested (52) that the nucleation of the γ' phase in a highly alloyed coating occurs preferentially in those regions rich in alloying elements. Such regions can be the refractory metal-rich precipitates at grain boundaries in the outer coating region.

The result of the degradation of the coating is a reversal of the original coating process with the progressive formation of phases lower in aluminium that the β phase. Figure 43 illustrates γ' progression with time.

Corti et al (22) in their study on the platinum-enriched superalloys showed that platinum alloying additions increase the lattice parameter of γ' phase in Ni-Cr alloys, thus improving creep properties at higher temperatures which they attributed to both the improved temperature stability imparted to γ' by platinum and the improved solid strengthening of γ matrix to which platinum also partitions. In this study a slight increase in lattice parameter of γ' has been observed (Table 30).

CONCLUSIONS

The aluminisation of platinum-coated IN-738 produced coatings whose morphology and chemistry are highly dependent upon the thickness of the platinum layer, pack activity and the temperature and time of aluminising.

In all cases platinum is found to remain most concentrated at the surface of the coating. Three main types of platinum-aluminide coating can be distinguished. One, usually obtained using a relatively thick (>10 μm) Pt layer is characterised by an outer layer of Pt_2Al_3 above other narrow layers. The Pt concentration decreases towards zero as the diffusion zone is approached. The second type, usually formed with a thin (5 μm)Pt layer is characterised by a marked interaction with the substrate. An outer layer of $PtAl_2$ is followed by a layer of NiAl containing fine precipitates of a chromium rich phase. Beneath this, high concentrations of chromium and other refractory elements are formed similar to those produced by aluminizing IN-738 without the presence of platinum. The third type, characterised by an outer ($PtAl_2$ + NiAl) duplex structure is usually obtained by a post-platinising heat treatment prior to aluminizing.

Further heat treatment of these types of coating for up to 1200 hours at 1000°C has shown the development of different microstructure leading to a (Pt,Ni)Al or (Ni,Pt)Al outer layer and widmanstatten α phase plates extending into the substrate.

Due to the kinetics of the aluminizing process, only the intermetallics $PtAl_2$, Pt_2Al_3 and PtAl are generally found in aluminizing structures.

This study has demonstrated that the deposition of a platinum layer onto IN-738 prior to aluminization leads to the reduction, or even elimination of refractory metal elements in the outer region of the coating. However, a relatively high level of chromium throughout the platinum aluminide structure has been found ($\sim$ 6 wt.%) after long term heat treatment. A similar behaviour is also apparent for cobalt. The finger like regions found between the outer coating and the substrate contain high Cr and refractory metal concentration similar to those found for non-Pt-coated IN-738.

The phase constitution of as-formed and subsequently heat treated coatings on Pt-coated IN-738 can be represented by diffusion paths on pseudo-ternary diagrams. The application of these diagrams is limited by the complexity of the phases that formed, i.e. the number of elements they contain and also the number of phases which co-exist in the same region of coating.

The presence of the noble metal in the coating seems to enhance the oxidation resistance (particularly at $1000^{o}C$) in oxygen atmosphere. The reason for this improvement in the oxidation behaviour may be due to the improved adherence of Al_2O_3, scale, but this could be only one cause for this improved performance of these coatings. The exact mechanism by which platinum improves the adhesion of Al_2O_3 scale on coatings has not been determined, however, oxide protrusions extending into the coating have been observed in specimens, having a $PtAl_2$ surface, oxidised at $1000^{o}C$ in oxygen for more than 400 hours. Therefore, mechanical keying of oxides could be behind the improved adhesion of Al_2O_3 scale on coatings.

REFERENCES

1. C. SIMS, High temperature alloys for gas turbines, edited by D. Coutsouradis, P. Felix, H. Fishmeister, L. Habraken, Y. Lindblom and M.O. Speidel, Applied Science Publishers, 1978.

2. R.R. SIVAKUMAR and L.L. SEIGLE, Met. Trans. 7 1073 (1976)

3. M.R. JACKSON and J.R. RAIRDEN, NBS, Sp-496, P. 423 (Jan. 1977).

4. M.P. JANSSEN and G.D. RIECK., Trans. Met. Soc. AIME, 239, 1372 (1967).

5. R.T. DeHOFF, K.J. ANUSAVICE and C.C. WAN, Met. Trans. 5, P. 113 (1974).

6. W. GOWARD, Proceedings of the Symposium on Properties of High Temperature Alloys, Edited by Z.A. Foroulis and F.S. Pettit, (1976).

7. G. LEHNERT and H. MEINHARDT, J. Electrodeposition and Surface Treatment 1 (1972/1973) p. 189.

8. R. HUCH and W. KLEMM, Z. Anorg. Allegem CHem. Vol. 329, (1964) .

9. A.S. DARLING, G.C. SELMAN and R. RUSHFORTH, Plat.Met.Rev. 14, No. 4, p. 124 (1970).

10. F. FERRO and R. CAPELLI, Atti. Accad. Na.2. Lincei-Rend.cl Sci. fis. Met. e nature 45 Nos. 1-2 p. 54 (1968).

11. A. MAGNELI, L. EDSHAMMAR and T. DAGERHAMN, Final Technical Report No. 1 under contract DA-91-591-EnC-2734 (AD426927) p. 49, (1963).

12. P.M. ARZHANYI and R.T. SEKHANSKAYA, Zashchitta metallov. Vol. 7 No. 2,pp. 212-214, March-April, 1971.

13. D. CHATTERJI, R.C. DEVRIES and J.F. FLIESCHER, Jrnl. Less Common Metals, 42, pp. 187-198 (1975).

14. J.J. COMER, Acta Cryst. 17, pp. 444-445 (1964).

15. T. CHATTOPADHYAY and K. SCHUBERT, Jrnl. Less Common Metals, 41, pp. 19-32 (1975).

16. M.R. JACKSON and J.R. RAIRDEN, Met. Trans. A. 8A, p. 1697 (1977).

17. G. LEHNERT and H.W. MEINHARDT., Electrodepos surface Treat. 1 p. 71, 1972/1973.

18. W. GOWARD, Battle Columbus Labs. Ohio Metals & Ceramics Info., Proc. of the 1976 Tri-Service Conference on Corrosion (Dec. 1977).

19. R. SEELIG and R. STUEBER, High Temp-High press, 10, pp. 207-213 (1978).

20. T. E. STRANGMAN, E.J. FELTEN and ULLOW, American Ceramic Soc. 78th Annual Meeting, Cincinnati, Ohio May 2-5 (1976).

21. R.J. WING and I.R. McGILL, Platinum Metals Rev. 25(3) Page 94,1981.

22. C.W. CORTI, D.R. COUPLAND and G.L. SELMAN, Platinum Metals Review 24 (1), P.2. 1980.

23. P.G. CAPPELLI, High Temperature Alloys for Gas Turbines, Ed. by D. Coutsouradis, P. Felix, H. Fishmeister, L. Habraken, Y. Lindblom, M.O. Speidel, Apolied Science Publishers (1978).

24. S.R. LEVINE and R.M. CAVE, J. Electrochemical Soc. 121(2) Aug. 1974 pp. 1051-1069.

25. G.H. MARIJNISSEN, H.V. FAMEREN and J.A. KOLSTERMANN, High Temperature alloys for gas turbines, Ed. by D. Coutsouradis, F. Felix and H. Fishmeister, L. Habraken, Y. Lindblom and M.O. Speidel, Applied Science Publishers 1978.

26. R.R. SIVAKUMAR, J. Met. Sci, 17, p. 1843 (1982).

27. R. PICHOIR, Materials and Coatings to resist High Temperature Corrosion Ed. by D.R. Holmes and A. Rahmel, Applied Science Publishers.

28. B. GUPTA, A. SARKHEL, SHANKARS and L.L. SEIGLE, Sixth Semi-Annual Report 1/6/75 to 3/11/75, NASA Research Grant NGR-33-015-160 NASA Sci. and Tech. Inf. P.O. Box 33, College Pk. md.

29. G.F. HANCOCK, Phys. Status Solidi, 7(A) 535 (1971).

30. M.P. JANSSEN, Met. Trans. 4, 1623 (1973).

31. R.A. SHALIN and A. MARTIN, J. Met. 8, 567 (1956).

32. L.S. CASTLEMAN and L.L. SEIGLE, Trans. Met. Soc. AIME 212, 589, (1958).

33. A.J. BRADLEY and A. TAYLOR, Proc. Roy. Soc. 159, 56 (1937).

34. E.W. ELCOCK and C.W. McCOMBIE, Phys. Review, 109, 605, (1958).

35. E.W. ELCOCK, Proc. Phys. Soc. 73, 250, (1959).

36. P.A. FLYNN and G.M. McMANUS, Phys. Rev. 124, 54 (1961).

37. C.S. GIGGINS and F.S. PETTIT, Oxide Scale Adherence Mechanisms and the Effect of Yttrium, Contract F33615, 72-c.1702, 1975, Wright Patterson Airforce Base, Ohio Aerospace Research Lab.

38. K. BUNGART, Protective Diffusion layer on Nickel and/or Cobalt Base Alloys - U.S. Patent 3,677,789 (1972).

39. E.J. FELTEN and F.S. PETTIT, Oxide. Met. 10, No. 3 pp. 189-223 (1976).

40. E.J. FELTEN, Oxide Met. 10 No. 1. pp. 23-28 (1976).

41. J. FOUNTAIN, F.A. GOLIGHTLY, F.H. STOTT and G.C. WOOD, Oxide Met. 10, No. 5 pp. 341-345 (1976).

42. G.C. WOOD, J.G. FOUNTAIN and F.H. STOTT, Oxid. Met. 14 No. 1,p. 47, (1980).

43. J.E. RESTALL, Metallurgia, p. 676, 46 (1979).

44. GAS TURBINE International, July/August, 1977 p. 32.

45. J.CELLAND, Proc. 3rd NAVSEC Conference (Bath) 1976, Session 3, paper 5.

46. G. KATZ and R. WEISS, 3rd NAVSEC Conference (Bath) 1976, Session 1, Paper 2.

47. L. APRIGLIANO and G. WALKER, Proc. 3rd NAVSEC Conference (Bath) 1976, Session 3, Paper 4.

48. A.R. STETSON and V.S. MOORE, Proc. of the 1974 Gas Turbine Materials in Marine Environment Conference, Castine, MCIC Report, 75-27, 1975.

49. J.F. NORTON, Platinum Metals Review 4, 21, p. 122 (1977).

50. T. FLATLEY, Ph.D. Thesis, University of Sheffield (1969).

51. G.V. BEETON. Jrnl. Sci. Instruments 2, 252, (1969).

52. G.W. GOWARD, D.H. BOONE and C.S. GIGGINS, Trans ASM 60 P. 228 (1967).

53. S. RIDEOUT, W.D. MANLEY, E.L. KAMEN, B.S. LEMENT and P.A. BECK, Trans. TSM-AIME, 191 p. 872 (1951).

54. H. YAKOWITZ, R.C. MYKLEBUST and K.F.J. HEINRICH, NBS Technical Note 796 (1973).

55. K.F.J. HEINRICH, H. YAKOWITZ and D. VIETH, Proc. 7th Nat. Conf. on EPMA (1972).

56. S.J.B. REED, Brit. Jrnl of Appl. Phys. 16, 913 (1965).

57. J. BOWKER, Ph.D. Thesis Sheffield University (1978).

58. D.E. COATES and J.S. KIRKALDY, Jrnl. Crystal Growth 3, 4, 549 (1968).

59. J.S. KIRKALDY, Can. Jrnl. Phys. 36, 917 (1958).

60. J.S. KIRKALDY and F.G. FEDAK, Trans. Met. Soc. AIME, 224, 490, (1962).

61. J.W. RUTTER and B. CHALMERS, Can. Jrnl. Phys. 31, 15 (1953).

62. W.W. MULLINS and R.F.J. SEKERKA, J. Appl. Phys. 35, 444 (1964).

63. G.W. GOWARD and D.H. BOONE, Oxid. of Metals, 3, 475, (1971).

64. C.W. HAWORTH 'Environmental degradation of High Temperature Materials' Inst. of Metallurgists Conf. Proceedings Series 3, 1, 6/23, (1980).

65. J.R. RAIRDEN and M.R. JACKSON, Jrnl. Vac. Sci. Techn. 17 (1) Jan-Feb, P. 77-80 (1980).

66. A. TAYLOR, J. Inst. Met. 81 251 (1952).

67. J. SCHRAMM, Z. Metallk. 33, 403, (1941).

68. K.R. PETERS, D.P. WHITTLE and J. STRINGER. Corros. Sci. 16, pp. 791-804 (1976).

69. J.W. SCULTZ and W.R. HULSIZER, Proc. of the 1975 Gas Turbine Materials in Marine Environment Conference, MCIC, Columbus, Ohio, 1974, pp. 735-57.

70. H. MORROW, D.L. SPONSELLER and E. KALNS, Met. Trans. 5 pp. 673-83 (1974).

71. A.K. SARKEL and L. SEIGLE, Met. Trans. 7A, 1899 (1976).

72. G.F. HANCOCK and B.R. McDONNEL, Phys. Status solidi, 4(A), 143, (1971).

73. O. HAUFFE, Oxidation of Metals and Alloys, Plenum Press, New York (1965), p. 64.

74. H.J. BEATTIE and W.C. HAGEL, Trans. Met. Soc. AIME, 233, No. 2 pp. 277-287 (1965).

75. W.J. BOESCH and J.S. SLANEY, Met. Progr. 86, No. 7, pp. 109-111 (1964).

76. P.A. BECK, Electronic Structure and Alloy Chemistry of the Transition Elements,Interscience (New York) 1963.

77. C.R. WOODYATT, H.J. BEATTIE and C.T. SIMS, Trans. Met. Soc. AIME 236 No. 4 pp. 519-527 (1966).

78. M.J. FLEETWOOD, J. Inst. Metals, 98 pp. 1-7 (1970).

79. T.K. REDDEN, Trans. Met. Soc. AIME, 242, pp. 1695-1702, (1968).

80. G.W. GOWARD and D.H. BOONE, Oxid. Met. 3, No. 5, (1971).

81. C.H. WELLS and C.P. SULLIVAN, ASM Trans. 61, pp. 149-155, (1968).

82. A. Strang, Proc. Conf. NL, Behaviour of High Temp. Alloys in Aggressive Environments, Cttee of European Communities, p. 595.

83. L. BRANDIS, G. LEHNERT and W. SCHMIDT, Thyssen Edelst. Tech. Ber. 7 Band, 1981, Heft 1.

84. R. LOWRIE, J. Metals 4, pp. 1093, (1952).

85. R.E. SMALLMAN and P.S. DOBSON 'Vacancies, 76' 193, 1977, London, Metals Society.

86. A. KUMAR, A .NASRALLAH and D.L. DOUGLASS, Oxid. Met. 8, 227, (1974).

87. J. HARRIS, Acta Metall., 26, P. 1033, (1978).

88. J.K. TIEN and F.S. PETTIT, Metall. Trans 3, 1587 (1972).

89. C.S. GIGGINS and F.S. PETTIT,'Oxide Scale Adherence Mechanisms' contract F33615, 71-C-1702, 1975, Wright Patterson Air Force Base, Ohio, Aerospace Research Laboratories.

90. R. HUTCHINGS and MH. LORETTO, Met. Sci. 12, 503, 1978.

91. H.L. FRASER, M.H. LORETTO, R.E. SMALLMAN and P.J. WASILEWSKI, Phil. Mag. 28, 639 (1973).

92. F.S. PETTIT, Trans. AIME 239, p. 1296, (1967).

93. I.M. ALLAM, H.C. AKUZUE and D.P. WHITTLE, Oxid. Met. 14 No. 6, p. 517 (1980).

94. H. FISHMEISTER, Mem. Sci. Rev. Metall 62, 211 (1965).

95. F.A. GOLIGHTLY, F.H. STOTT and G.C. WOOD, Oxid. Met. 10 163, (1976).

96. G.W. GOWARD, J. Met. 22,31,(1970).

97. G. LLEWELYN, ASTM, STP, 421, p. 3 (1967).

98. A. HICKEL and R.W. HECKEL, Met. Trans. A. 6A, 431 March, (1975).

ACKNOWLEDGEMENTS

I would like to express my sincere thanks to my Supervisors, Dr. C.W. Haworth and Professor B.B. Argent for their guidance and advice throughout this work.

I am indebted to the University of Technology, Baghdad, IRAQ for financial assistance.

I am also grateful to members of the technical staff, in particular, Mr. J. Horsefield, for his help in the use of the electron probe microanalyser.

Finally I would like to thank Mrs. Joan Kaine for her prompt and efficient typing of this thesis.

A P P E N D I X 1

A correction program for electron probe micro-analysis

(Sheffield FRAME 3 - C.W. Haworth and J.W. Horsefield)

The programe is an adapted version of the N.B.S. Program Frame (Yakowitz et al (54)). The mass fraction C of the element being measured is computed from the X-ray intensity ratio K according to the expression :-

$$C = K\,(ZAF)$$

K can be input as a ratio relative to a pure element or relative to a compound standard (for which the chemical composition must be specified). The program normally iterates from K → C can be run to calculate K values given C values.

Atomic number correction

$$Z = \frac{R_{spec}}{R_{std}} \times \frac{S_{std}}{S_{spec}}$$

Values of R (Back scatter coefficient) are derived for over-voltage $U = E_o/E_c$ corresponding to the radiation being measured, for each element measured in the specimen. The equation used is :-

$$R = R_1 - R_2 \operatorname{Ln} (R_3 \bar{Z} + 25)$$

where $R_1 = 8.73 \times (10^{-3}U^3 - 0.1669U^2 + 0.9662U - 0.4523)$

$R_2 = 2.703 \times (10^{-3}U^3 - 5.182) \times (10^{-2}U^2 + 0.302U - 0.1836)$

$R_3 = (0.887U^3 - 3.44U^2 + 9.33U - 6.43)\ /U^3$

$U = E_o/E_c$ $\bar{Z} = \Sigma_i C_i Z_i$, if $U > 10$ then U is set = 10. This expression for R is simpler than 5th order approximations used by Duncumb et al.

The value $R_{spec} = \Sigma_i C_i R_i$

The stopping power S is calculated using Bethe's formula :

$$S = \frac{Z}{A} - \frac{1}{E} \text{Ln} (1166\ \bar{E}/J)$$

where an average value $\bar{E} = (E_o + E_c)/2$, related to the element being measured.

This procedure is adequate provided $U > 1.5$

The ionisation potential is obtained from the approximation

$$J = 9.76Z + 58.5\ Z^{-0.19}$$

The atomic weights required are stored in the program.

Absorption correction (A)

This was the factor proposed by Heinrich et al (55)

$$\frac{1}{f} = 1 + 3 \times 10^{-6} (E_o^{1.65} - E_c^{1.65}) X + 4.5 \times 10^{-13} (E_o^{1.65} - E_c^{1.65}) X^2$$

where $X = \mu \text{cosec}\ \Psi$, Ψ is the X-ray emergence angle, and the absorption correction $A = f_{std}/f_{spec}$. This procedure is probably not as good as Philibert's Equation although neither should be used for small values of (X). A warning is printed

if $f_{std} < 0.75$ and the value of $f(X)_{spec.}$ is printed out. The mass absorption coefficients are calculated according to the equation $\mu = C \lambda^{n}$ where least squares fits have been used for the log of C and the exponent of n. Values of λ (wavelength of radiation used) and the various values of E_c for each absorber are calculated by means of bits based on Moseley's Law and different values of C, n are used depending on which branch of the absorption curve is applicable. This procedure results in a smoothing of the absorption data and agreement to within a few percent is generally found, if the measured radiation falls within 100 ev, - 30 ev of an absorption edge then the absorption coefficient data is uncertain and another line should be used.

Fluorescence correction (F)

The factor F uses the following provision to decide whether a fluoresence correction is required. If E_ℓ is the energy of the line possibly causing fluorescence, then if $o < E_\ell - E_k \leq 5$ fluorescence of the K shell is assumed and if $0 < E_\ell - E_L \leq 3.5$ then fluorescence of L radiation is taken to occur.
If fluorescent radiation occurs the program prints a message to this effect, calculates all the mass absorption coefficients required, takes

$\gamma_k = 0.88$ or $\gamma_L = 0.75$, computes fluorescent yields using an empirical fit and then computes the fluorescent correction using the method of Reed (65).

The iteration procedure used is a hyperbolic approximation :-

$$\frac{1 - K_A}{K_A} = \frac{d\,(1-(A))}{C_A}$$

where a is a constant for the measurement of element A. The calculation is terminated after three iterations since this has proved to be adequate.

	Ni	C	Co	Cr	Mo	W	Ta	Nb	Al	Ti	B	Zr
Wt%	61.42	0.17	8.5	16.0	1.75	2.6	1.75	0.9	3.4	3.4	0.01	0.1
At%	59.33	0.79	8.17	17.47	1.02	0.79	0.57	0.57	7.15	4.03	0.06	0.06

Table 1 composition of IN-738 superalloy.

Phase	Colour	Type	Å	d	M.P.°C
Al	Silver	Cubic	a = 4.049	2.697	660
$PtAl_4$	White	χ-brass	a = 19.23	5.7	806 peri
$(Al_{21}Pt_5)$?		?			1121 peri
$PtAl_3$	Ivory	?			
$PtAl_2$	Golden yellow	Fluorite	a = 5.910	8.016	1406 peri
Pt_2Al_3	Blue-violet	Ni_2Al_3	a = 4.22	9.878	1521
		Hexagonal	c = 5.17		
PtAl	Pink	Fe Si	a = 4.865	12.82	1554
Pt_3Al_2	Whitish	?	?	—	1397 peri
Pt_5Al_3	Silver	Rh_5Ge_3	a = 5.413	15.36	1465
			b = 10.73		
			c = 3.95		
Pt_2Al (h)	—	Ni_2Si	a = 7.898		
			b = 5.401		
			c = 4.055		
Pt_2Al (r)		Pt_2Ga (r)	a = 16.306		
			b = 3.919		
			c = 5.433		
Pt_3Al	White	Cubic $AuCu_3$	a = 3.87	17.47	1556
$Pt_{13}Al_3$	White	Tetragonal super	a = 7.698	?	—
(80 At% Pt)		Structure	c = 7.844		
Pt	Silver	Cubic	a = 3.924	21.45	1778

Table 2 phases observed in the Pt-Al system. (after HUCH and KLEMM (8), and CHATTOPADHYAY and SCHUBERT (15)).

Ni_2Al_3

Ref.	D $cm^2 sec^{-1}$	Temp. C^o	Comp. (Ni at%)		method of Determinati
Janssen &	$7.1x10^{-9}$	610	36.3	40.8	EPMA
Rieck(4)	10^{-7}	1000 extrapolated			Boltzman - matano
Janssen & Rieck(4)	$6.5x10^{-9}$	610	36.3	40.8	EPMA Wagner-Eq.
Castleman & Seigle (32)	$5x10^{-10}$	610	36.3	40.8	Wagner Eq.
NiAl					
Janssen (30)	$6x10^{-10}$	1000	62		EPMA
	$2.7x10^{-9}$	1000	62		Boltzman.
	$11.0x10^{-9}$	1200	62		
Hancook & Mcdonnel (72)	$1.0x10^{-12}$	1000	49		D_{Ni}*

Table 3 diffusion data for Ni_2Al_3 and NiAl.

	Spectrometer crystal	Bragg angle	Counter	Peak
Pt	mica	$35^{o}14$	flow	M
Ni	LiF	$48^{o}45$	sealed	K
Al	mica	$49^{o}25$	flow	K
Cr	LiF	$69^{o}22$	sealed	K
Co	LiF	$52^{o}55$	sealed	K
W	mica	$40^{o}56$	flow	M
Mo	mica	$31^{o}00$	flow	L

Table 4 optimum EPMA operating conditions. P.H.A was set with no window, discriminator threshold of 0.5V, amplifier set at a gain of 100, time constant between 1 and 3.3 sec. and the voltage on the counter adjusted ($\sim$ 1780V for sealed counter, $\sim$1340V for flow counter) so as to give a pulse height of 2V.

	Ni	Al	Cr	Co	W	Mo	Ti	Nb	Fe
EPMA with FRAME 3 ZAF correction program	60.7	4.2	17.4	8.5	2.4	0.8	3.8	-	-
Point analysis using EDS on the SEM, link system ZAF4FLS DOS VERSION	59.9	3.4	17.7	8.3	3.7	1.8	2.4	0.8	0.8
Chemical analysis (as given by the alloy supplier)	61.4	3.4	16.0	8.5	2.6	1.75	3.4	0.9	-

Table 5 comparison between EPMA, point analysis on the SEM and chemical analysis in wt% for the bulk IN-738, it is clear that high values for Al and Ti had been obtained using EPMA , this may be due to the absorption correction used in FRAME 3 correction program, while the high values for W and Mo obtained using EDS on the SEM could be explained on the basis that their lines are interfering with other lines (especially when Pt is present).The results of EPMA and point analysis were in good agreement,however we think that EPMA results are more accurate.

		Al	Ni	Cr	Co	W	Ti	Mo	Nb	Fe	T%
Example of blue etched ppts. (Al_3Ti) type.	Wt%	40.8	3.5	5.2	0.0	11.9	5.9	9.1	8.1	0.0	84.6
	At%	74.06	2.92	4.9	0.0	3.17	6.03	4.65	4.27	0.0	
Matrix	Wt%	30.6	53.7	1.6	4.18	0.0	0.0	0.0	0.0	0.0	90.1
	At%	52.74	42.5	1.43	3.3	0.0	0.0	0.0	0.0	0.0	
Example of brown etched ppts. Al_9Cr_4/ Al_8Cr_5 type.	Wt%	32.3	7.1	36.8	1.5	5.3	1.3	1.9	0.0	1.1	87.5
	At%	55.76	5.63	32.97	1.19	1.34	1.26	0.92	0.0	0.92	
Matrix	Wt%	29.3	46.4	4.4	6.19	0.0	1.08	0.0	0.0	0.7	88.2
	At%	51.68	37.6	4.03	5.00	0.0	1.07	0.0	0.0	0.6	
Lamella finger-like phase	Wt%	3.7	34.3	30.9	8.5	7.8	3.8	5.1	0.0	2.0	96.1
	At%	8.21	34.97	35.5	8.6	2.54	4.75	3.18	0.0	2.14	
Matrix	Wt%	9.5	49.7	16.9	7.5	3.6	7.05	1.9	0.9	1.3	98.3
	At%	18.8	45.26	17.38	6.8	1.05	7.87	1.06	0.52	1.24	

Table 6 Composition of precipitates and finger-like phase found in simple aluminide coating with the matrices associated with them.

		Pt	Al	Ni	Cr	Co	W	Ti	Mo	Nb	Fe	T%
σ phase in outer coating	Wt%	--	0.6	15.5	40.0	12.3	18.0	1.8	8.5	1.3	1.6	100
	At%	--	1.44	17.1	50.0	13.5	6.3	2.4	5.7	0.9	1.8	--
Matrix	Wt%	--	17.7	65.0	5.8	6.9	0.93	2.6	0.0	0.0	0.96	100
	At%	--	31.7	53.5	5.4	5.6	0.24	2.6	0.0	0.0	0.83	--
Acicular σ phase	Wt%	2.44	0.3	5.87	62.3	2.04	9.33	0.15	4.99	0.0	0.41	87.8
	At%	0.85	0.76	6.8	81.5	2.36	3.4	0.21	3.5	0.0	0.5	--
Matrix	Wt%	41.53	10.5	30.1	6.2	3.4	3.8	1.27	0.0	2.7	0.5	100
	At%	15.46	28.26	37.2	8.66	4.19	1.5	1.93	0.0	2.1	0.65	--

Table 7 Composition of two different sigma phases found in the outer and inner coatings after long time heat-treatment.

d spacing, Å	Relative intensity	∝	NiAl	Ni_3Al	TiC
2.53	M			110	
2.48	W				111
2.38	W	311			
2.19	M				200
2.15	MS	410			
2.079	S			111	
2.04	S	202	110		
1.98	M	212			
1.945	S	411			
1.90	M	331			
1.80	MS			200	
1.78	S	312			
1.67	VW		111		B220
1.55	VW				
1.43	VW		200		
1.32	VW	541			
1.26	W	532		220	
1.18	W		211		
1.08	M			311	

Table 8 diffusion zone phase identification of heat treated plain aluminized coating at 1000C for 640hrs. sigma phase identification after Beattie and Ver Snyder (1957).

d spacing, Å	Relative intensity	$PtAl_2$ (obs.)	NiAl	d $PtAl_2$ (calc.)
3.4	VS	111		3.41
2.95	S	200		2.95
2.09	VS	220		2.09
2.03	W		110	
1.77	M	311		1.78
1.70	W	222		1.70
1.47	MW	400		1.48
1.44	VW		200	
1.35	MW	331		1.36 D
1.33	W	420		1.32 D
1.20	M	422		1.21 D

Table 9 X-ray diffraction results for the as-coated coating treatment A (calculated d values were compiled given the structure of $PtAl_2$ is CaF_2 type, having lattice parameter a=5.91 , Schunk 1969).

d spacing, Å	Relative intensity	Pt_2Al_3 (obs.)	d Pt_2Al_3 (calc.)
5.22	S	001	5.16
3.63	S	100	3.64
3.4	M	101	3.43
2.95	VS	102	2.98
2.59	M	222	2.59
2.11	VS	110	2.11
1.94	M	111	1.95
1.81	W	200	1.83
1.72	M	003, 201	1.72
1.63	W	112	1.63
1.55	M	103	1.56
1.49	M	202	1.49
1.37	W	210	1.38
1.33	M	113	1.33

Table 10 X-ray diffraction results for the as-coated coating treatment B (calculated d values were compiled given that the structure of Pt_2Al_3 is similar to Ni_2Al_3 having lattice parameters; a=4.22 , c=5.17 , Schunk 1969).

layer	thickness (µm)	composition At%							
		Pt	Al	Ni	Cr	Co	W	Ti	Mo
Pt_2Al_3	30	44.96	55.04	-	-	-	-	-	-
$(Pt,Ni)_2Al_3$	1	31.75	52.61	14.95	-	0.69	-	-	-
(Pt,Ni)Al	½	44.1	44.2	11.1	-	0.52	-	-	-
(Pt,Ni)Al	2	31.3	37.38	22.65	6.35	2.33	-	-	-

Table 11 average composition in At% resulted from point analysis using EDS on the SEM for the different layers found in the outer coating region of the as-coaed treatment B (see figure14 for optical micrograph).

Phase		Composition				
		Pt	Al	Ni	Cr	Co
$PtAl_2$	Wt%	64.8	18.0	12.0	1.5	1.3
	At%	26.47	53.1	16.3	2.3	1.7
(Ni,Pt)Al	Wt%	30.0	23.6	32.6	2.37	3.15
	At%	9.18	52.3	33.1	2.6	3.19

Table 12 Results of point analysis using EDS on the SEM of the duplex layer formed in the inner coating region of the as-coated treatment C.

d spacing, A°	Relative intensity	$PtAl_2$	NiAl	Al_2O_3
4.90	VW			
3.50	W			012
3.39	VS	111		
2.93	MS	200		
2.85	W		100	
2.54	VW			104
2.37	VW			110
2.32	VW	--	--	--
2.26	VW	--	--	--
2.07	S	220		
2.02	MS		110	
1.75	MS	311		
1.7	W	222	111	
1.45	W		200	200
1.35	MW	331		

Table 13 X-ray diffraction results for coating treatment E (duplex coating).

layer	thickness (Um)	composition At%							
		Pt	Al	Ni	Cr	Co	W	Ti	Mo
$(Pt,Ni)Al_2$	10	22.2	53.5	12.3	8.0	1.35	0.0	1.5	0.9
(Ni,Pt)Al	18	3.4	45.9	41.7	3.38	4.0	0.36	0.6	0.47
NiAl	12	0.18	47.7	45.1	2.47	4.11	0.2	0.23	0.0

table 14 Results of point analysis using EDS on the SEM of different layers formed after heat treating coating A for 5hrs at 1000 C (see fig.21).

---

layer	thickness (Um)	composition At%							
		Pt	Al	Ni	Cr	Co	W	Ti	Mo
(Pt,Ni)Al	10	26.5	34.7	23.8	9.79	3.3	0.0	0.3	1.4
(Ni,Pt)Al	20	2.24	44.03	44.1	4.1	4.32	0.24	0.58	0.36
NiAl	25	0.12	49.44	42.0	3.16	4.88	0.22	0.18	0.0

table 15 Results of point analysis using EDS on the SEM of different layers formed after heat treating coating A for 50hrs at 1000 C (see fig 21).

d spacing, Å	Relative intensity	NiAl	Al_2O_3	d_{NiAl} (calc.)
4.08	VW			
3.45	VW		012	
2.9	MW	100		2.87
2.54	W		104	
2.38	VW		110	
2.08	M		113	
2.05	VS	110		2.02
1.78	W			
1.74	VW		024	
1.67	W	111		1.655
1.6	W		116	
1.44	VW	200		1.434
1.40	VW		124	
1.37	VW		030	
1.28	VW	210		1.285
1.27	W		208	
1.18	W	211		1.17

Table 16 X-ray diffraction results for coating treatment A after 1200hrs of heat treatment at 1000C. d calculated after ASTM hand book.

layer	thickness (µm)	composition At%				
		Pt	Al	Ni	Cr	Co
Pt_2Al_3	20	44.2	54.9	0.88	—	—
(Pt,Ni)Al	10	49.08	45.89	5.02	—	—
(Pt,Ni)Al	15	31.54	38.8	24.5	3.15	2.01

Table 17 Results of point analysis using EDS on the SEM for the layers formed on coating B after 5hrs heat treatment at 1000C (see fig.23).

layer	thickness (µm)	composition At%							
		Pt	Al	Ni	Cr	Co	W	Ti	Mo
(Pt,Ni)Al	30	48.3	50.7	0.97	—	—	-	—	—
(Pt,Ni)Al	5	45.5	42.6	11.85	—	—	-	—	—
PtAl+NiAl	20	18.03	39.7	35.2	2.85	2.96	0.0	0.57	0.57

Table 18 Results of point analysis using EDS on the SEM for the layers formed on coating B after 50hrs heat treatment at 1000C (see fig.23).

d spacing, Å	Relative intensity	PtAl	NiAl	Al_2O_3	d_{PtAl} (calc.)
4.08	W				
3.45	W			012	
3.42	M	110			3.44
2.72	M	111			2.80
2.54	MW			104	
2.38	VW			110	
2.15	VS	210			2.17
2.08	S			113	
2.05	M		110		
1.91	M	211			1.98
1.74	VW			024	
1.7	W				
1.68	M		111		
1.6	VW			116	
1.45	VW	311	200		1.46
1.4	VW			124	
1.37	VW			030	
1.29	MW	321	210		1.30
1.19	VW		211		
1.15	MW	411			1.14

Table 19 X-ray diffraction results for coating treatment B after 120Ch of heat treatment at 1000C, d(calc.) values were compiled given that the structure of PtAl is FeSi type having lattice parameter of a=4.865 (HUGH et al( )).

layer	thickness (μm)	composition At%							
		Pt	Al	Ni	Cr	Co	W	Ti	Mo
$(Pt,Ni)_2Al_3$	20	37.7	52.6	8.35	1.19	-	-	-	-
(Ni,Pt)Al	10	1.5	43.1	46.0	2.56	5.8	-	-	-

Table 20 Results of point analysis using EDS on the SEM for the layers formed on coating C after 5hrs of heat treatment (see figure 25).

layer	thickness (μm)	composition At%							
		Pt	Al	Ni	Cr	Co	W	Ti	Mo
(Pt,Ni)Al	40	12.08	28.7	45.5	6.4	4.1	0.29	2.11	0.75

Table 21 Results of point analysis using EDS on the SEM for the layer formed in the outer coating region of coating treatment C after 55hrs of heat treatment (see figure 25).

d spacing, Å	Relative intensity	PtAl	NiAl	Al_2O_3
3.42	VW	110		012
2.90	VW		100	
2.14	M	210		
2.05	S		110	
1.91	W	211		
1.66	M		111	116
1.19	M		211	220

Table 22 X-ray diffraction results for coating treatment C after 1000hrs of heat treatment at 1000C.

layer	thickness (Um)	composition At%							
		Pt	Al	Ni	Cr	Co	W	Ti	Mo
Pt_2Al_3	30	41.13	56.19	2.68	-	-	-	-	-
(Pt,Ni)Al	5	27.5	39.9	28.2	2.48	1.14	0.24	-	-
(Ni,Pt)Al	20	8.67	44.3	41.98	1.46	2.9	0.13	0.19	-

Table 23 Results of point analysis using EDS on the SEM of the layers formed on coating D after 5hrs heat treatment (see fig.28).

---

layer	thickness (Um)	composition At%							
		Pt	Al	Ni	Cr	Co	W	Ti	Mo
(Pt,Ni)Al	5	41.7	47.9	10.09	-	0.27	-	-	-
(Pt,Ni)Al	40	20.29	32.1	38.7	3.64	3.48	0.21	0.99	-

Table 24 Results of point analysis using EDS on the SEM of the layers formed on coating D after 55hrs heat treatment (see fig.28).

d spacing, Å	Relative intensity	PtAl	NiAl	Al_2C_3
3.42	M	110		012
2.72	VW	111		
2.54	VW			104
2.14	S	210		
2.05	M		110	
1.99	MW	211		
1.96	MW			202
1.69	MW		111	
1.26	M	321	210	
1.19	VW	400		220
1.15	W	411	211	

Table 25 X-ray diffraction results for coating treatment D after 1000hrs of heat treatment at 1000C.

layer	thickness Um	composition At%							
		Pt	Al	Ni	Cr	Co	W	Ti	Mo
(Ni,Pt)Al	60	5.14	31.6	49.49	5.36	5.87	0.12	2.1	0.3

Table 26 average composition of the outer coating layer of the duplex structure coating E after 156hrs heat treatment as determined using point analysis EDS on the SEM.

layer	thickness Um	composition At%							
		Pt	Al	Ni	Cr	Co	W	Ti	Mo
(Ni,Pt)Al	110	5.39	25.99	54.75	5.62	5.95	0.1	1.95	0.2

Table 27 composition of the outer coating layer of the duplex structure coating E after 516hrs heat treatment as determined using point analysis EDS on the SEM, (see figure 31).

Coating treatment	As-Coated structure	H.T 5 h	H.T 50 h	H.T 1000-1200 h
A	$PtAl_2$	$PtAl_2$	PtAl	NiAl
	NiAl	NiAl	NiAl	α
			α	
B	Pt_2Al_3	Pt_2Al_3	PtAl	PtAl
	PtAl	PtAl	PtAl+NiAl	$\gamma' + \alpha$
			α	
C	$PtAl_2$	Pt_2Al_3	PtAl	NiAl+PtAl
	$PtAl_2$+NiAl	NiAl	PtAl+ α	α
D	Pt_2Al_3	Pt_2Al_3	PtAl	PtAl+NiAl
	$PtAl_2$	PtAl+NiAl	NiAl+ α	α
	$PtAl_2$+NiAl	NiAl		
E	$PtAl_2$+NiAl		NiAl*	NiAl** + γ'
	NiAl		NiAl+ α	NiAl+ α

Table 28 Structures developed on heat-treating different coating structures obtained in this study.

* H.T for 156 h.

** H.T for 516 h.

Surface	D $mg^2/cm^4.sec^{-1}$ 1000°C	900°C	800°C	Oxide
(Ni,Pt)Al	$1.22x10^{-7}$	$2.43x10^{-8}$	$1.15x10^{-8}$	Al_2O_3
(Pt,Ni)Al+(Ni,Pt)Al	$2.13x10^{-7}$	$1.73x10^{-7}$	$1.98x10^{-8}$	Al_2O_3
(Pt,Ni)Al	$2.89x10^{-7}$	$7.3x10^{-8}$	$5.2x10^{-8}$	Al_2O_3
Pure(NiAl)	$2.2x10^{-5}$	$5.2x10^{-7}$	---	Al_2O_3

Table 29 oxide growth rate constant (D) at different temperatures for the different Pt-Al and Ni-Al surfaces.

d spacing, Å	Relative intensity	NiAl	Ni_3Al	Al_2O_3
3.48	MW			012
2.89	M	100		
2.55	MW		110	104
2.37	W			
2.08	M		111	113
2.04	VS	110		
1.8	MW		200	
1.74	W			024
1.67	W	111		
1.60	W		210	116
1.44	MW	200		
1.40	W			124
1.37	W			030

Table 30 phase identification of coating treatment A after prolonged oxidation and heat treatment at 1000C,(see figure 43-C).

Phase	molar volume per atom	Pt-Al distance
Al	9.997	(2.864)
"$PtAl_4$"	10.286	—
$PtAl_3$	—	—
$PtAl_2$	10.142	2.561
Pt_2Al_3	9.545	2.57-2.99
PtAl	8.666	2.59-2.62
Pt_3Al_2	—	—
Pt_5Al_3	8.636	2.54-2.71
Pt_3Al	8.768	2.730
$Pt_{13}Al_3$	8.75	--
Pt	9.093	(2.774)

Table 31 molar volume per atom and Pt-Al distance in Å of different Pt-Al phases.

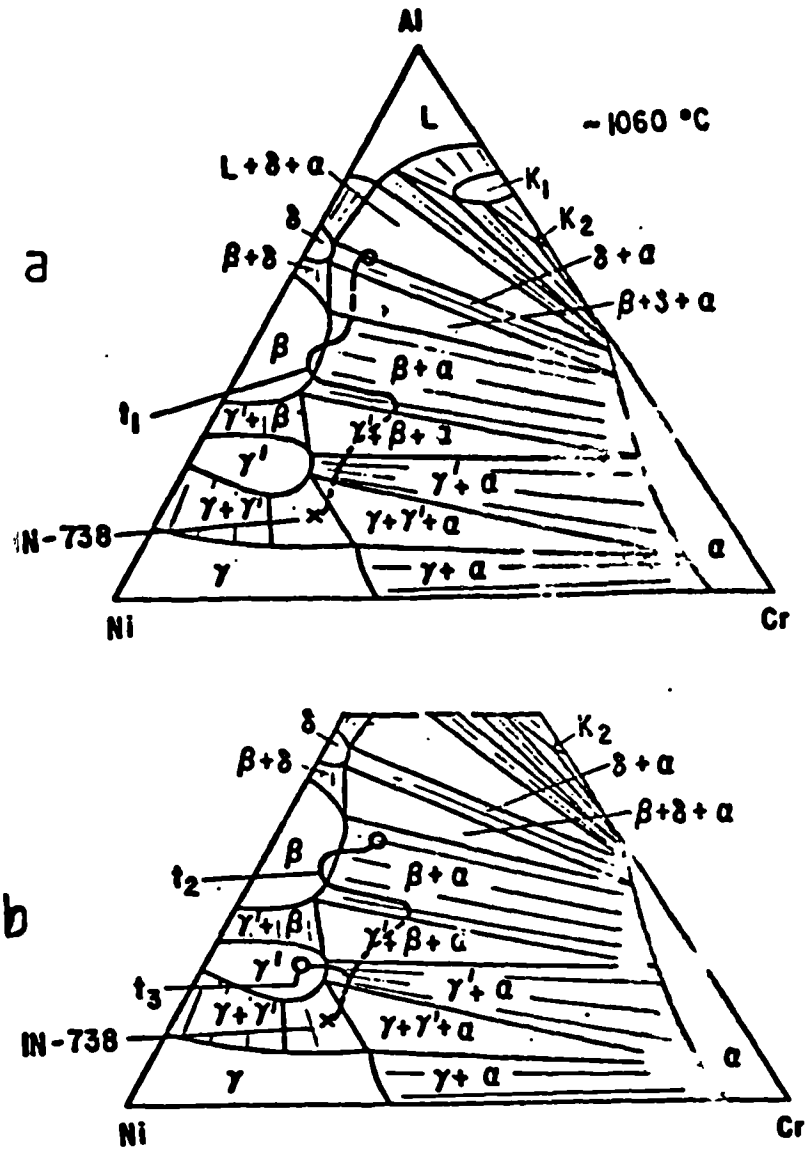

Figure 1 Phase diagram Ni-Cr-Al with diffusion paths describing

(a) simple aluminide coating formation on IN-738

(b) coating degradation.

(After JACKSON et al. 3)

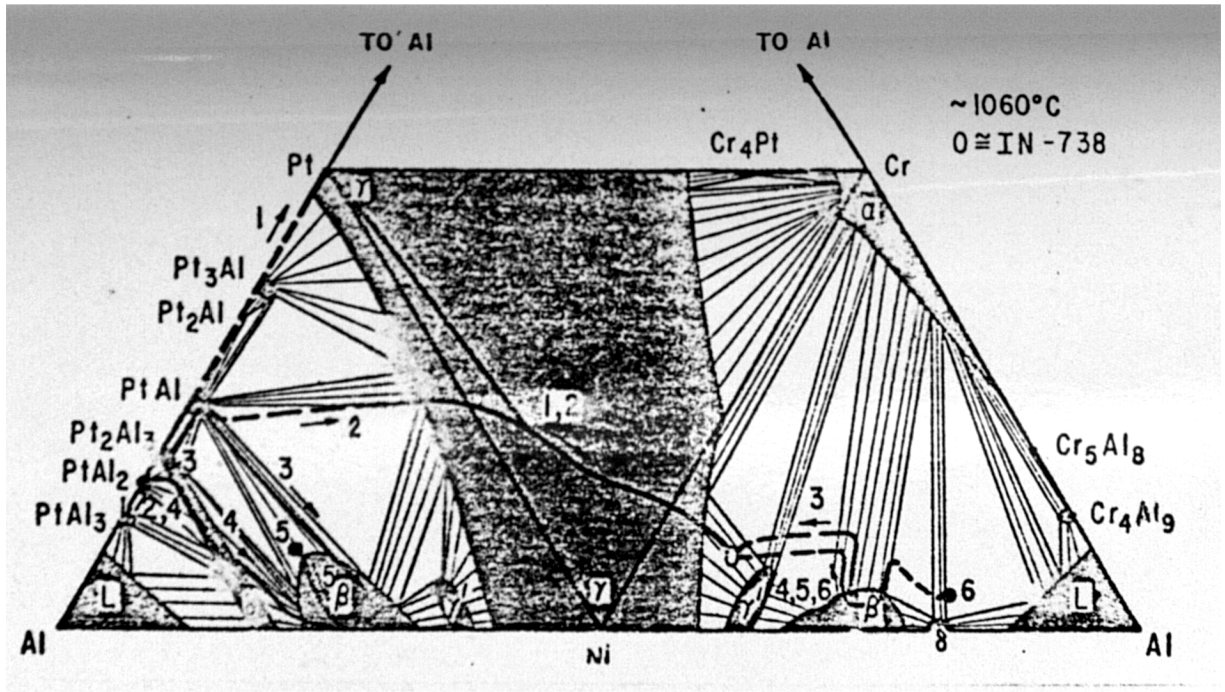

Figure 3 Schematic phase diagram for Ni-Cr-Al-Pt with diffusion paths describing platinum aluminide coating formation on IN-738 in a 1060°C pack;(1) aluminization with "infinitely thick" Pt layers, (2) 25Um thick Pt at 0h,(3) 25Um thick Pt at 3h,(4) 5Um thick Pt at 0h,(5) 5Um thick Pt at 3h,and (6) non-Pt coated IN-738 at 3h.

(After JACKSON et al. 3)

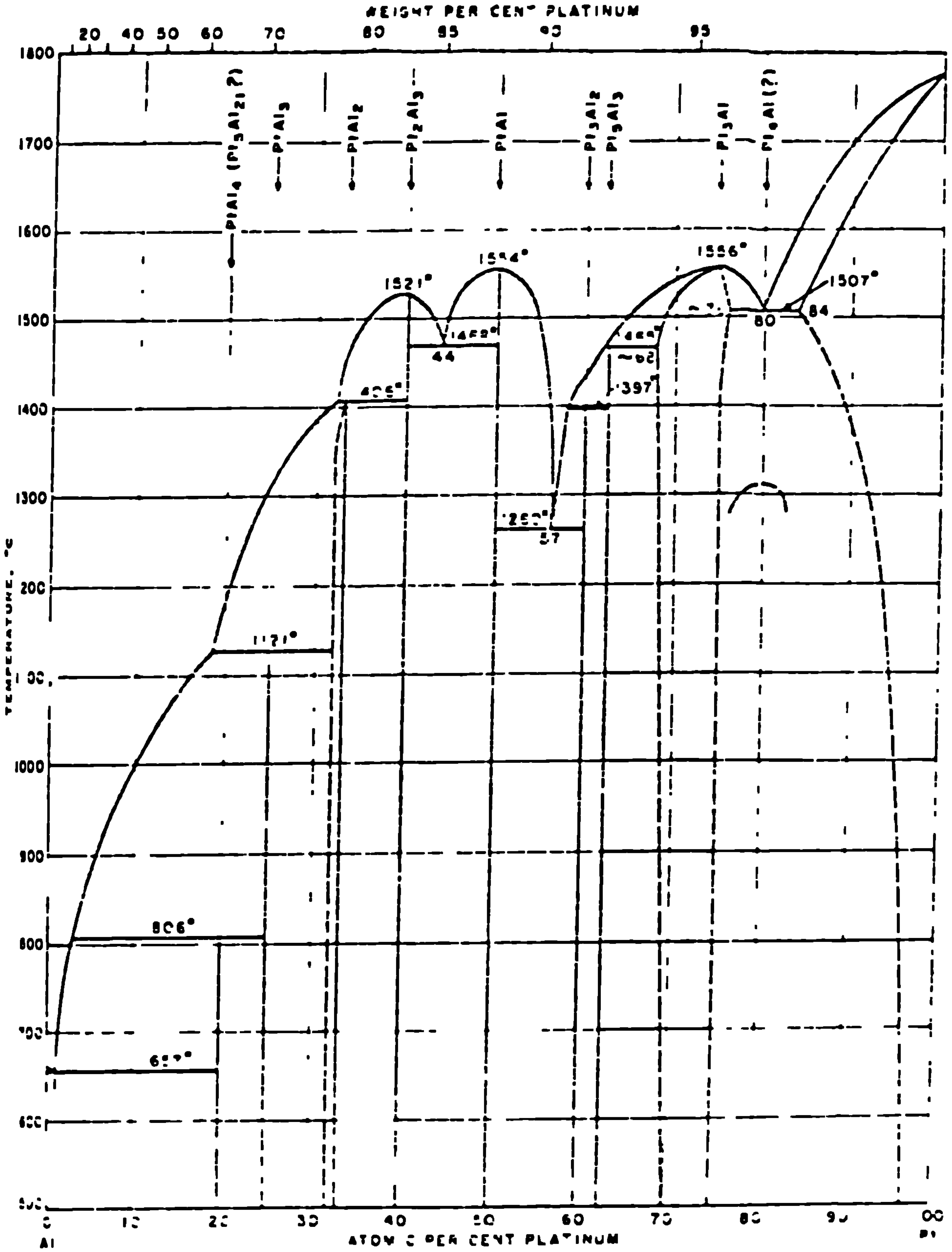
WEIGHT PER CENT PLATINUM
ATOMIC PER CENT PLATINUM
TEMPERATURE, °C
Al
Pt
PtAl4 (Pt5Al21 ?)
PtAl3
PtAl2
Pt2Al3
PtAl
Pt3Al2
Pt5Al3
Pt3Al
Pt4Al (?)
1521°
1554°
1556°
1507°
1405°
1468°
1397°
1260°
1121°
806°
657°
44
57
80
84

Fig 2 . Al-Pt

Figure 4

Schematic diagram of the reaction tube assembly.

A- Silica reaction tube

B- Gas admittance fitting

C- Constriction unit

D- Gas admittance tube

E- Balance

F- Balance cover

G- Rubber seal

H- Silica suspension rod

I- Heating tape

J- Specimen

K- Furnace

L- Gas mixture from injector

(After FLATLEY, 50)

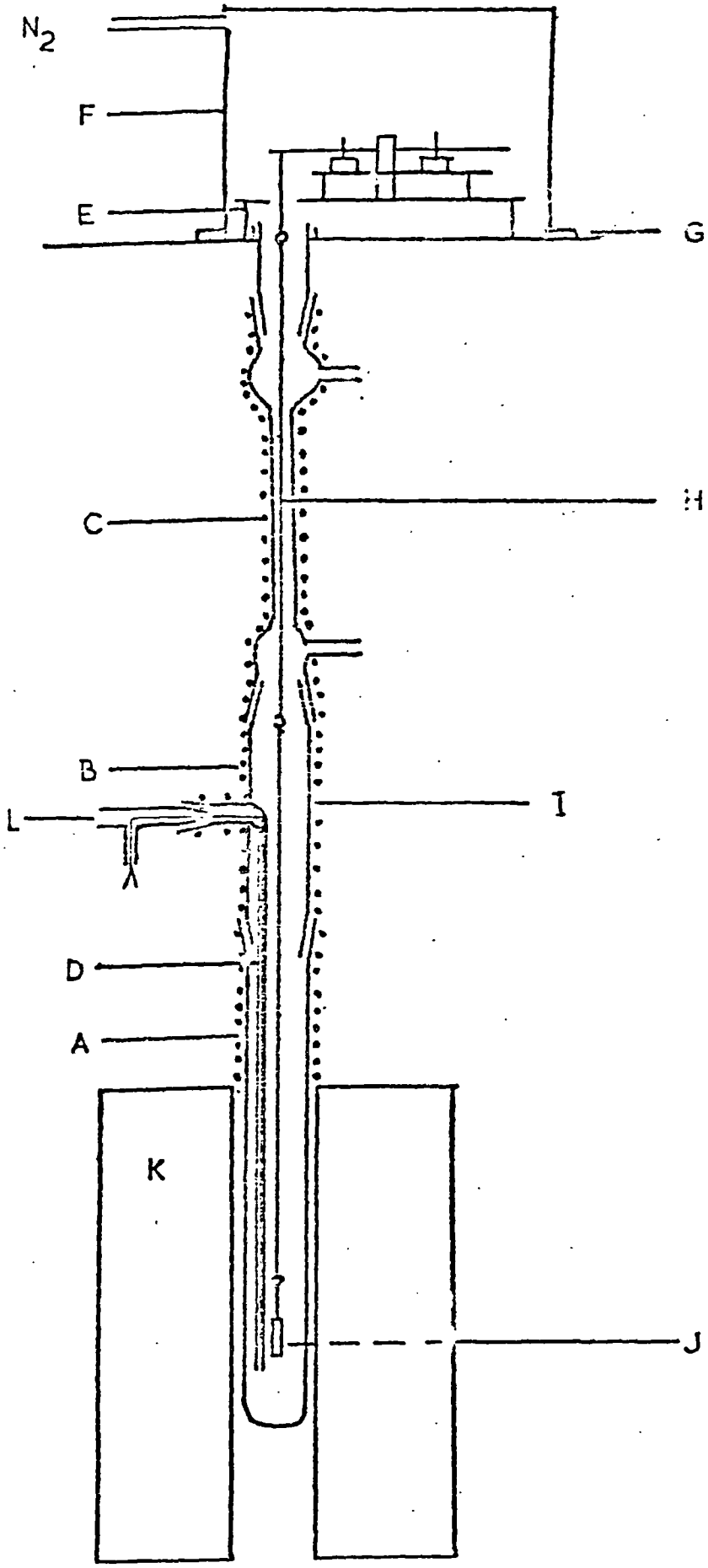
N_2
F
E
G
H
C
B
L
I
A
D
A
K
J

Figure 5 a- photograph of Balance

A- Restoring Coil
B- Damping Coil
C- Permanent Magnet
D- Centre of gravity adjustment
E- Pt. Suspension wire
F- Input and output leads
G- Photo cells
H- Light source
I- Stainless steel shim
J- Flag attached to beam to operate between G and H

(After Flatley, 50)

b- Photograph of the complete weighing assembly, including the balance, the recorder and the control unit.

(After Flatley, 50)

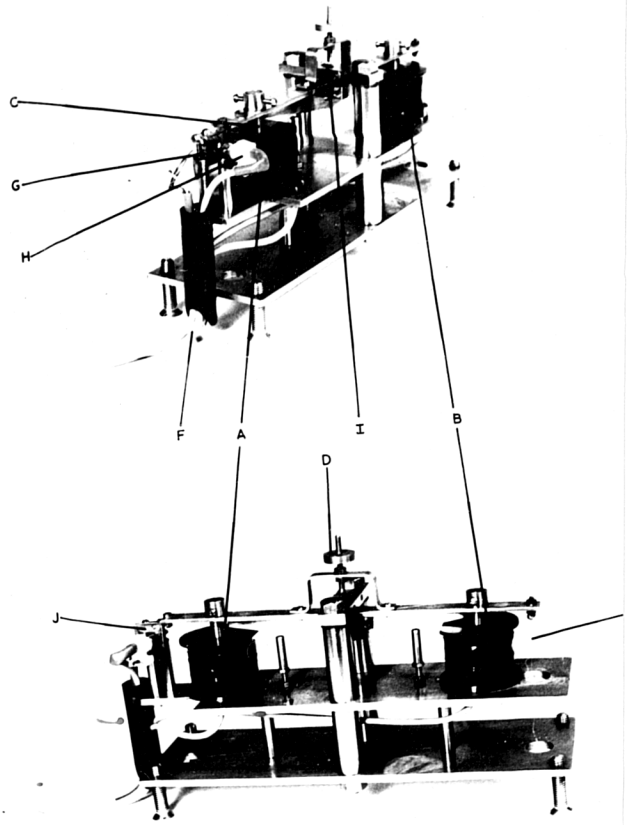
C
G
H
F
A
I
B
D
J

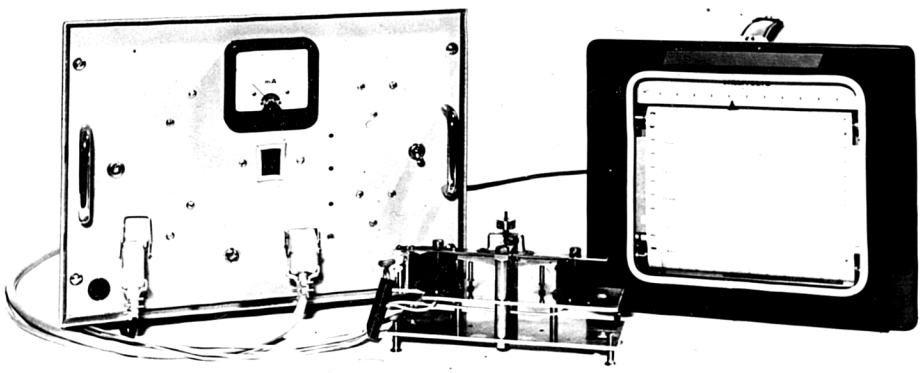

Figure 6

Calibration curve of balance.

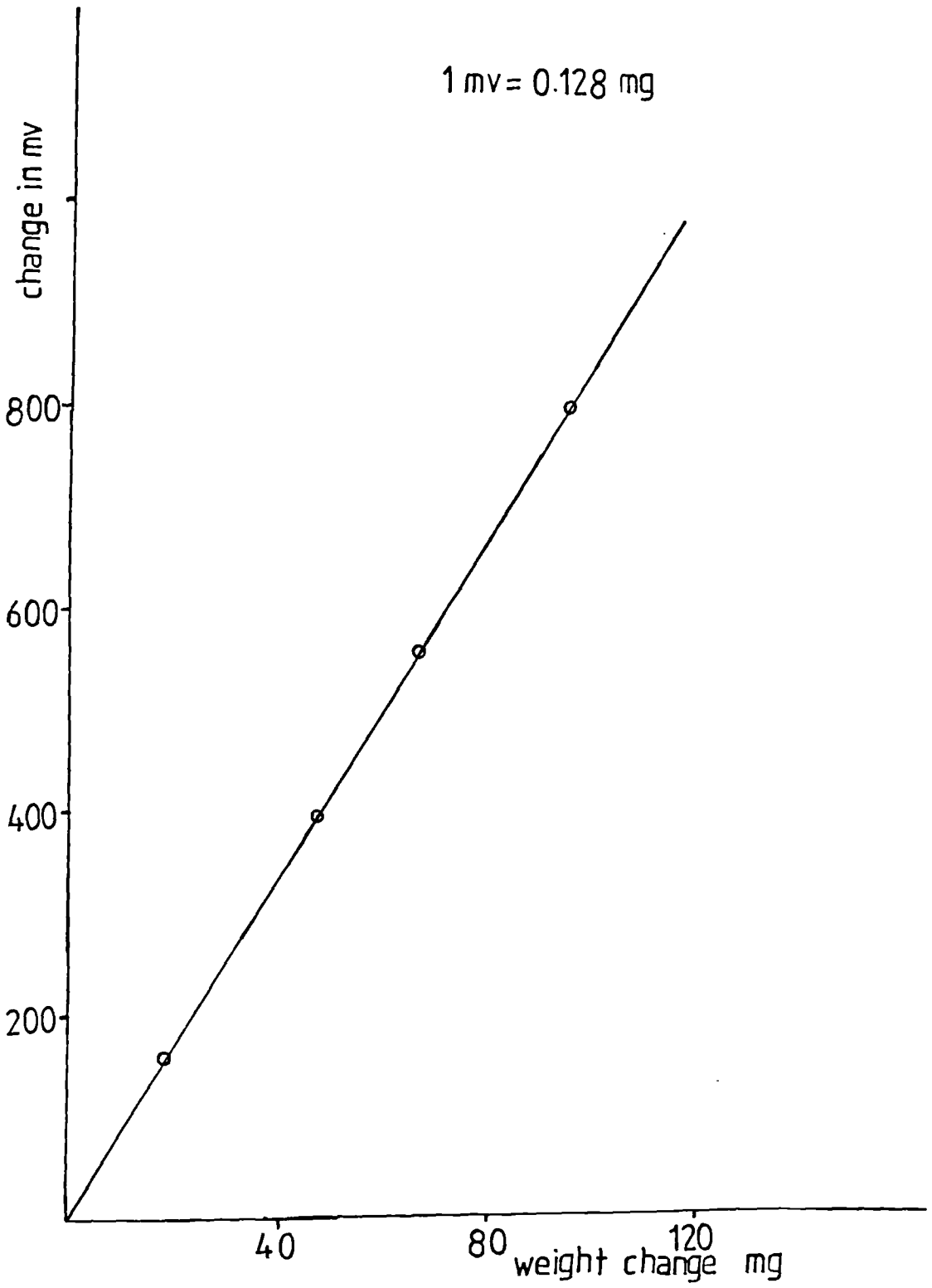
1 mv = 0.128 mg
change in mv
800
600
400
200
40
80
120
weight change mg

```
ANALY -? YES

                                        LIVETIME(SPEC)=     70
 ENERG      RES      AREA
    4.     89.44     45254
TOTAL  REA=    215737
......
PEAK A      .34 KEV OMITTED?
PEAK A     9.40 KEV OMITTED?

FIT IN EX= 3.54

ELMT    PP.CONC    ERROR(WT%)
 PT     41.501        .524
 AL      4.682        .094
 NI     24.407        .368
 CR      4.672        .142
 CO      2.603        .173
 TI       .599        .037
 NB       .359        .347* < 2 SIGMA*
 MO       .157        .244* < 2 SIGMA*
 W        .353        .260* < 2 SIGMA*
 FE       .610        .134

  [ 1 2 3 ZAF'S]

25.00 KV  A.O.I.=60.00 T.O.A.=40.00 COSINE=1.000

SPECTRUM:                                          HANNA

ALL ELMTS ANALYSED

ELMT     ZAF      %ELMT
 PT     .760     55.321
 AL     .533      8.717
 NI    1.054     23.148
 CR     .960      4.865
 CO     .998      2.614
 TI     .864       .693
 NB     .522       .000
 MO     .533       .000
 W      .689       .000
 FE    1.031       .592
TOTAL             95.950
```

Figure 7 A typical example of computer printout.

Where, a flat specimen was used, tilted to 30° when the take off angle (TOA) was 40° and the angle of incident of the electron beam (AOI) was 60°. In all cases accelerating voltage of 25 KV have been used.

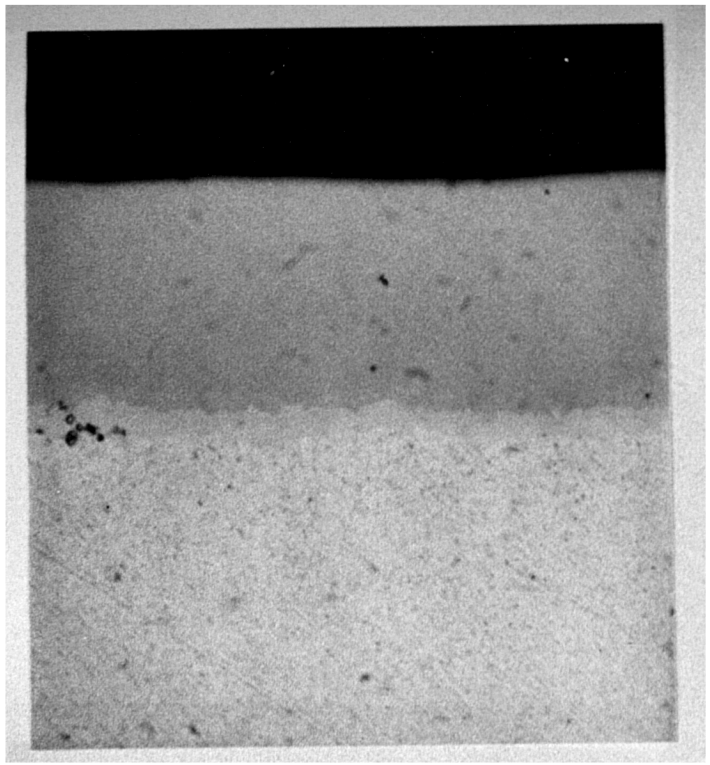

layer	thickness (μm)	Average composition, wt%			At.%	
		Al	Pt	Total	Al	Pt
-t Al_3	41	14.88	85.0	99.88	55.87	44.13
PtAl	2	9.9	88.4	98.3	44.75	55.25
Pt_3Al (?)	5	4.3	95.7	100.0	24.52	75.48

Fig. 8 Microstructcre and layer compositi n from top to bottom f Pt lumi ides formed on Pt in high activity Al pack.

-6
-5
-4
Log D
cm²/sec
0.7
0.8
0.9
1
1/T (10⁻⁵ K⁻¹)

Figure 9 LogD vs 1/T for the aluminisation of bulk Pt.

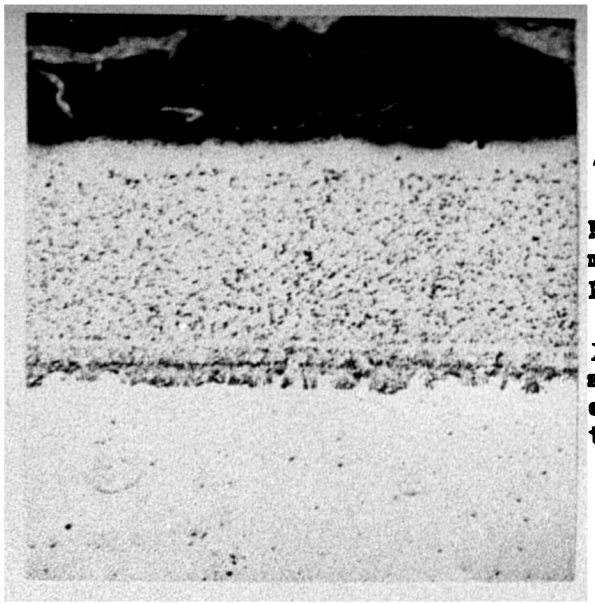

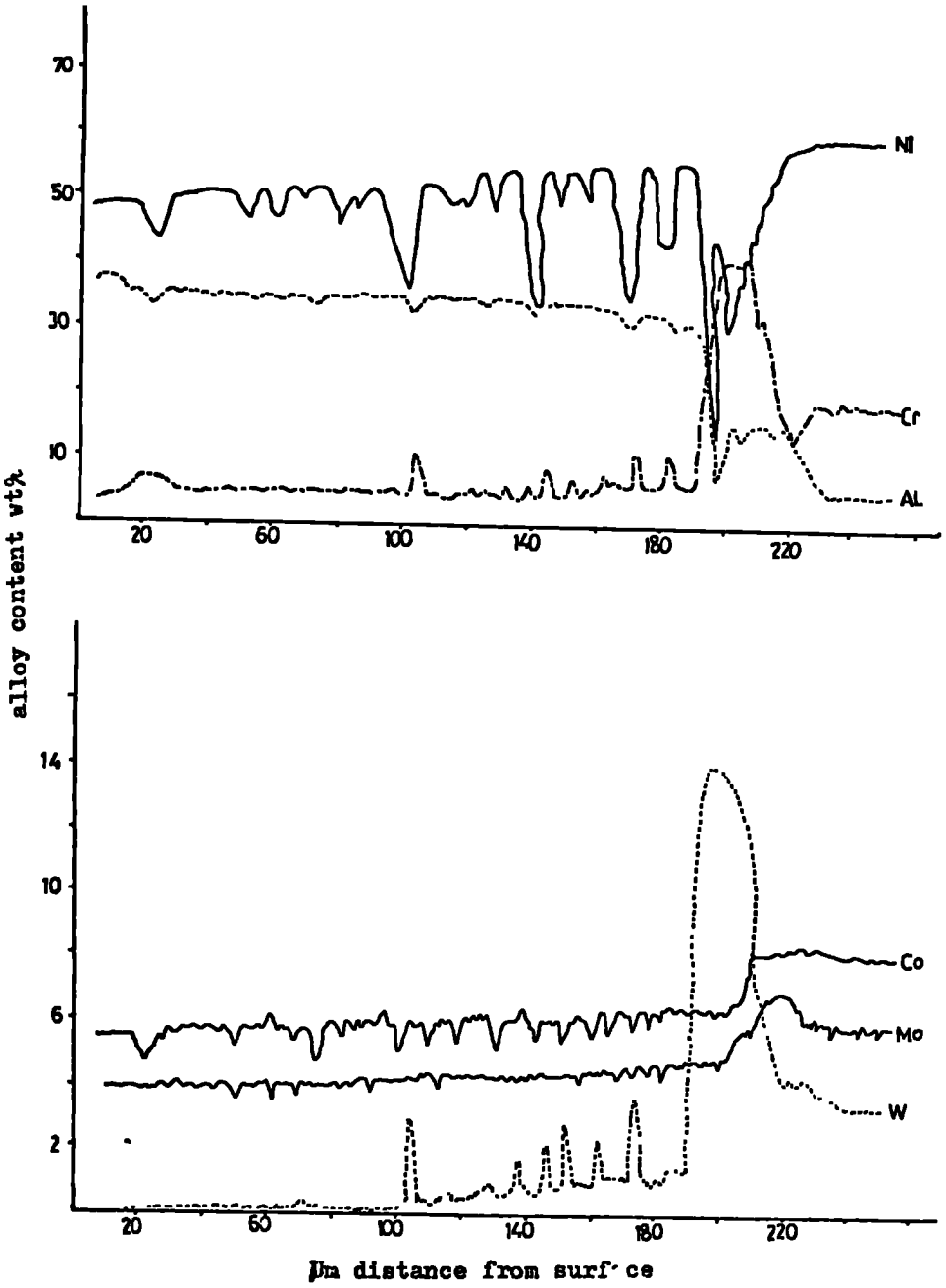

Fig.10 co ting mic s ruct ~ ard compositional profile through a plain aluminide IN-738 (5wt% Al p ck, 1000C, 20hrs), etched with etchant two.

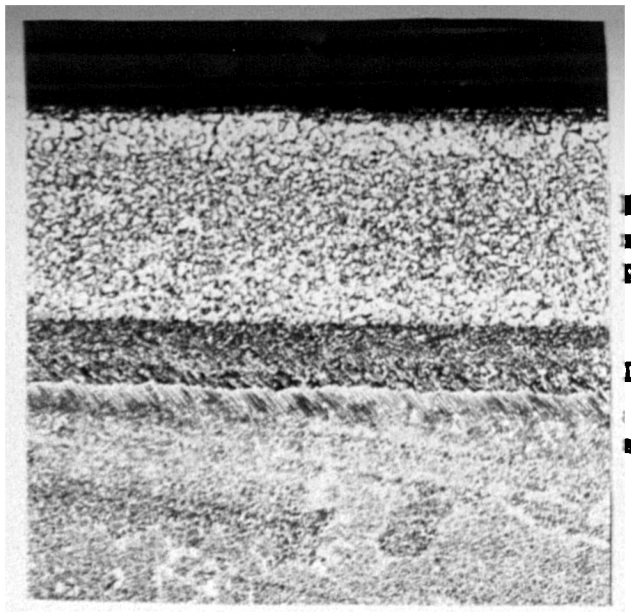

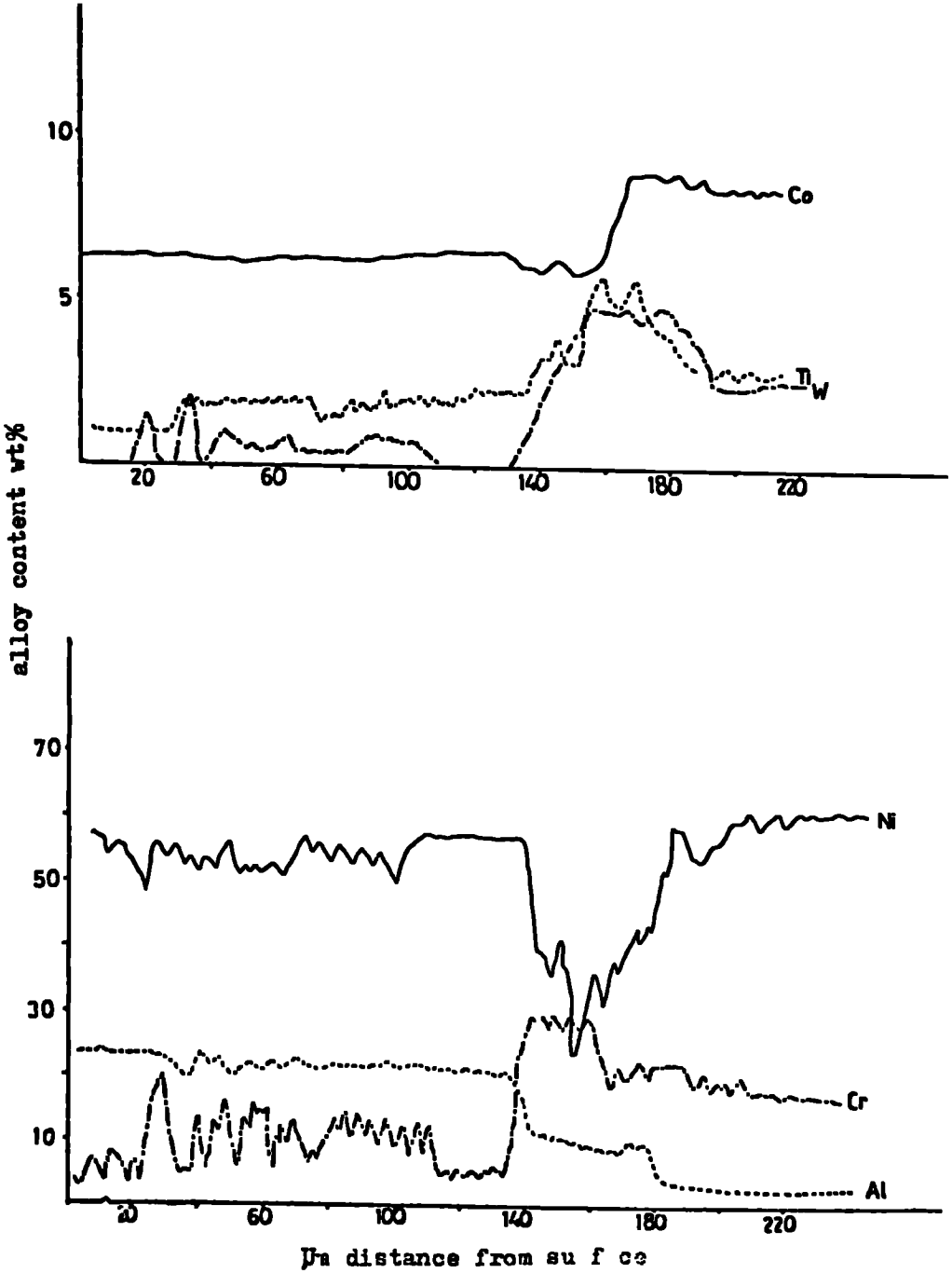

Fi .11c ating microstructure and compositional
rofile through a plain aluminide IN-738
after 1000 hrs of heat tre tment at 1000°C.

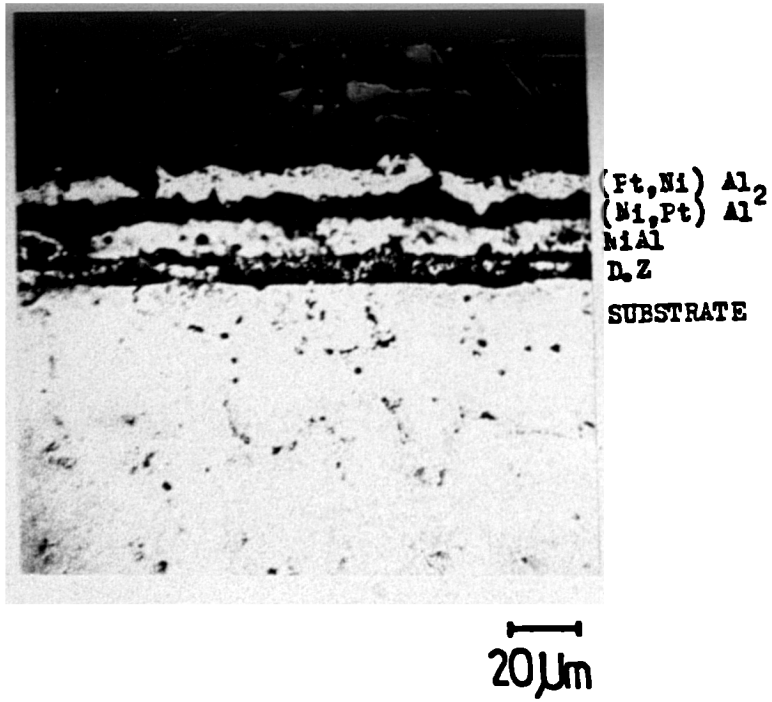

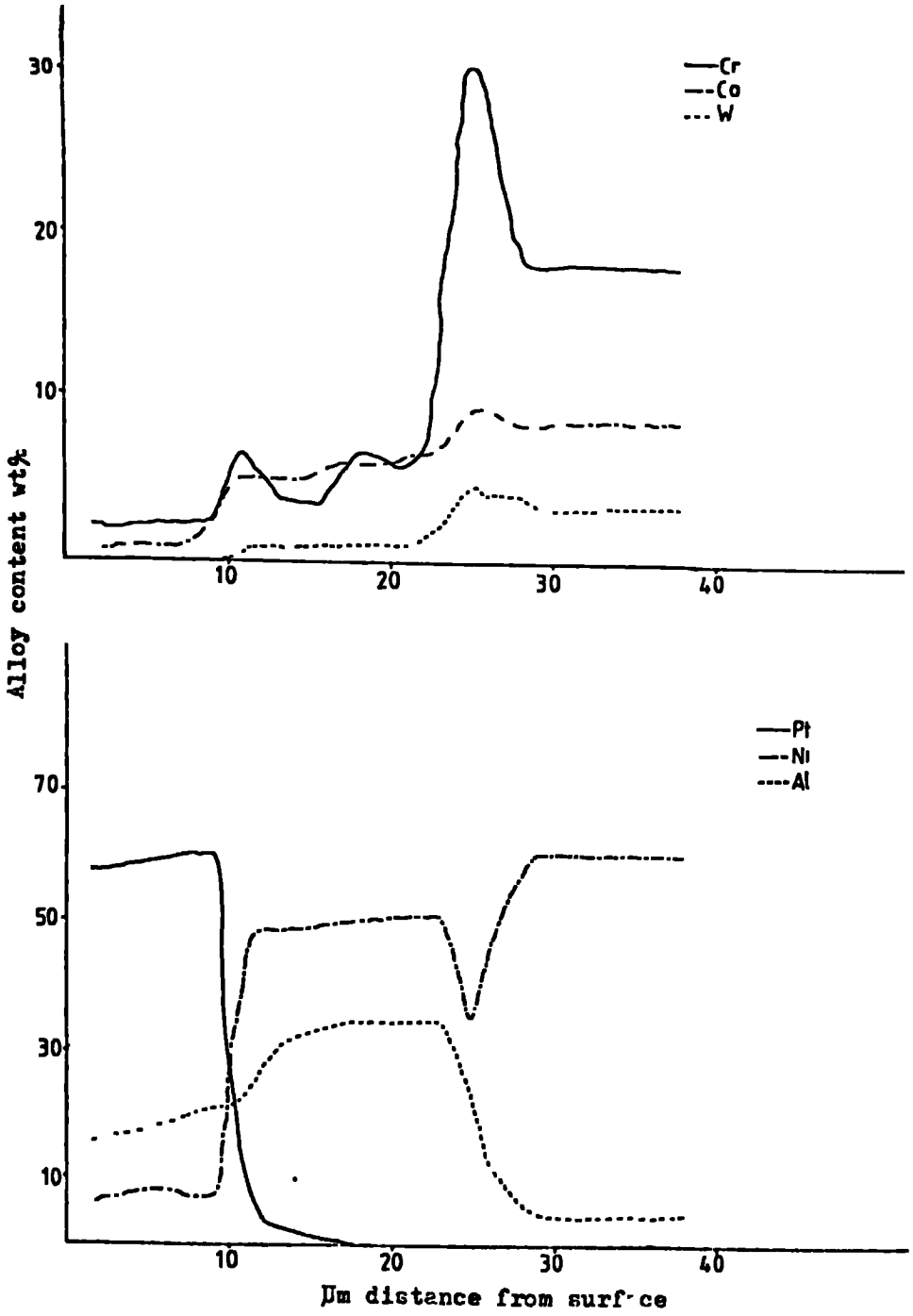

Fig.12 co ting structure and compositional profile through pack aluminized Pt-coated (5 µm thick) IN-738 for a 5 pct Al pack at 1000°C, after 2h. Code (A).

Figure 13 SEM micrograph showing surface topography of coating treatment A.

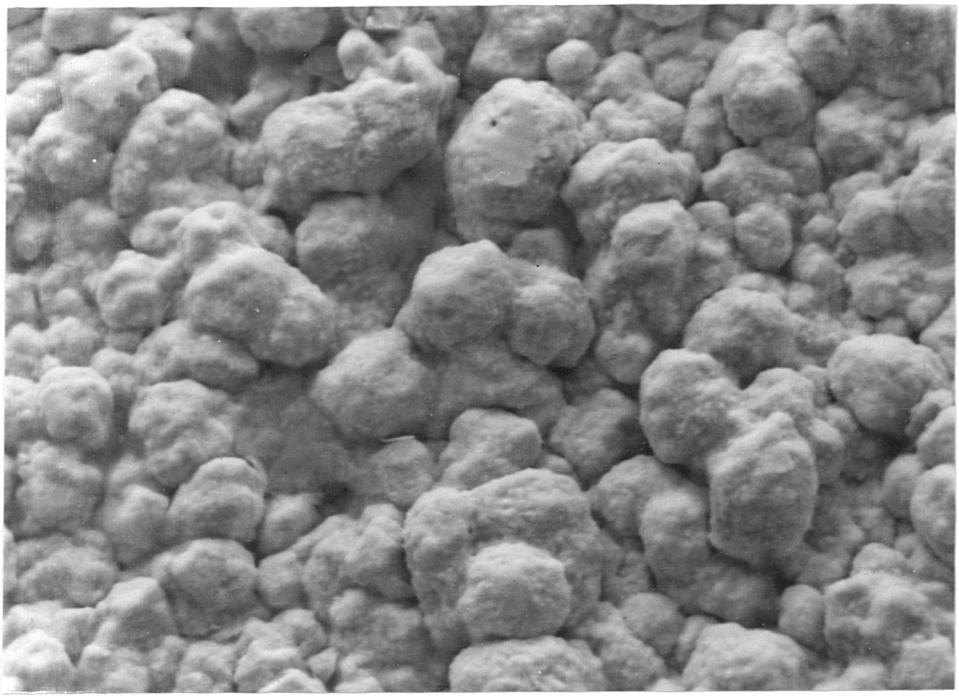

4 µm

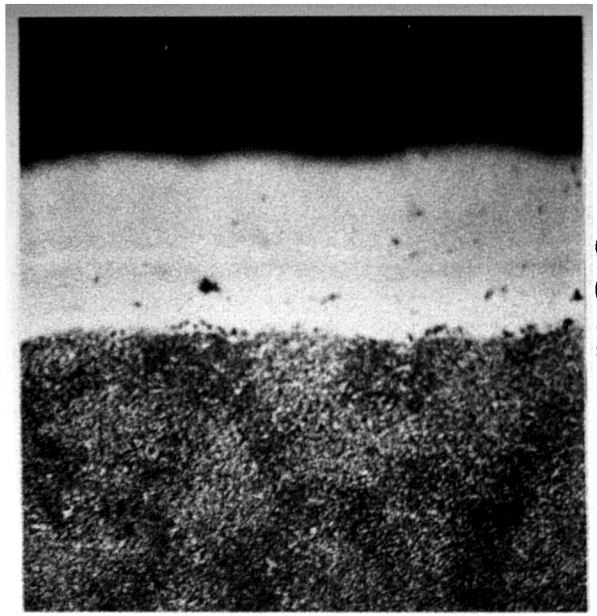

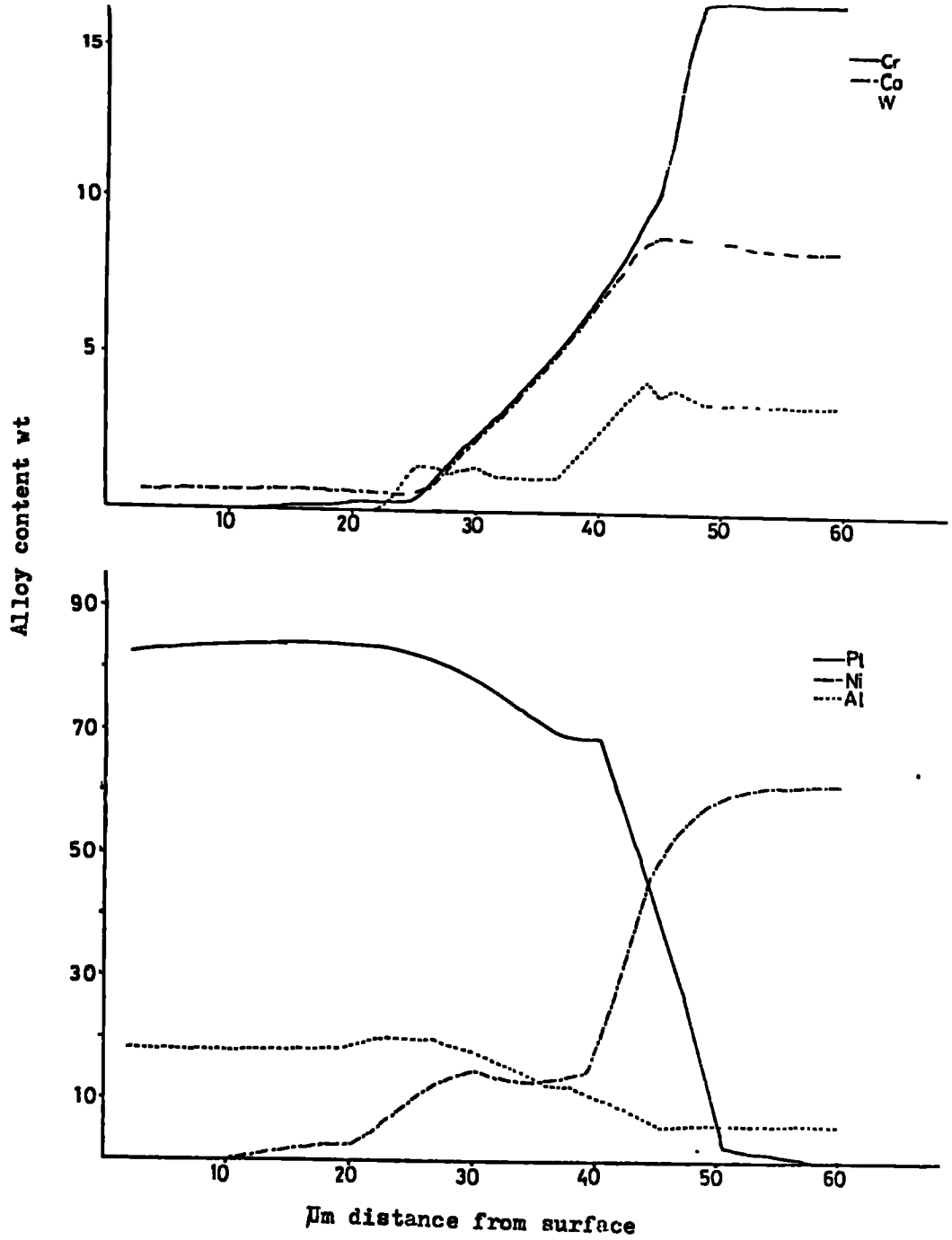

Fig.14 coating structure and compositional profile through pack aluminized Pt-coated (15 µm thick) IN-738 for a 5 pct Al pack at 1000°C, after 3h. Code (B).

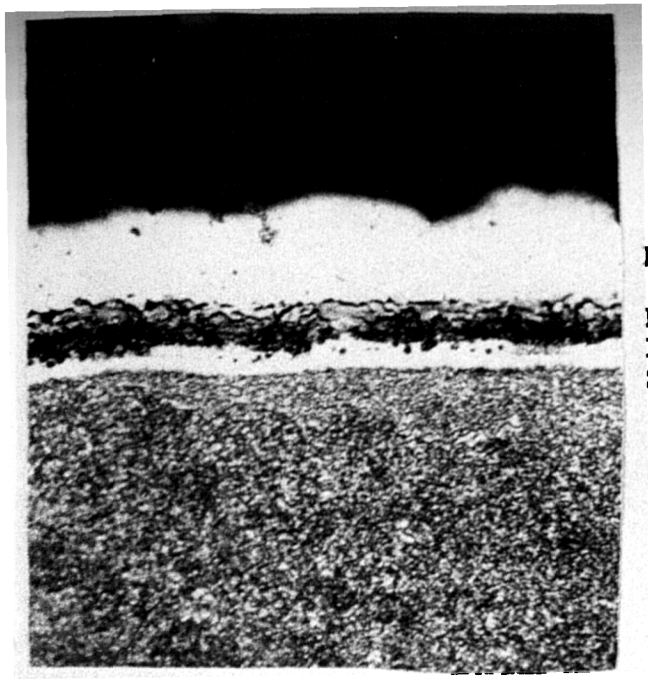

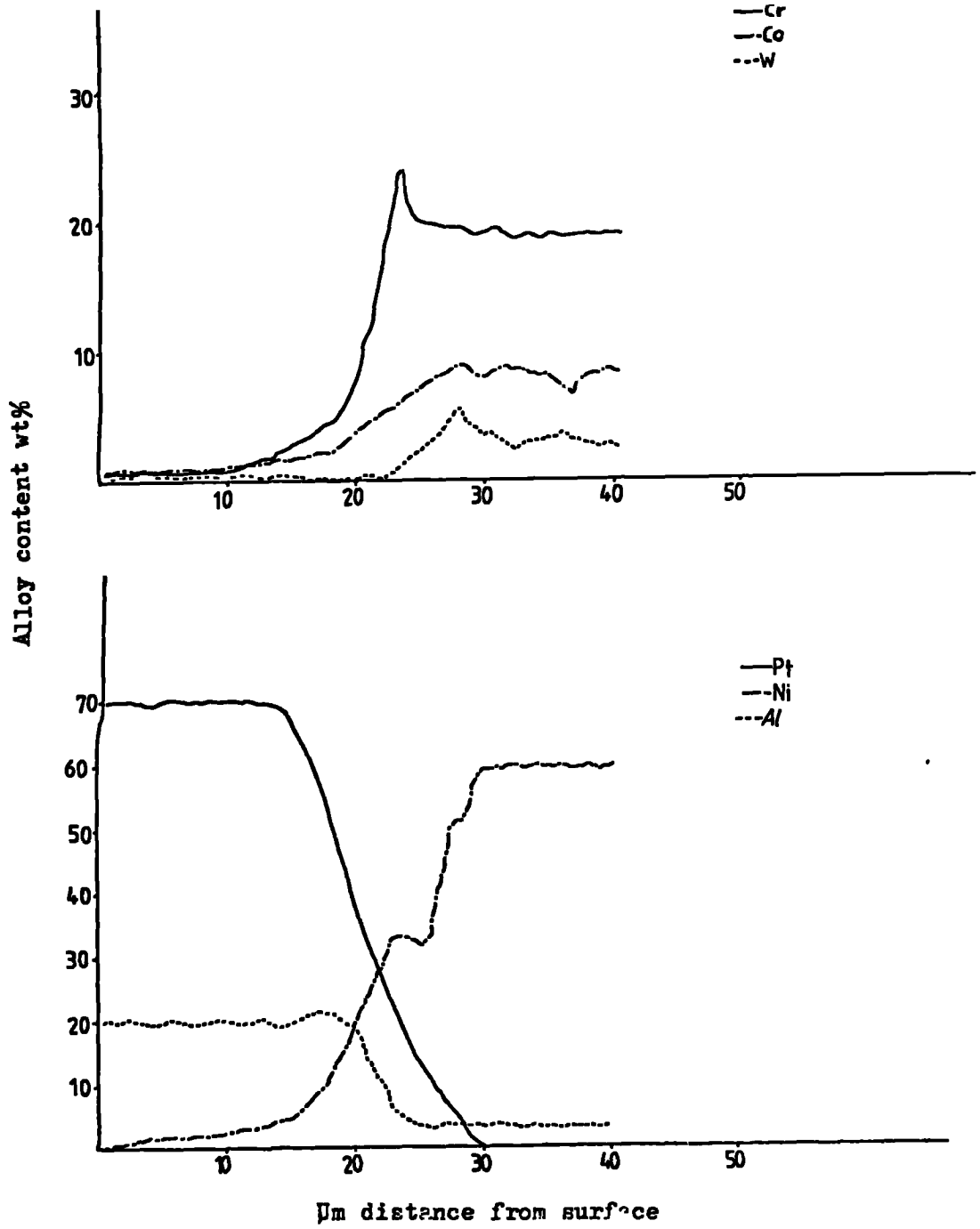

Fig.15 coating structure and compositional profile through pack aluminized Pt-coated (5 µm thick) IN-738 for a low activity pack at 1000°C, after 1h. Code (C).

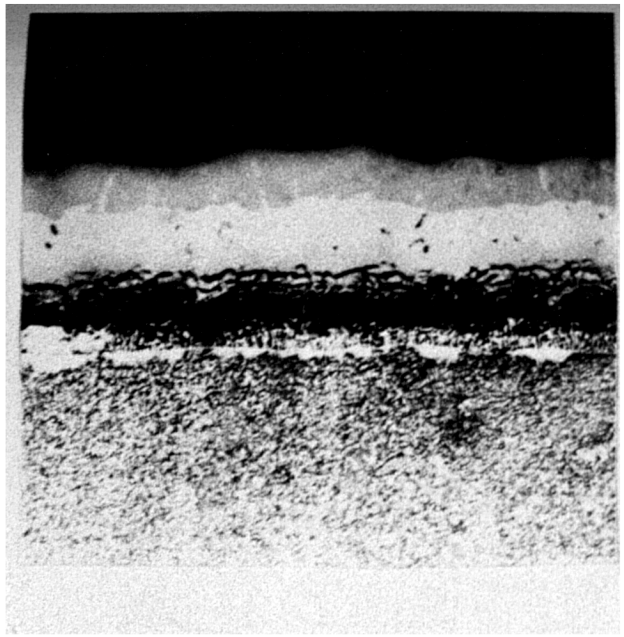

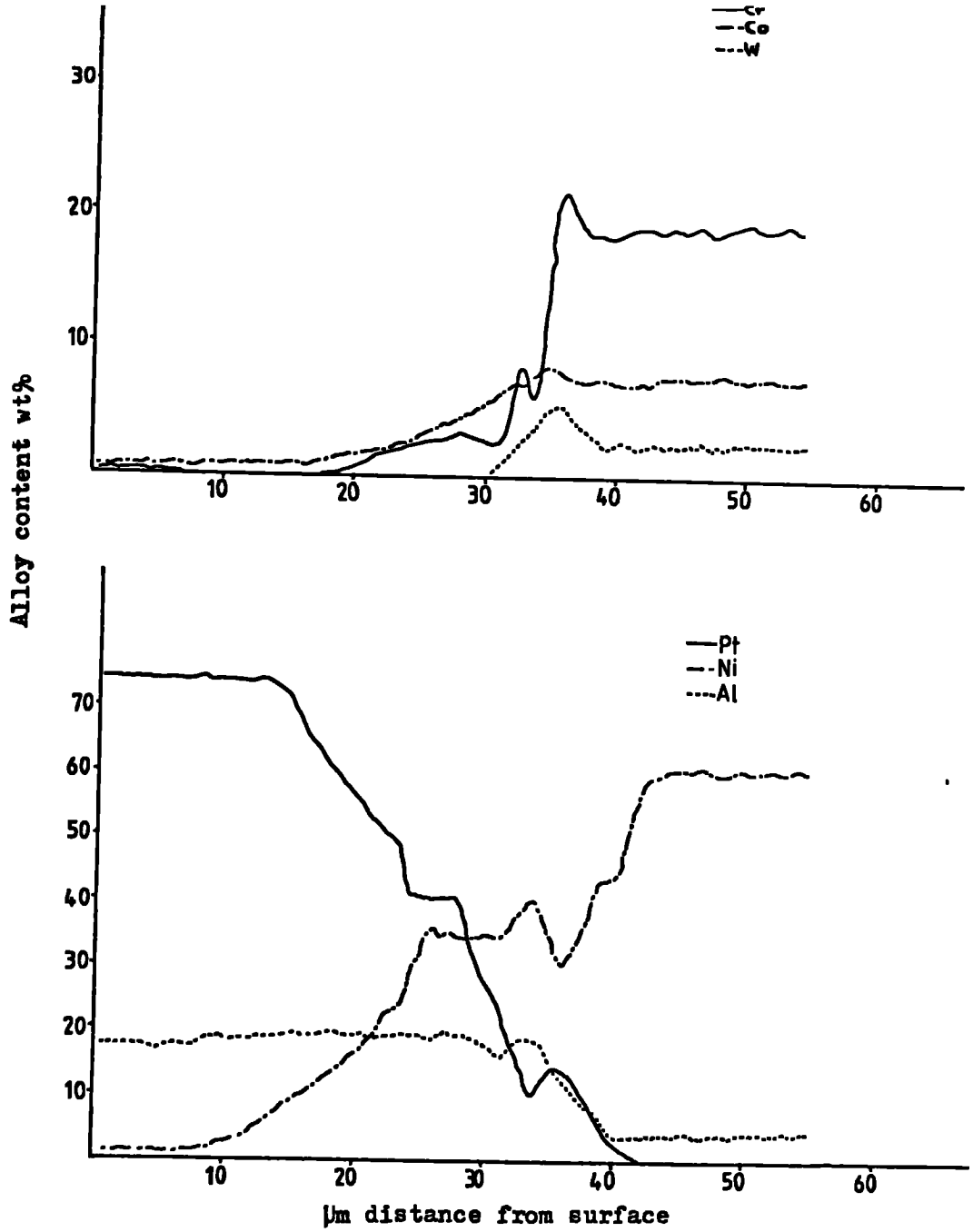

Fig.16 coating structure and compositional profile through pack aluminized Pt-coated (15 µm thick)IN-738 for a low activity pack at 1000°C, after 2 h. Code (D).

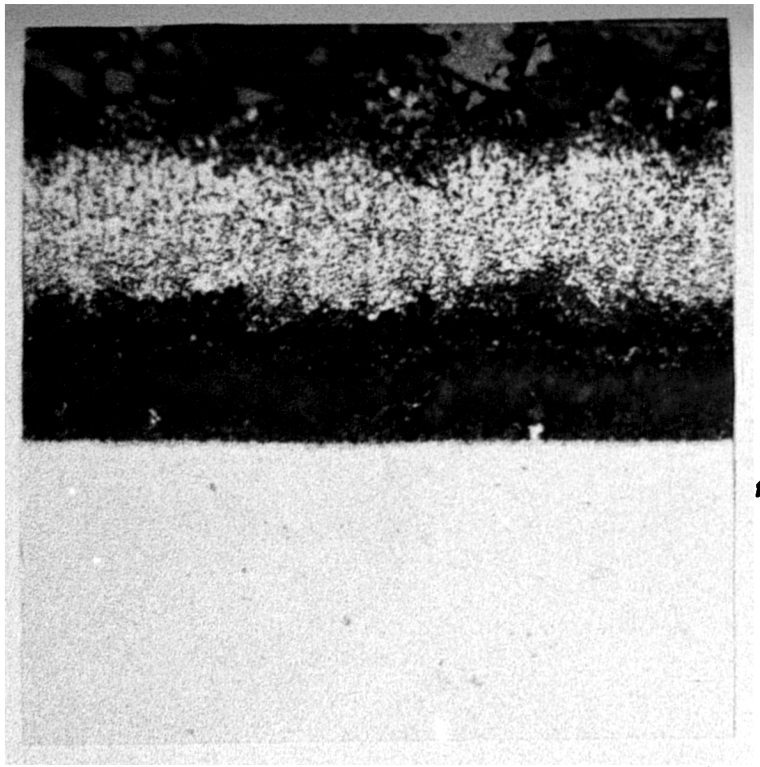

		Pt	Al	Ni	Cr	Co	W	Ti	Mo	Total
$PtAl_2$+NiAl	wt%	36.5	24.5	21.7	7.5	3.4	0.8	0.7	0.5	95.2
	At%	11.0	53.7	21.8	8.5	3.4	0.2	0.8	0.3	100.0
(Ni,Pt)Al	wt%	3.9	32.3	43.1	7.3	5.8	0.8	0.7	0.7	94.6
	At%	0.9	54.0	33.1	6.3	4.4	0.2	0.6	0.3	100.0

Fig.17 Coating microstructure and average composition, obtained by point analysis using EDS on the SEM, of a duplex($PtAl_2$+NiAl) coating, Code E. see section 3.6 for details.

Figure 18 Micro-hardness profile across coating treatment A (5 μm Pt) and coating treatment B (15 μm Pt), high activity pack.

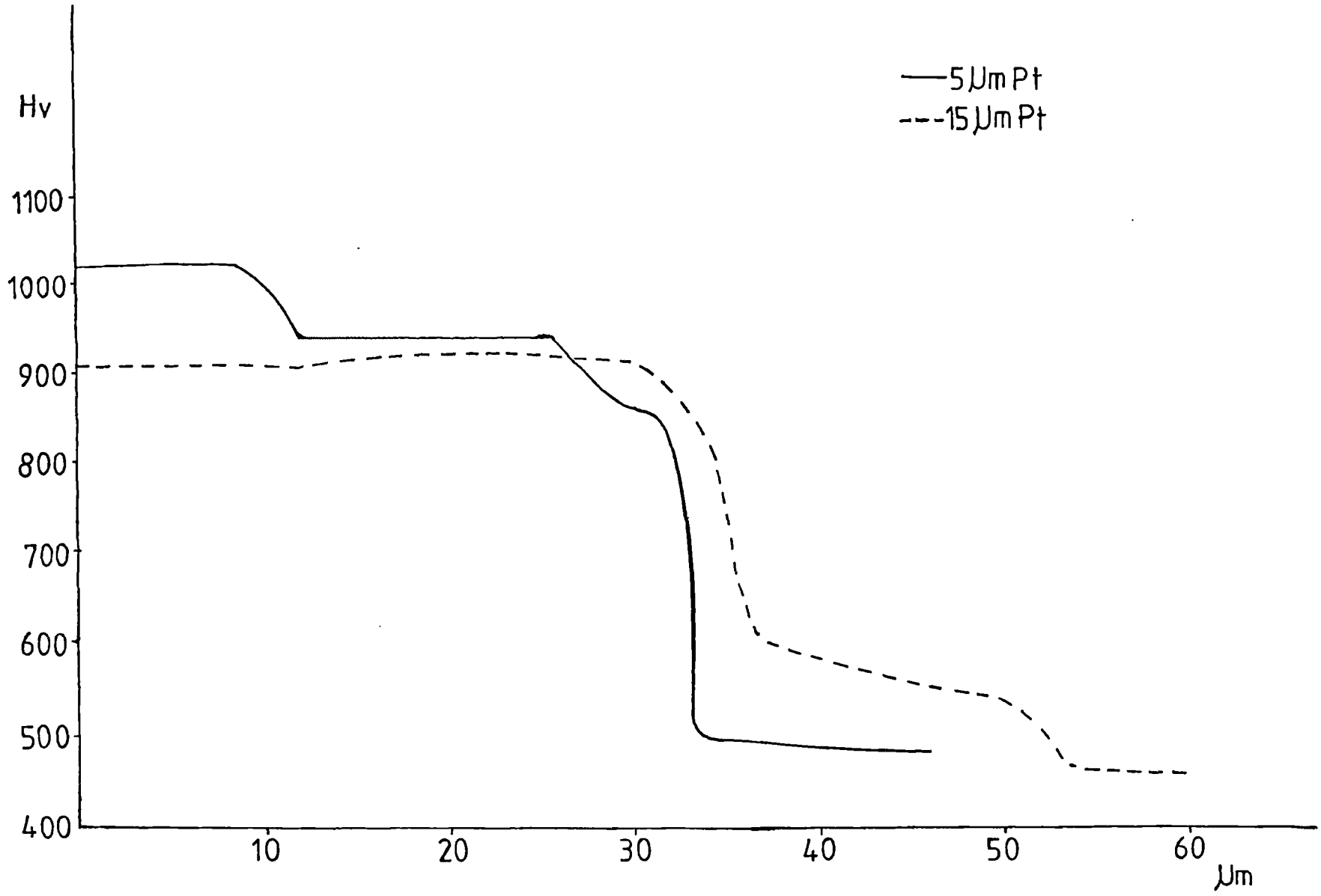
5 µm Pt
15 µm Pt
Hv
1100
1000
900
800
700
600
500
400
10
20
30
40
50
60
µm

Figure 19 Micro-hardness profiles across coating treatment C (5 μm Pt) and coating treatment D (15 μm Pt), low activity pack.

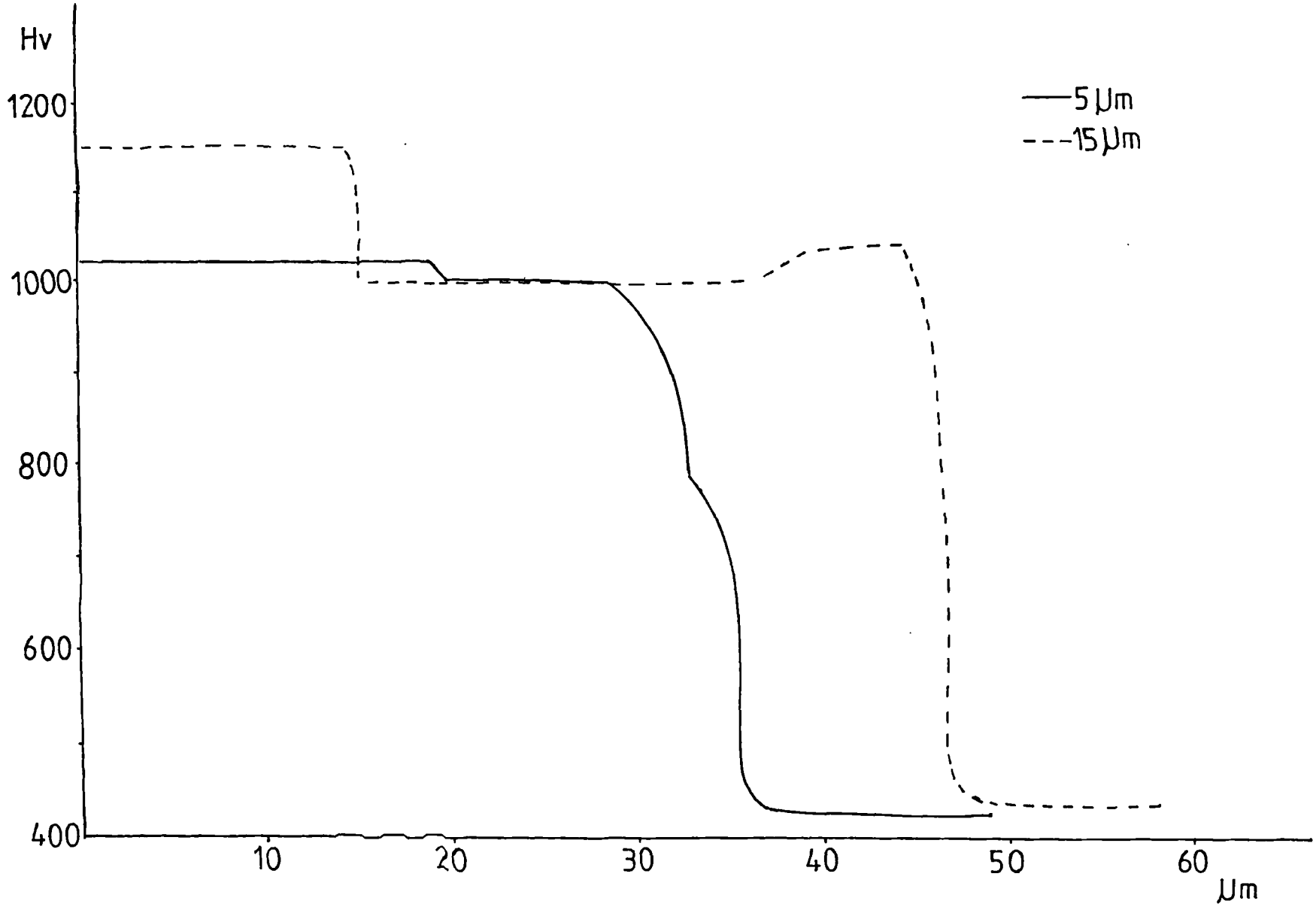
Hv
1200
1000
800
600
400
10
20
30
40
50
60
µm
5 µm
15 µm

Figure 20 Schematic phase diagram for Ni-Al-Pt with diffusion paths describing platinum aluminide coating formation on IN-738 in a 1000°C pack for (A) 5Um Pt using high activity pack, and (B) 15Um Pt using high activity pack, and (C) 5Um Pt using low activity pack, and (D) 15Um Pt using low activity pack, and (E) 15Um Pt duplex coating.

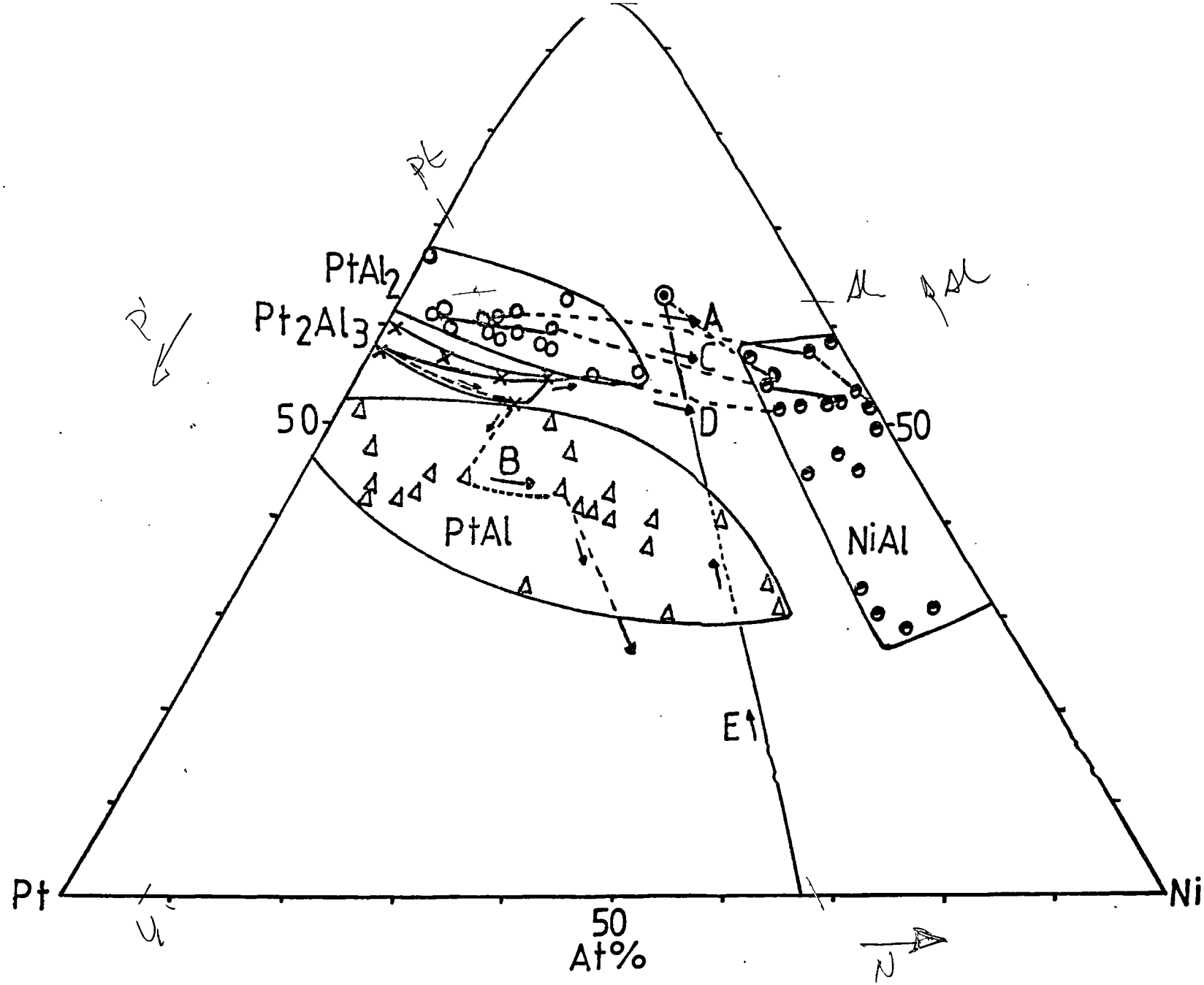
PtAl2
Pt2Al3
50
A
C
D
B
PtAl
NiAl
E↑
50
50
At%
Pt
Ni

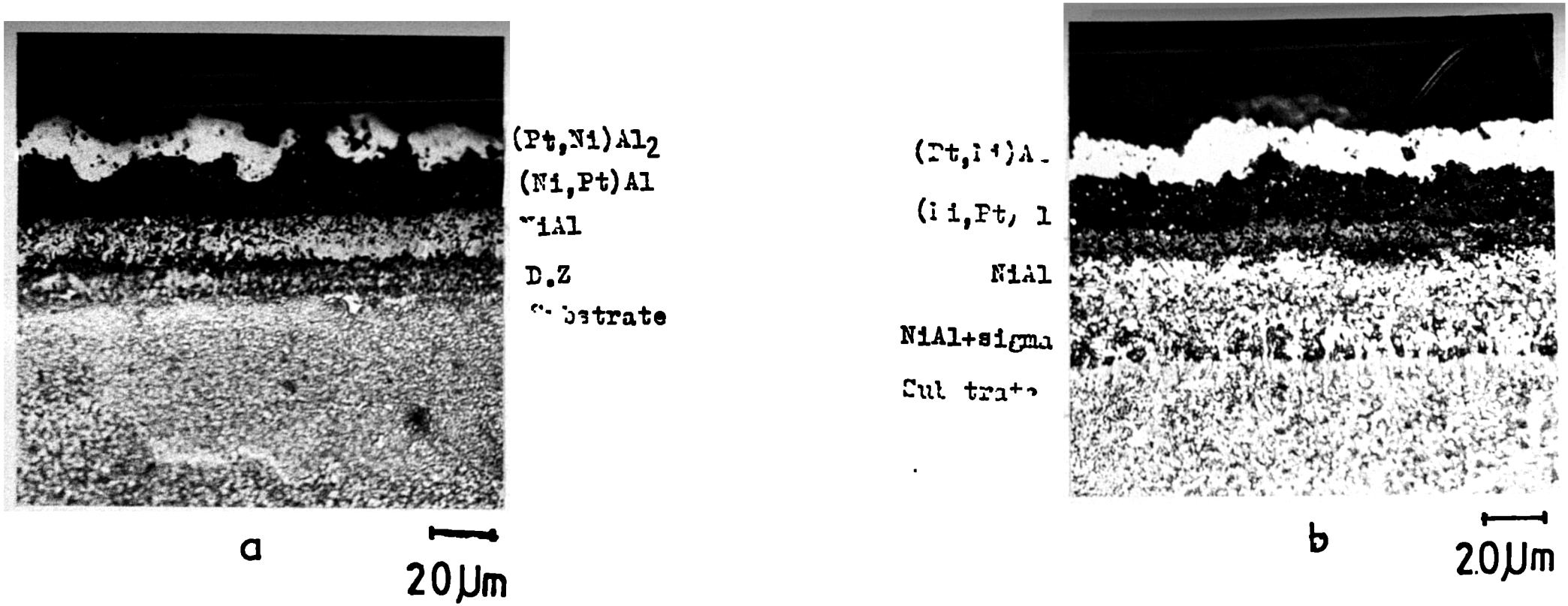

Fig.21 coating structure of heat treated 5Um Pt-coated,high activity pack after, a-5h. b-50h. Code (A).

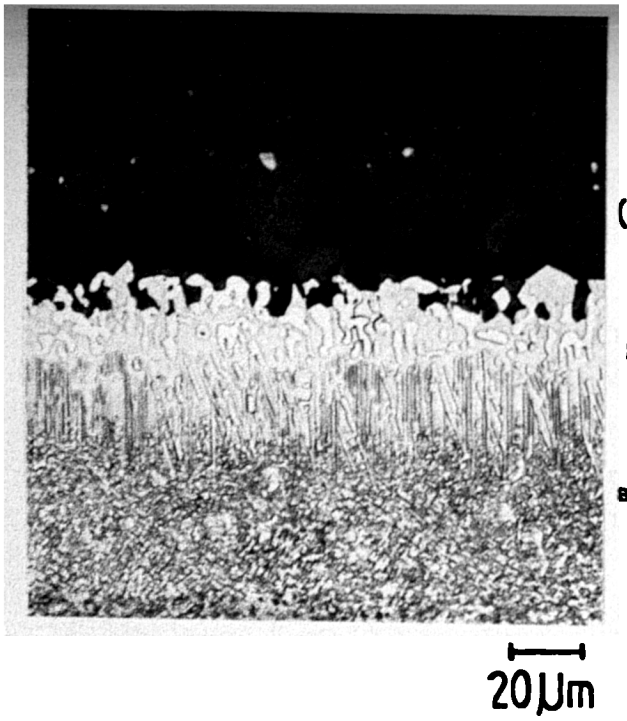

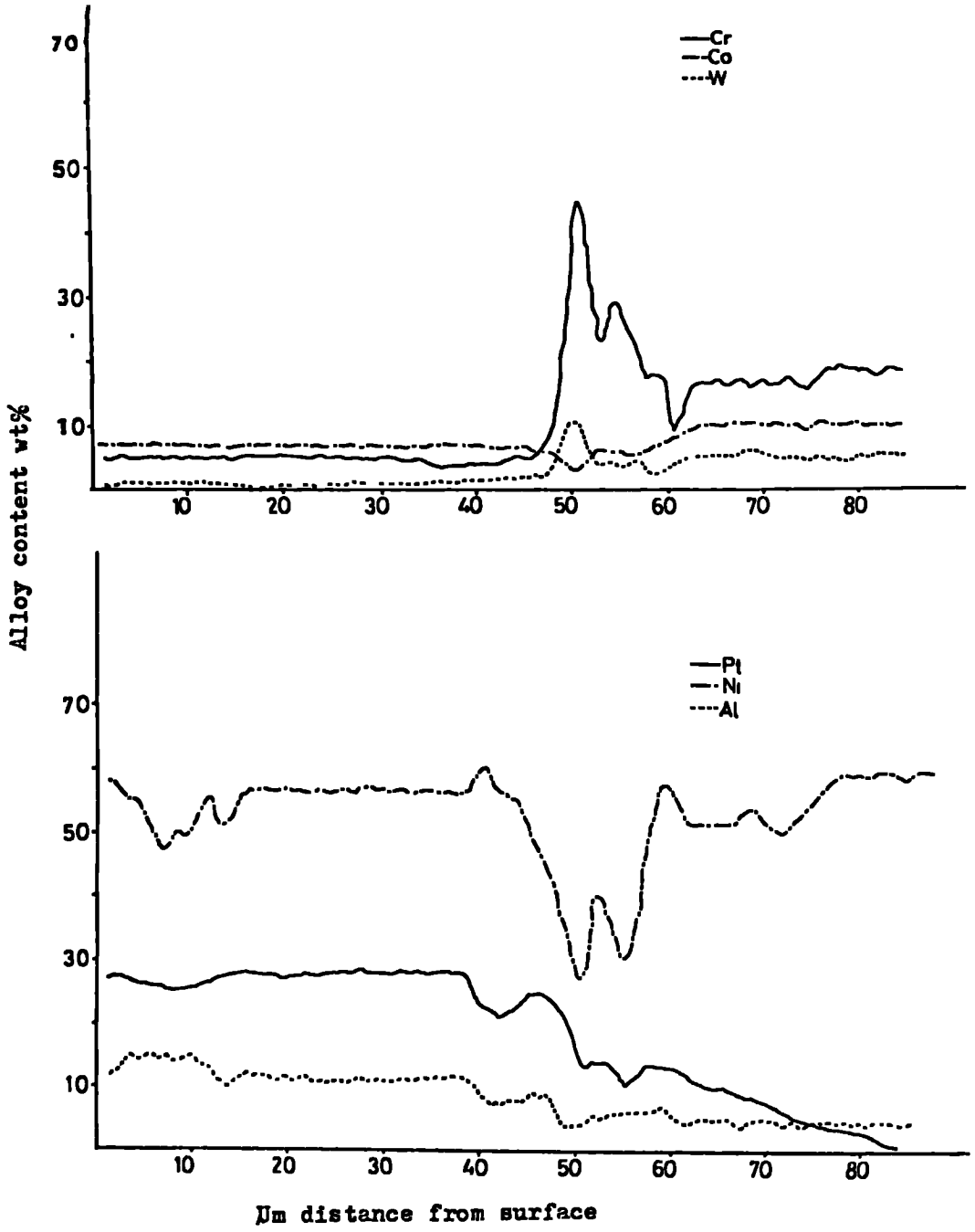

Fig. 22 coating structure and compositional profile through 5µm Pt-coated high activity pack after 1200h heat treatment at 1000°C. Code (A).

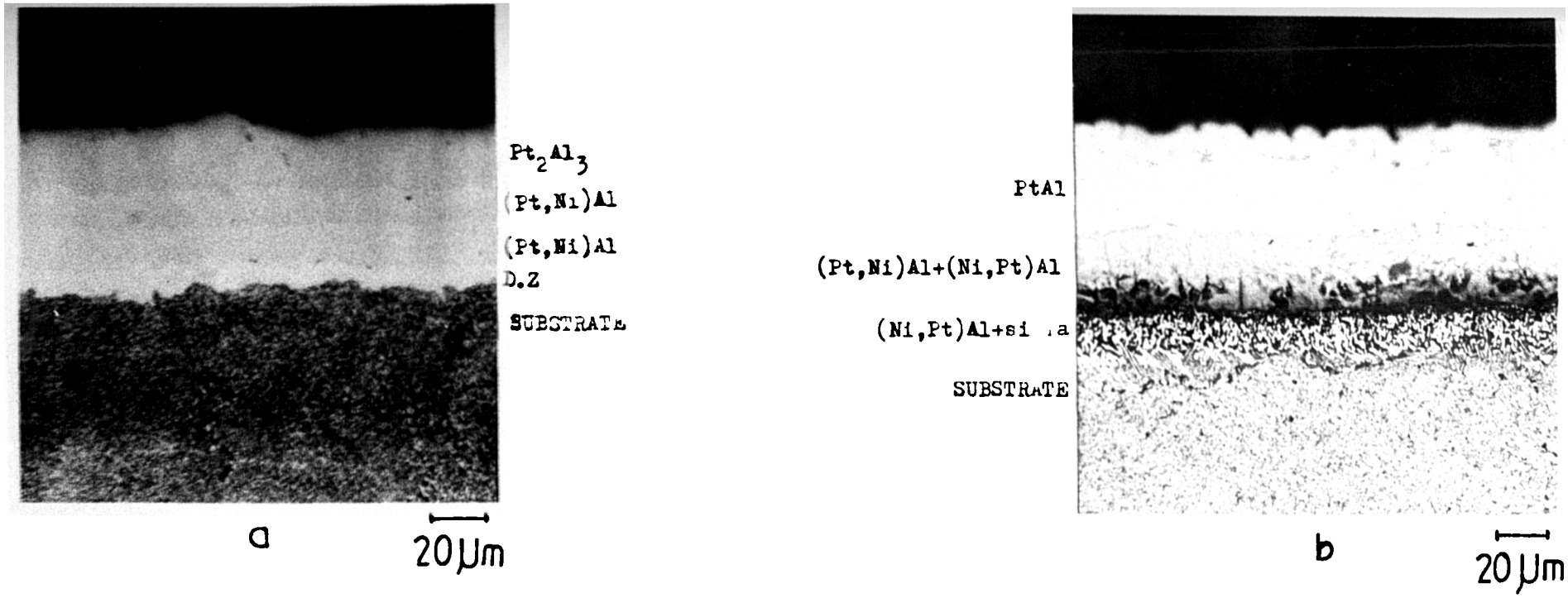

Fig.23 coating structure of heat treated 15Um Pt-coated,high activity pack after, a-5h. b-50h. Code (B).

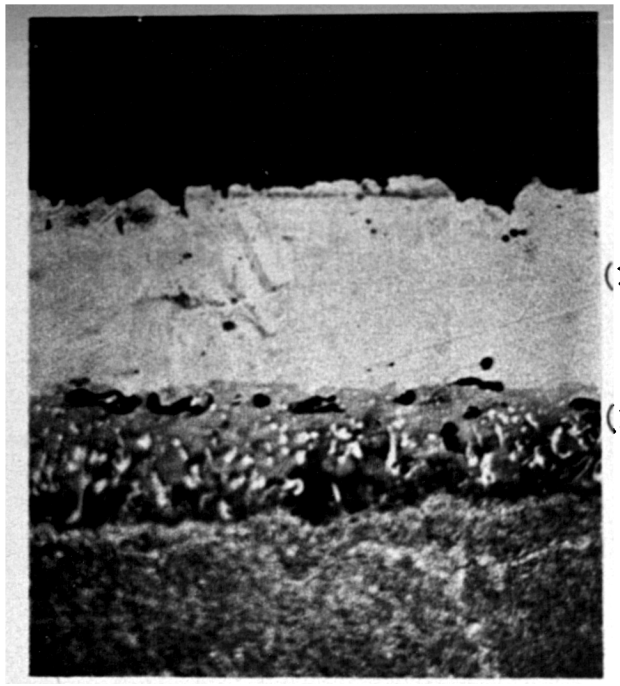

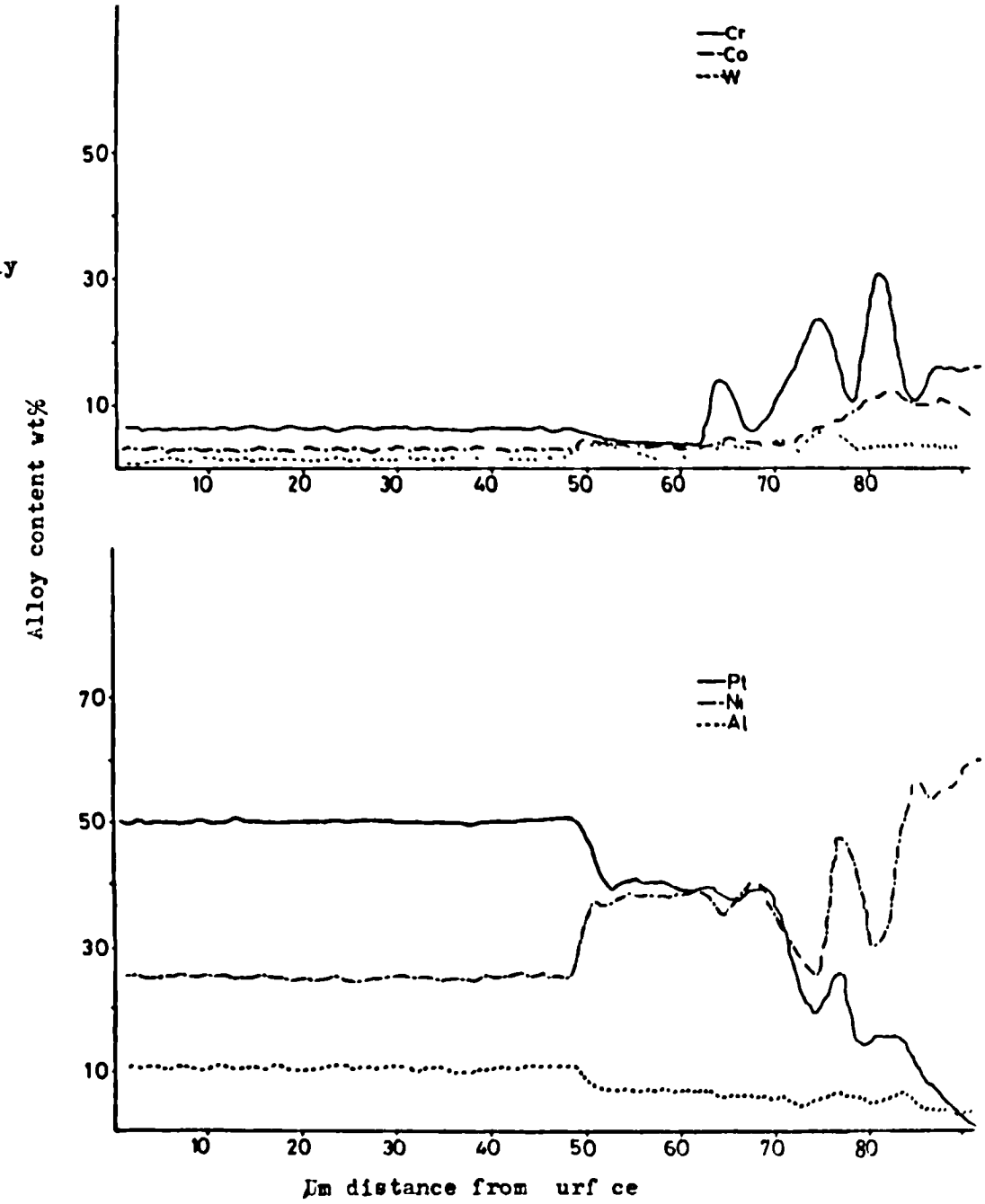

Fig.24 coating structure and compositional profile through 15µm Pt-coated high ctivity p ck after 1200h he t tre tment at 1000°C. Code (B).

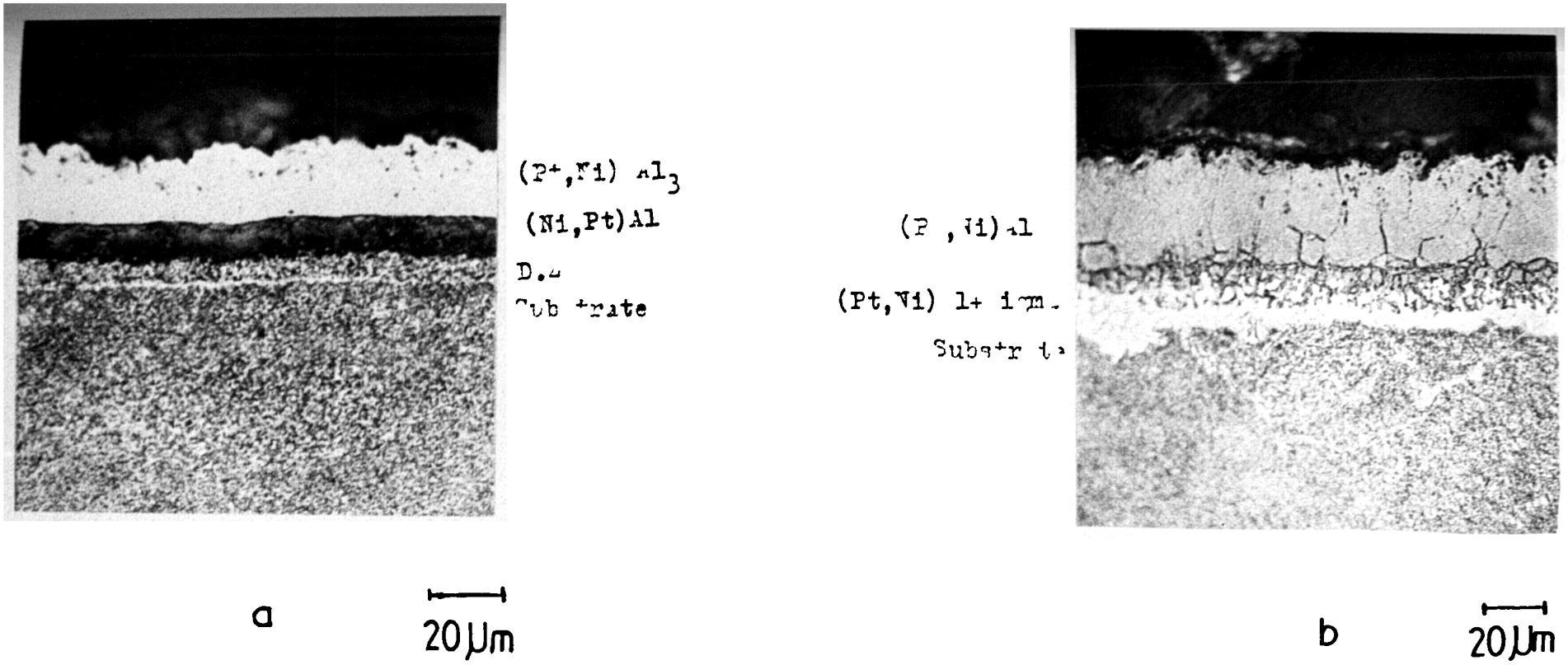

Fig.25 coating structure of heat treated 50m Pt-coated,low activity pack after, a-5h. b-55h. Code (C).

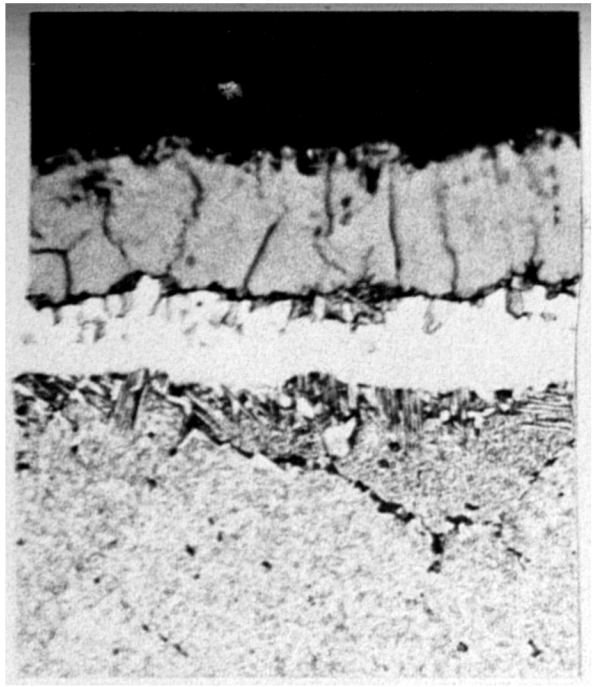

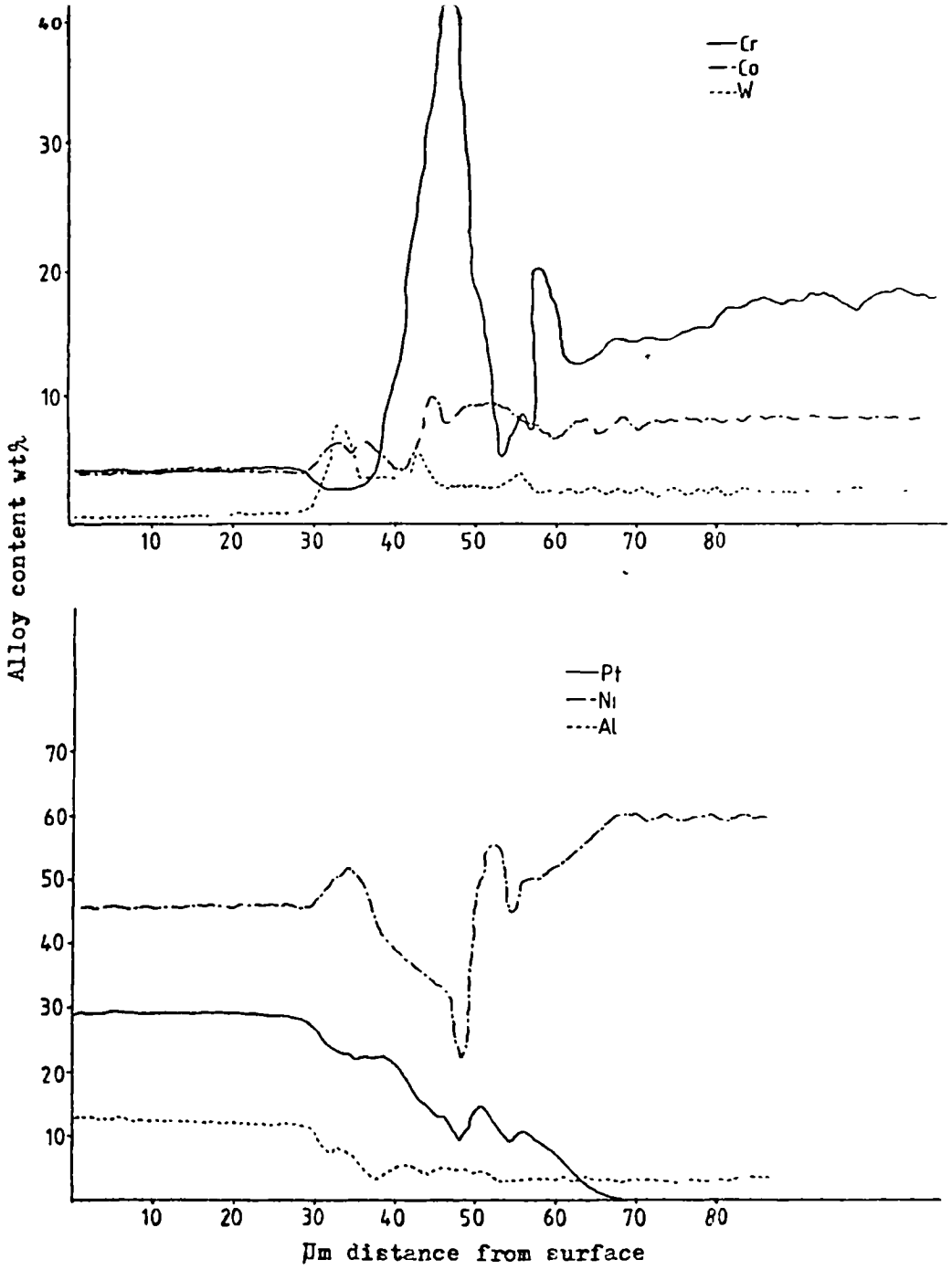

Fig.26 coating structure and compositional profile through low activity pack Aluminized Pt-coated (5µm) IN-738 after 1000h heat treatment at 1000°C. Code (C).

Figure 27 Lattice parameter of PtAl vs nickel content in At% .

A kx
4.7
4.75
4.8
4.85
At% Ni
10
20
30
40
50
60

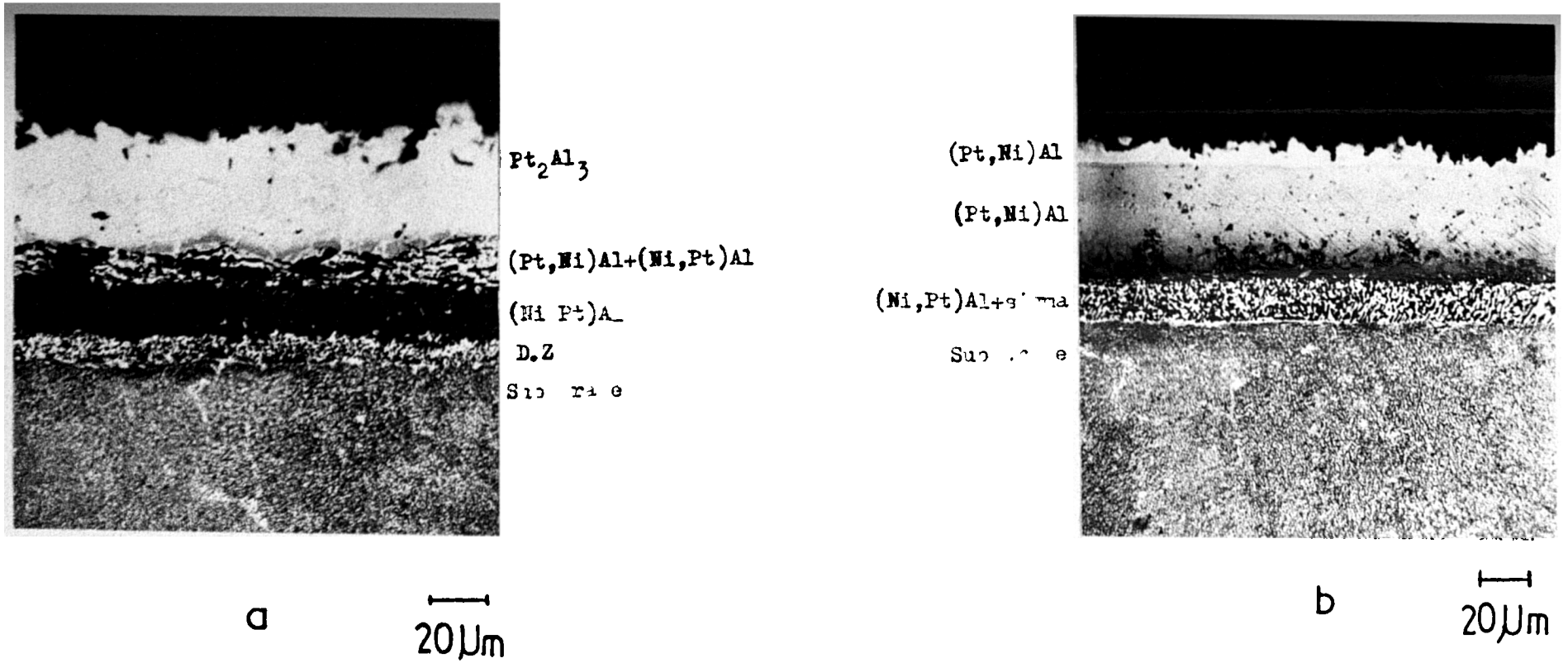

Fig. 28 coating structure of heat treated 15Um Pt-coated,low activity pack after, a-5h. b-55h. Code (D).

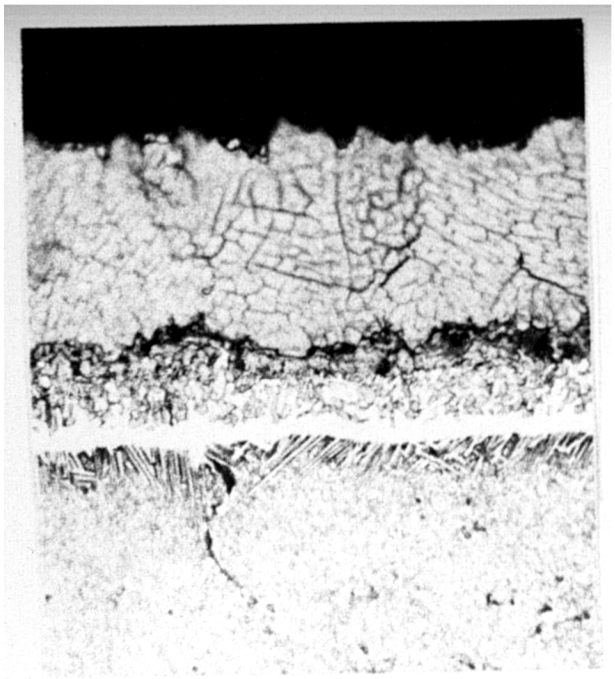

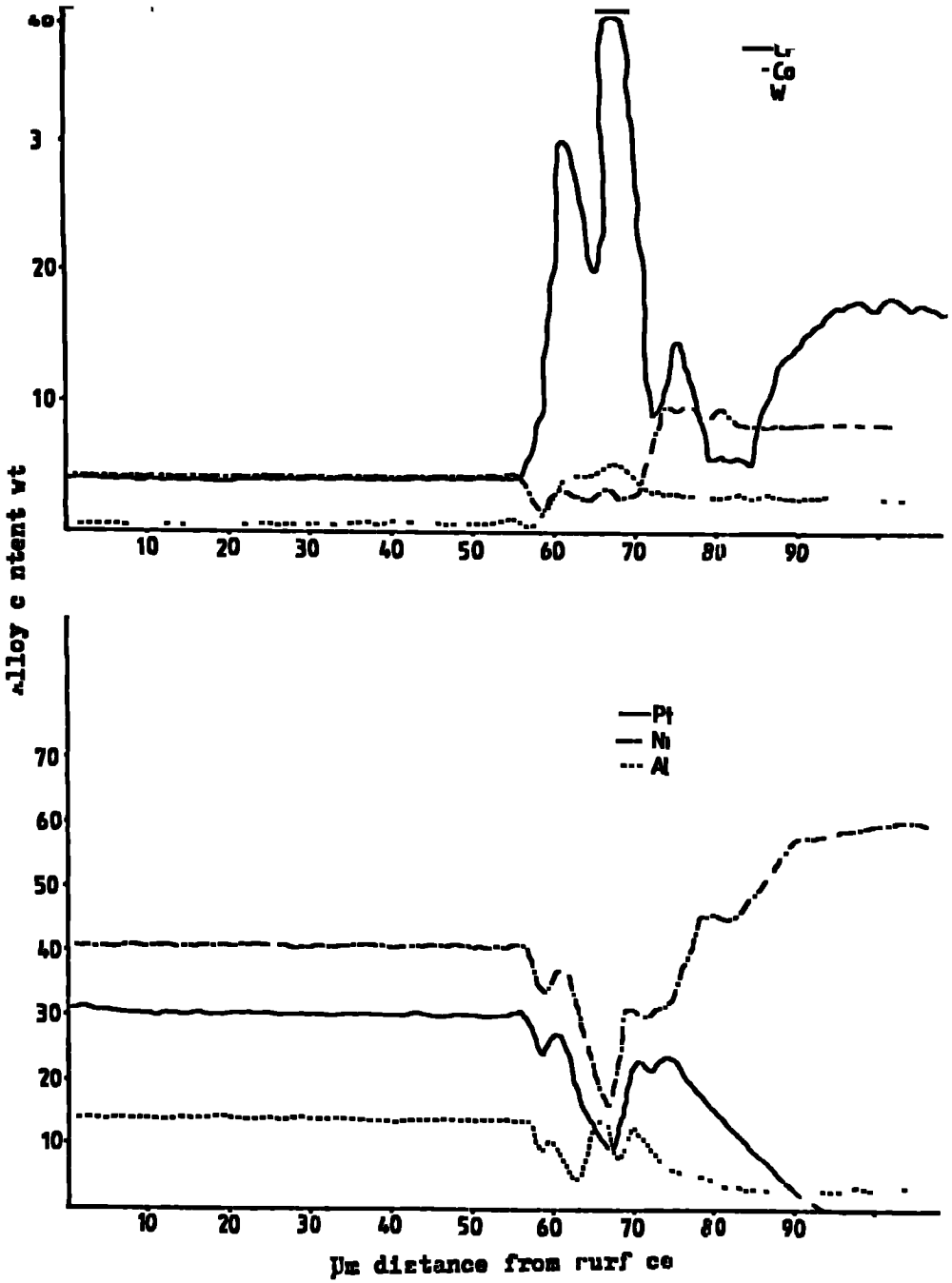

Fig. 29 coating structure and compositional profile through low activity pack Aluminized Pt-coated IN-738 after 1000h heat treatment at 1000°C. Code (D).

Figure 30 a- 28000X Transmission electron micrograph of a replica take from coating treatment D heat treated for 1000 hrs at 10C showing spheres of precipitated phase and dark extracted impingments.

b,c,d- Diffraction patterns from γ' phase(dark areas in TEM micrograph). contact printed from negative.

$\lambda L = 30$ mm Å

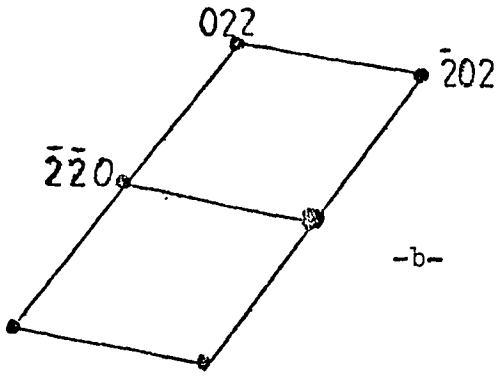

ZONE AXIS [$1\bar{1}1$]

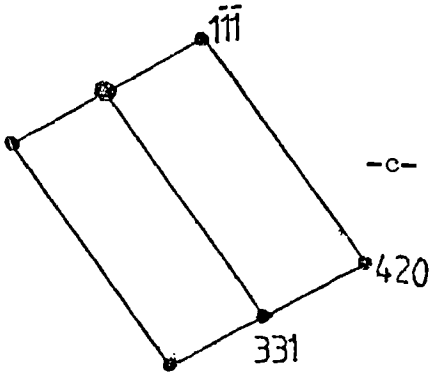

ZONE AXIS [123]

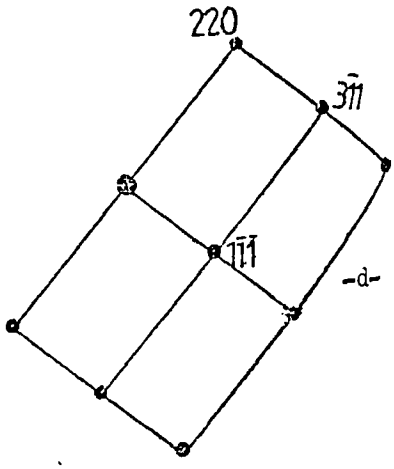

ZONE AXIS [$2\bar{1}1$]

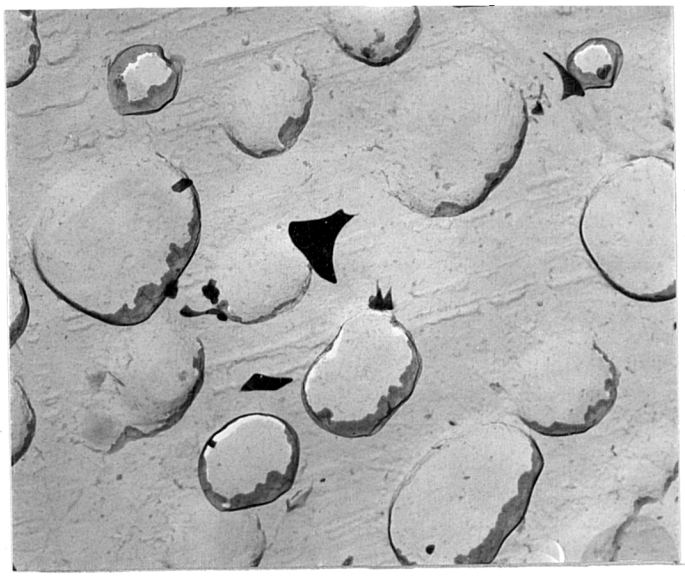

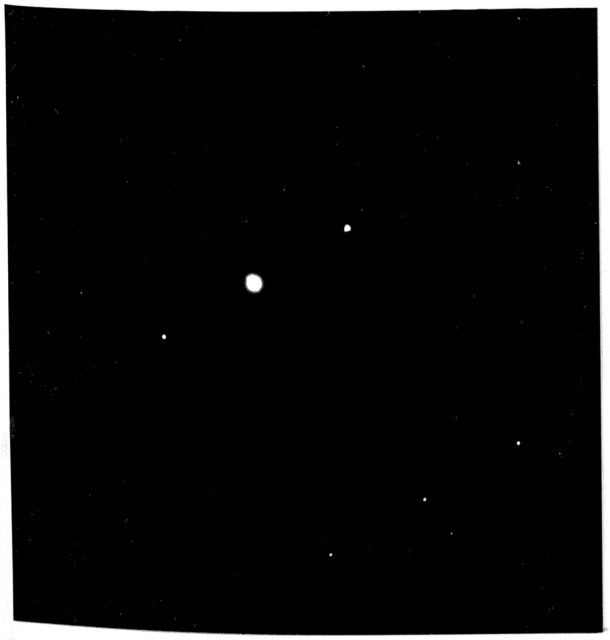

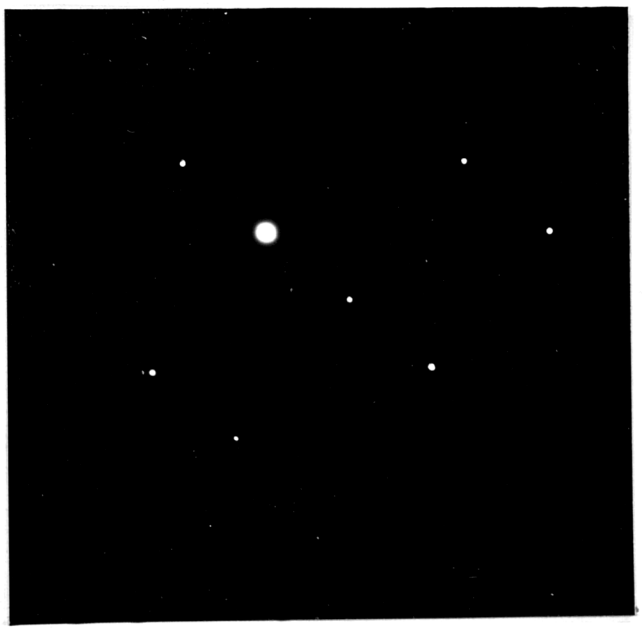

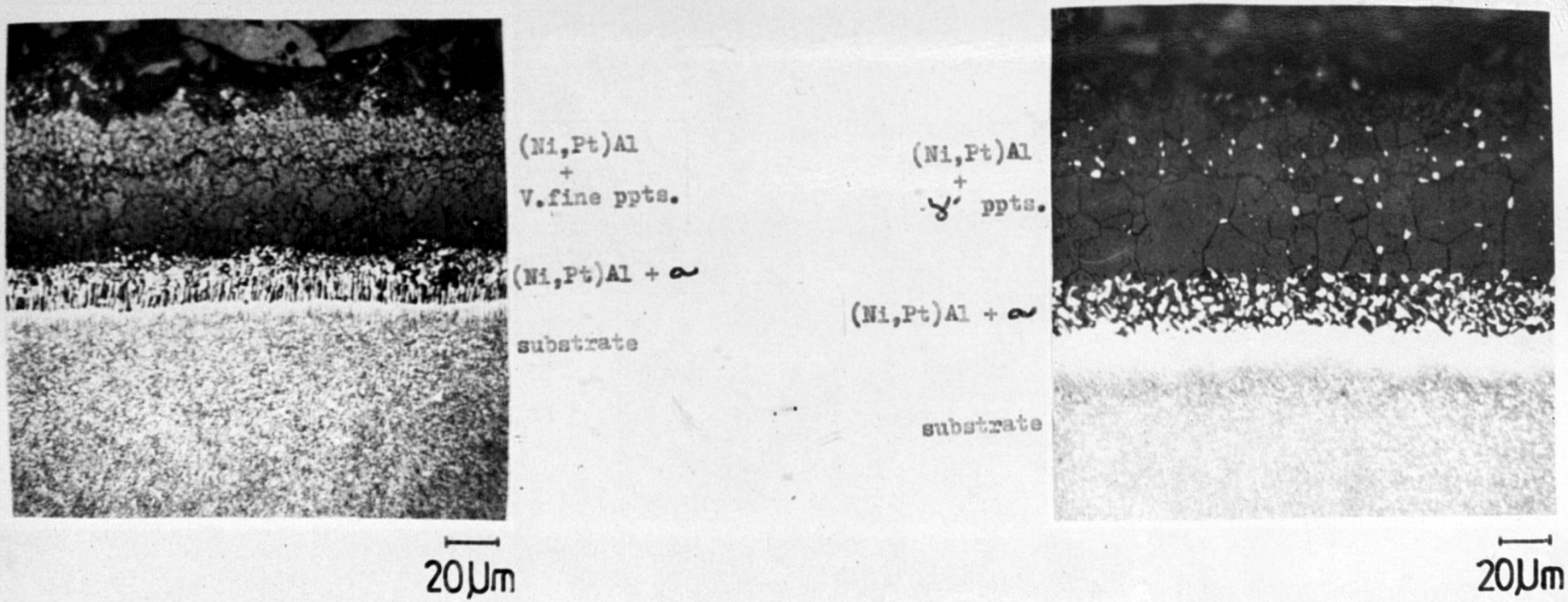

Fig. 31 Coating structure of heat treated duplex structure (coating E) after a-156 hrs. b-516 hrs. Elemental analysis is given in table

Figure 32 Weight gain versus time curves of oxidation of bare and aluminide coated IN-738 specimens in pure O_2 at 1 atm. pressure up to 5 h. at 950°C.

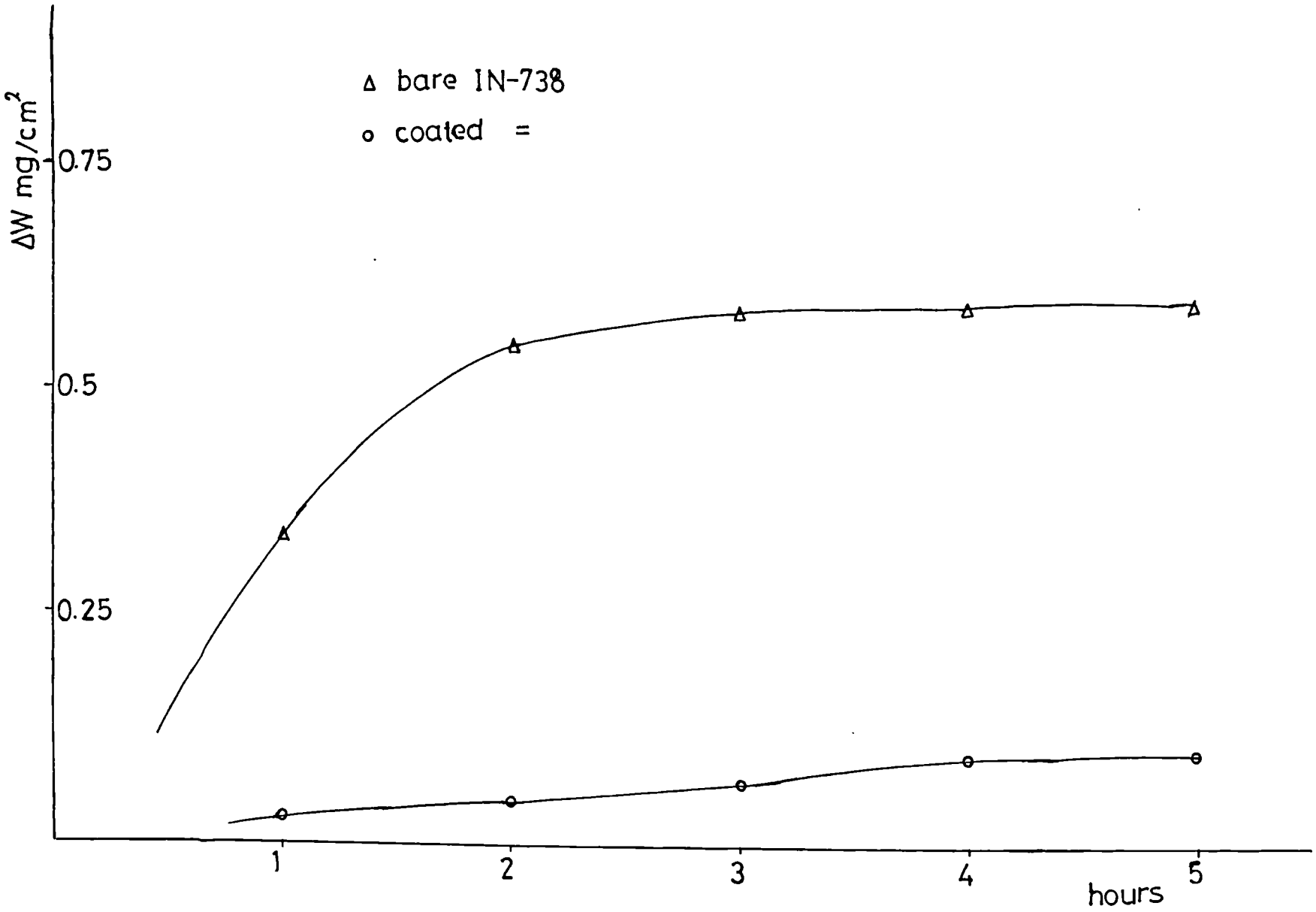
Δ bare IN-738
o coated =
ΔW mg/cm²
0.75
0.5
0.25
1
2
3
4
5
hours

Figure 33 Weight gain versus time curves of oxidation of simple aluminide coated IN-738 specimens in pure O_2 at 1 atm. pressure up to 5 h. at 900°C and 1000°C.

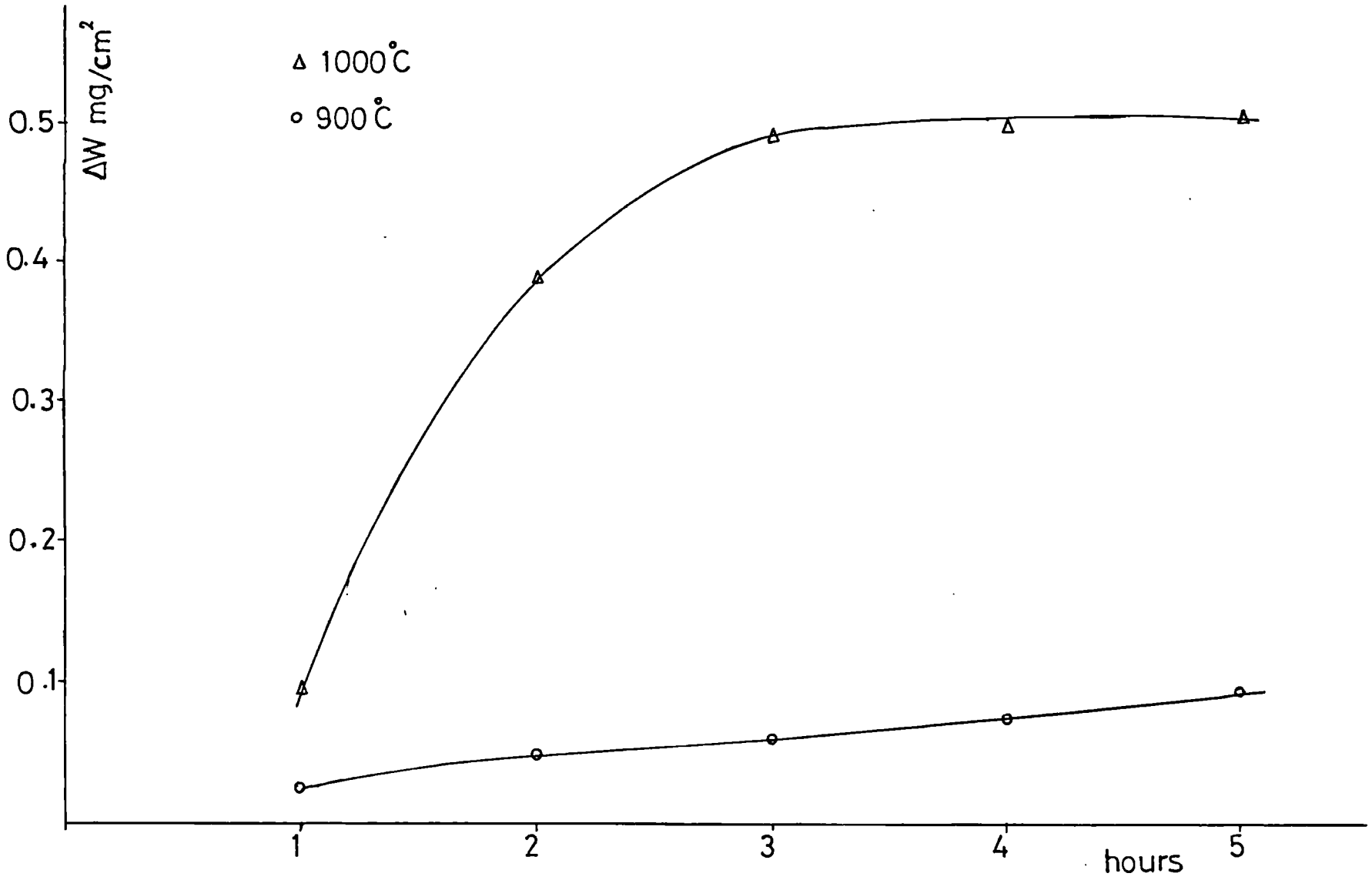
ΔW mg/cm²
Δ 1000°C
o 900°C
0.5
0.4
0.3
0.2
0.1
1
2
3
4
5
hours

Figure 34 As for figure 33, the data being replotted on weight gain squared (ΔW^2) versus time co-ordinates to test for parabolic behaviour at 900°C and 1000°C.

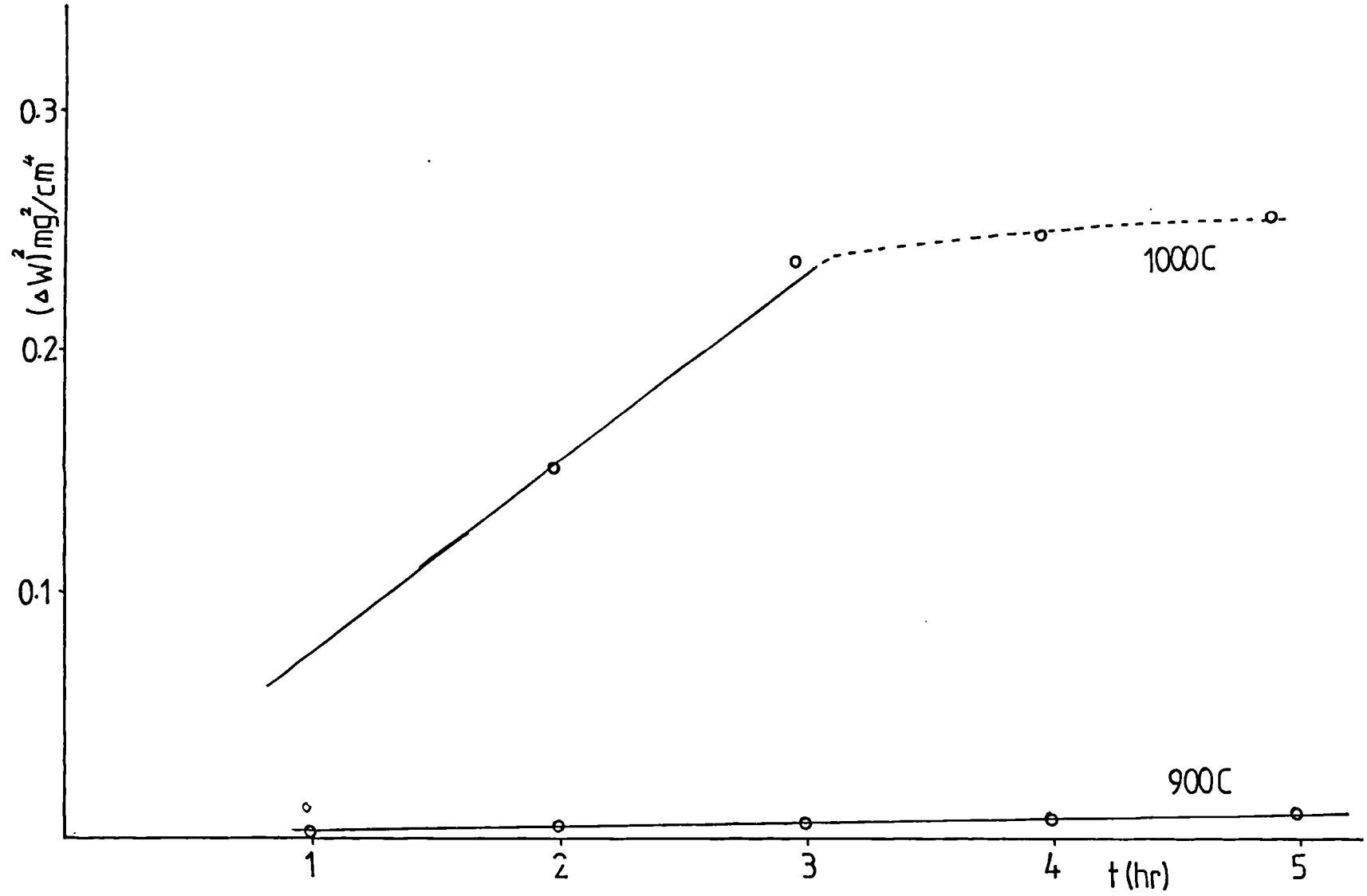
0.3
0.2
0.1
$(\Delta W)^2 mg^2/cm^4$
1000C
900C
1
2
3
4
5
t (hr)

Figure 35 Optical micrograph of simple aluminide IN-738 specimen oxidised in pure O_2 at 1 atm. pressure for 200 h. at 1000°C, specimen etched in etchant 2 ($KMnO_4$ solution).

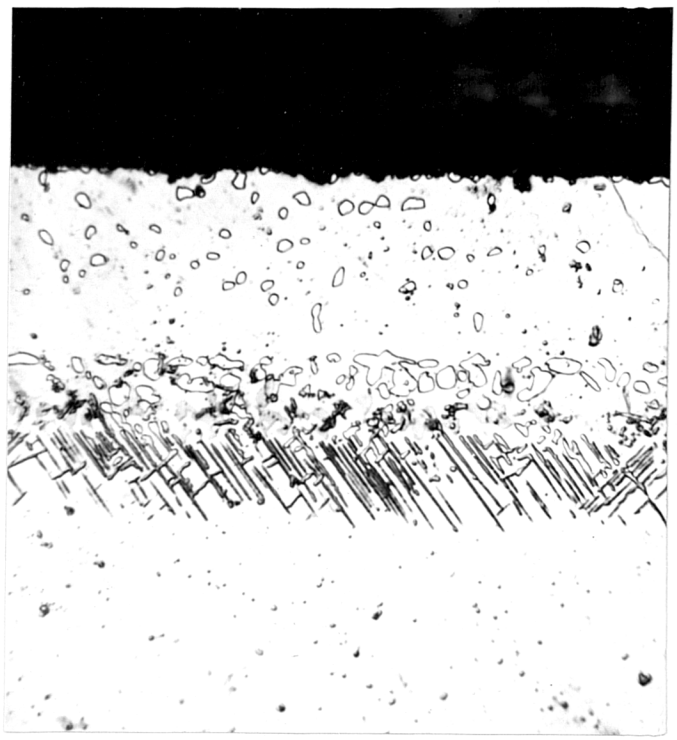

20 µm

Figure 36

The effect of temperature on the scaling kinetics of a PtAl surface in an atmosphere of Oxygen.

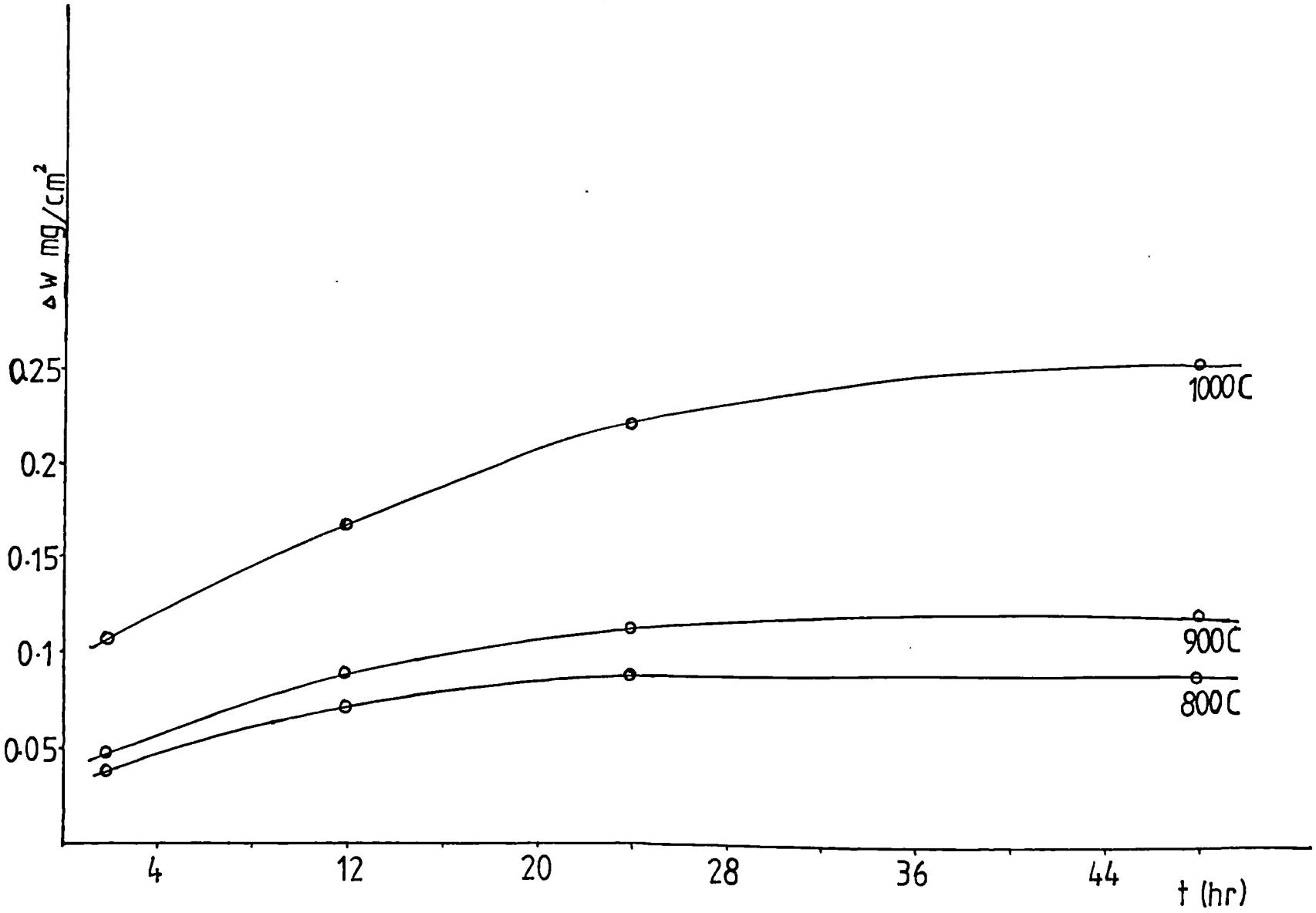
Δw mg/cm²
0.25
0.2
0·15
0·1
0·05
4
12
20
28
36
44
t (hr)
1000C
900C
800C

Figure 37

The effect of temperature on the scaling kinetics of a PtAl+NiAl surface in an atmosphere of Oxygen.

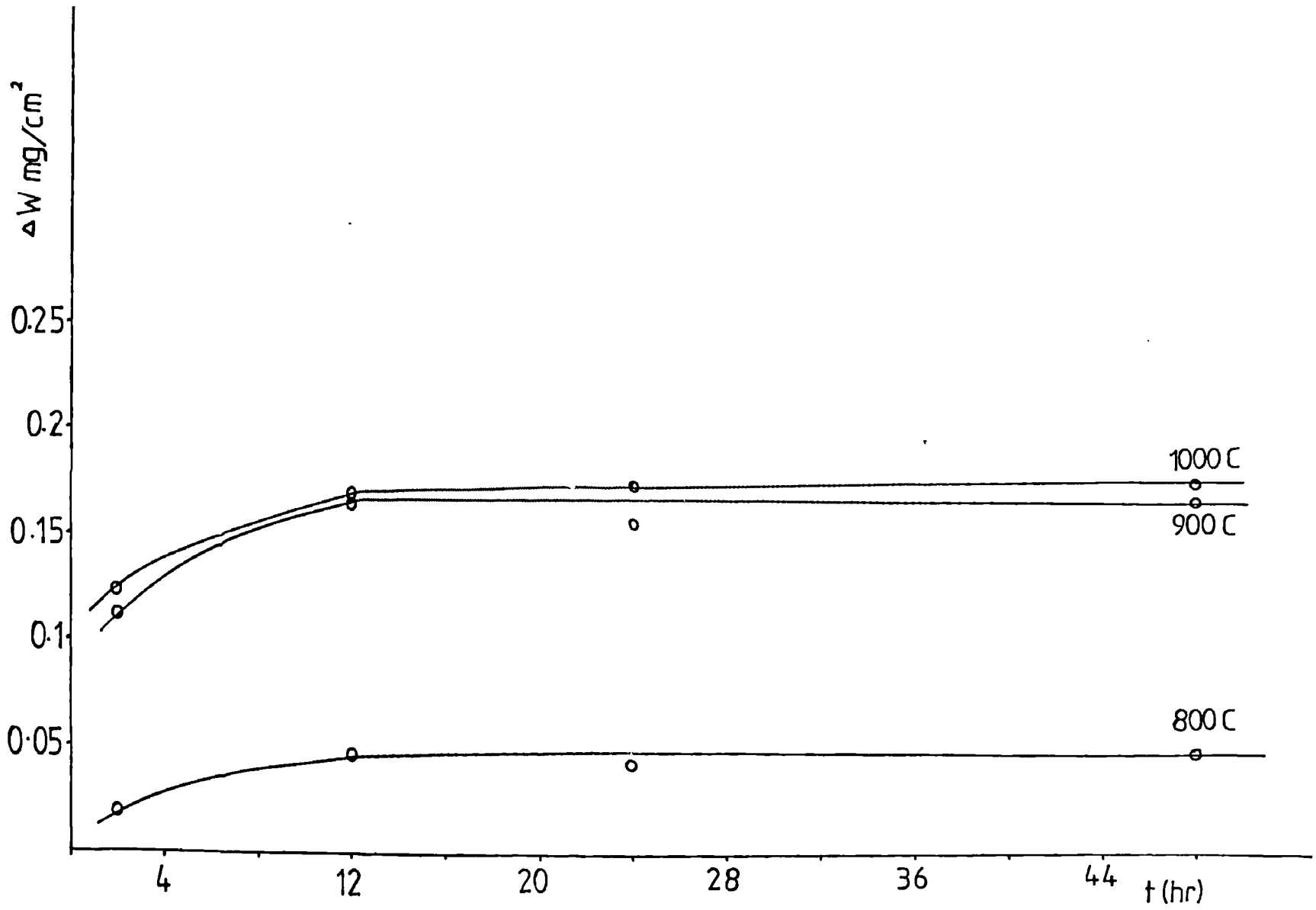
ΔW mg/cm²
0·25
0·2
0·15
0·1
0·05
1000 C
900 C
800 C
4
12
20
28
36
44
t (hr)

Figure 38

The effect of temperature on the scaling kinetics of (Ni,Pt)Al surface in an atmosphere of Oxygen.

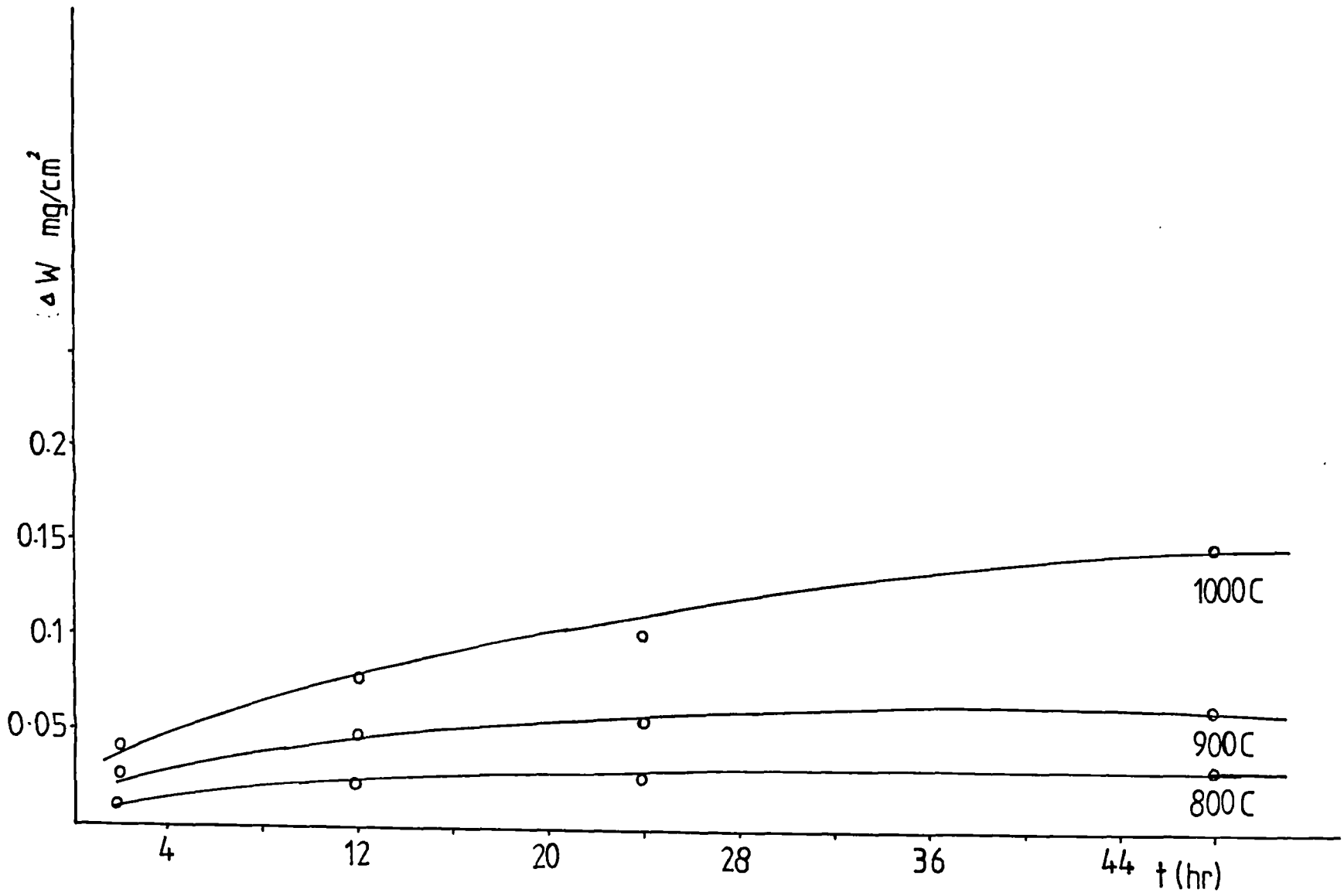
Δ W mg/cm²
0·2
0·15
0·1
0·05
4
12
20
28
36
44
t (hr)
1000 C
900 C
800 C

Figure 39

As for fig.36 the data being replotted on weight gain squered versus time co-ordinates to test for parabolic behaviour.

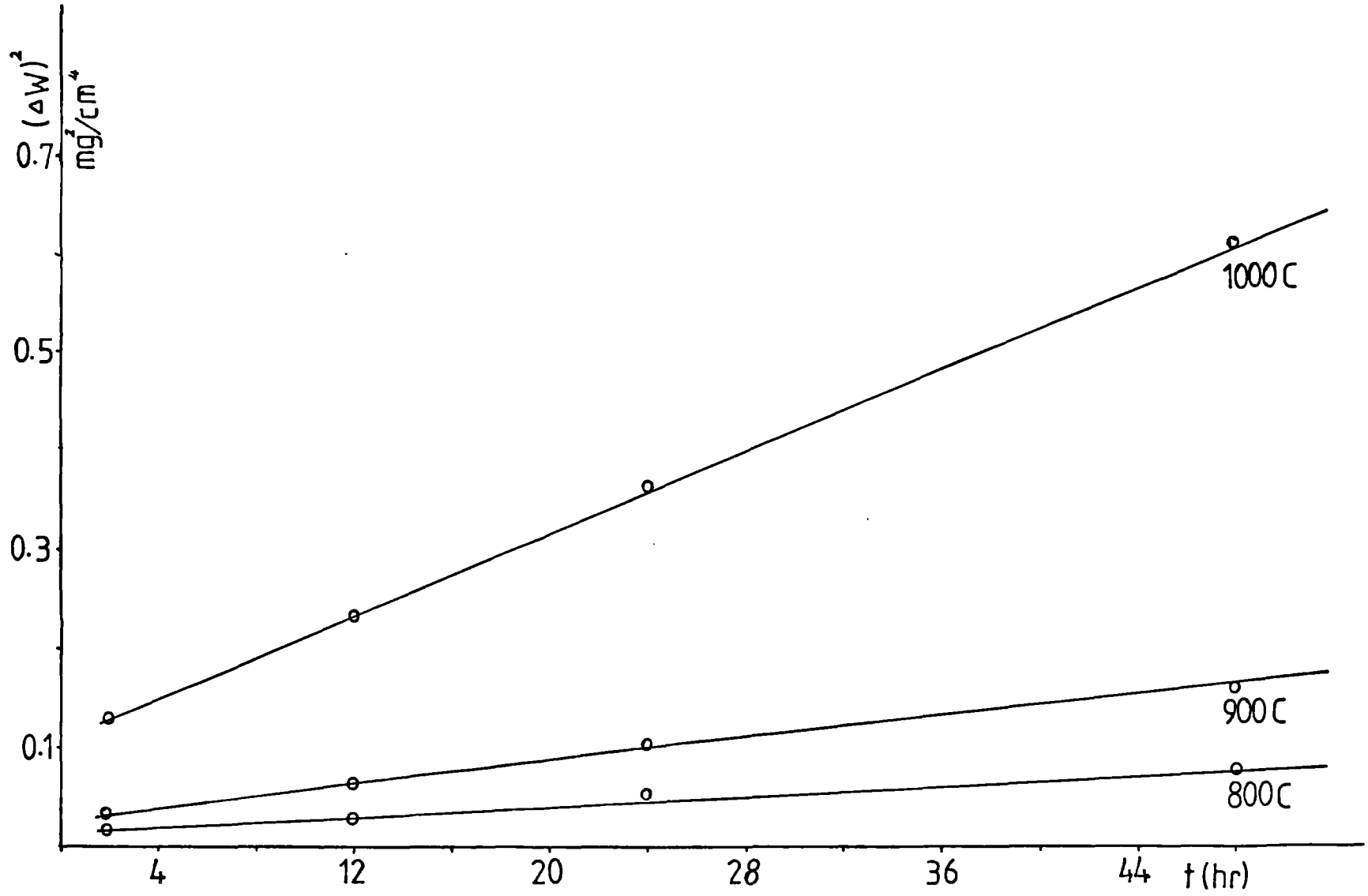
(ΔW)² mg²/cm⁴
0.7
0.5
0.3
0.1
1000 C
900 C
800 C
4
12
20
28
36
44
t (hr)

Figure 40

As for fig. 37 the data being replotted on weight gain squared versus time co-ordinates to test for parabolic behaviour.

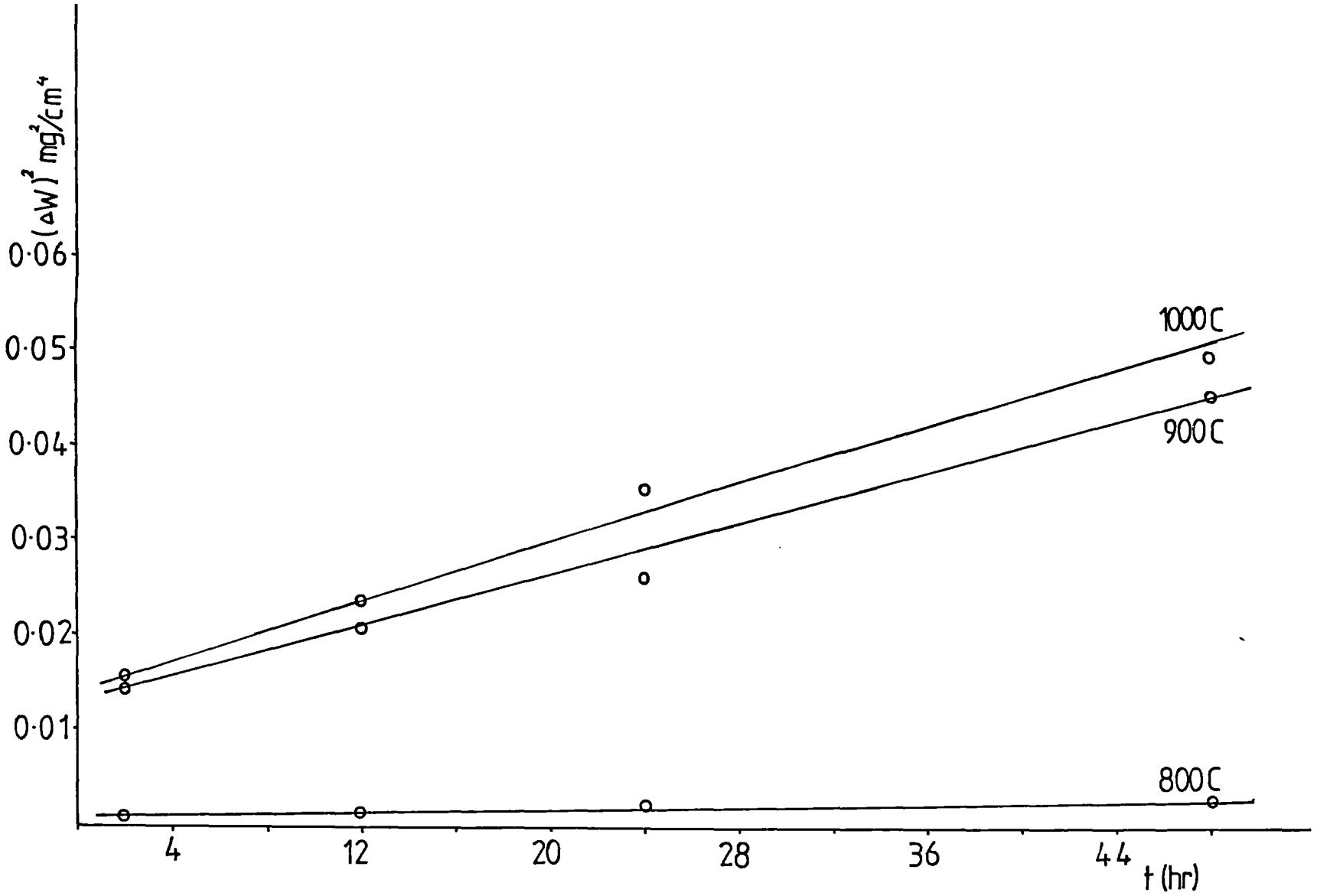
$(\Delta W)^2$ mg^2/cm^4
0·06
0·05
0·04
0·03
0·02
0·01
1000C
900C
800C
4
12
20
28
36
44
t (hr)

Figure 41

As for fig. 38 the data being replotted on weight gain squared versus time co-ordinates to test for parabolic behaviour.

0·01
0·03
0·05
(ΔW)² mg²/cm⁴
4
12
20
28
36
44
t (hr)
800C
900C
1000C

Figure 42 SEM micrographs showing:

a- Cross section of platinum-aluminised coating treatment A, Oxidised at 1000°C for 427 hrs in pure O_2, showing a thin adherent oxide layer and oxide protrusions.

b- Surface of oxide scale formed on the above specimen

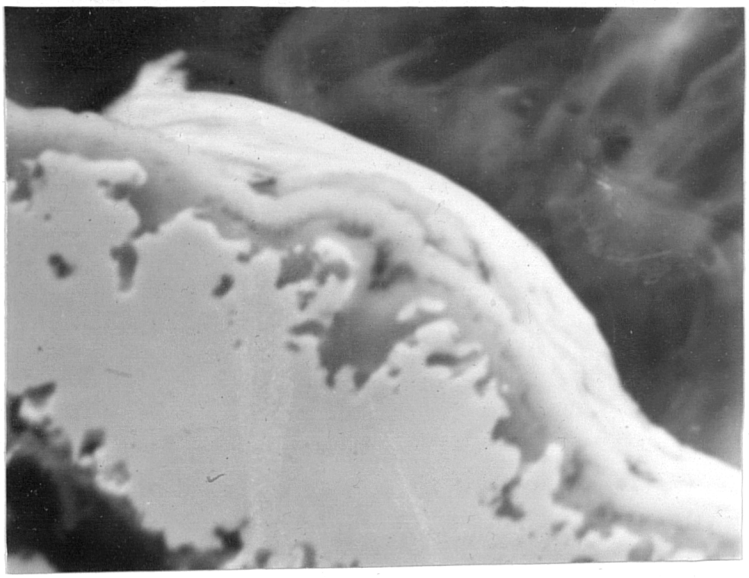

4 µm

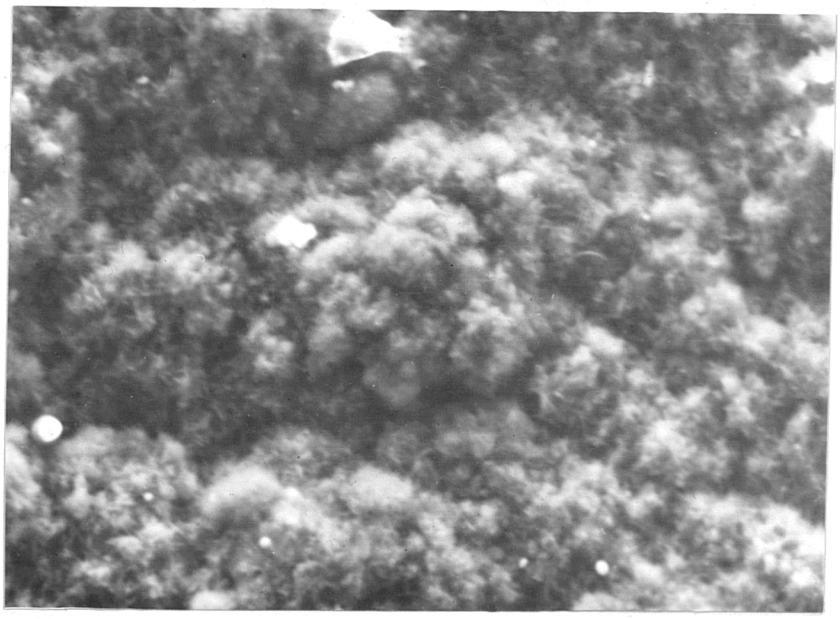

4 µm

Figure 43 microstructures and phase identities for platinum-aluminised IN-(coating treatment A) after oxidation at 1000°C in pure Oxygen, showing coating degradation, 20 micron markers shown.

a- 75 hr

b- 427 hr

c- 1200 hr . (including 550 hr of heat treatment at 1000°C).

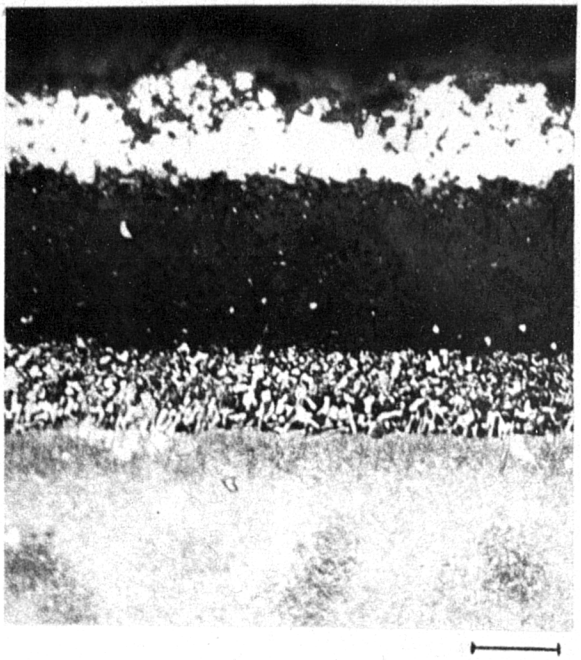
PtAl
(Ni,Pt)Al

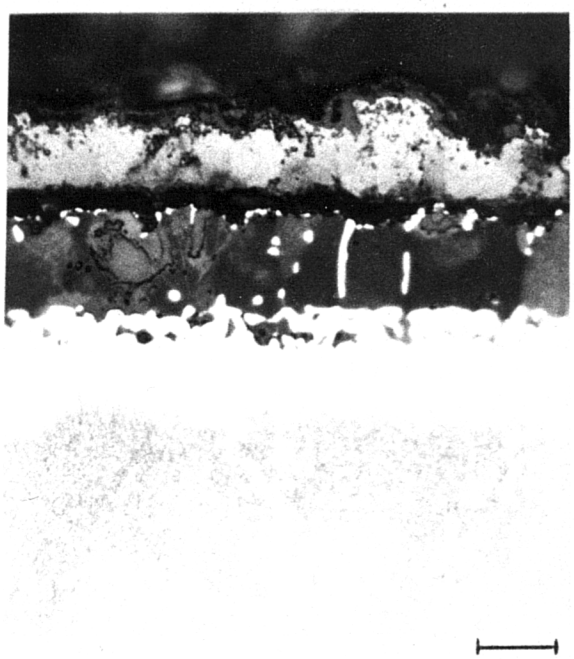
(Ni,Pt)Al
(Ni,Pt)Al+(Ni,Pt) Al

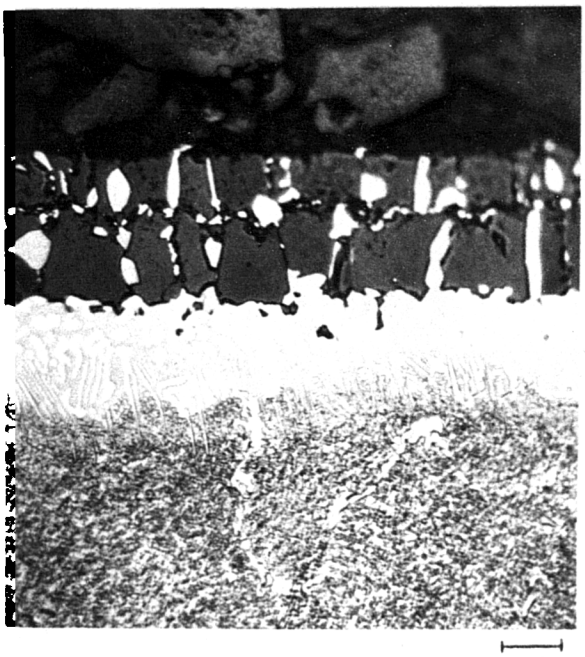
(Ni,Pt)Al+(Ni,Pt)3Al

Figure 44

a- Example of a diffusion path for a two phase diffusion couple after annealing for a time t . P and Q represent the terminal composition and R and S the interface compositions of the diffusion couple.

b- Concentration profile for component A across the diffusion couple.

C- Concentration profile for component C across the diffusion couple.

d- Diffusion path depicting a couple with a region of constitutional supersaturation in the α phase adjacent to the γ/α interface.

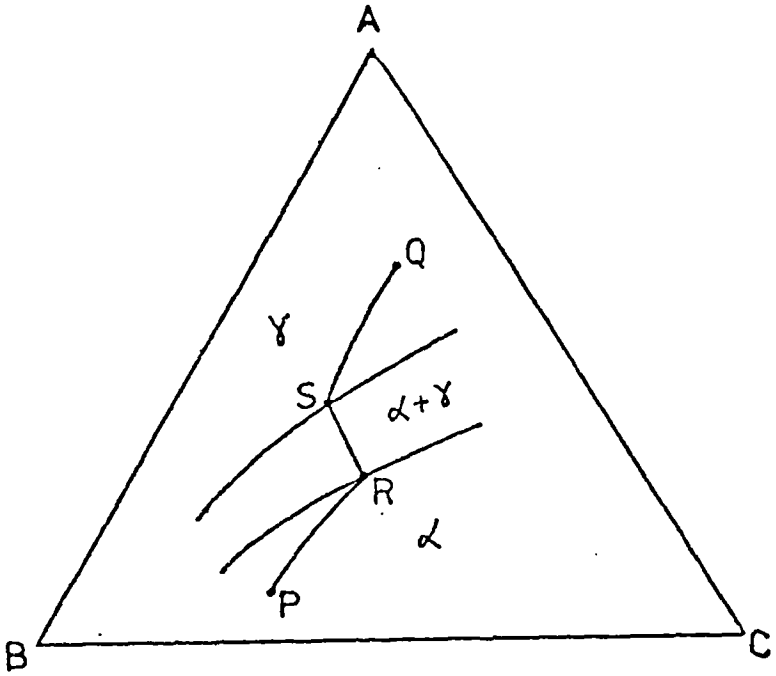
A
B
C
Q
S
R
P
γ
α+γ
α

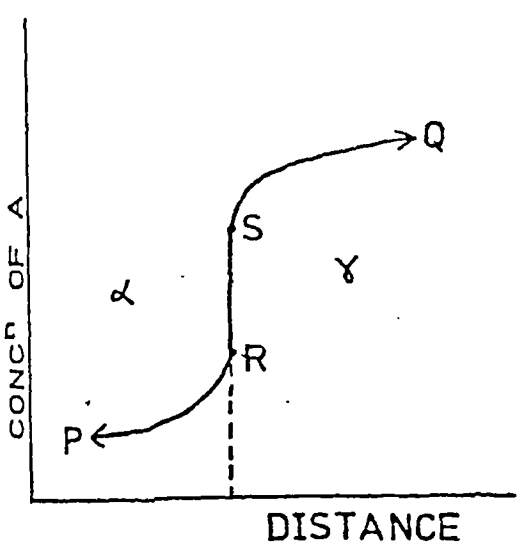
CONCⁿ OF A
Q
S
R
P
α
γ
DISTANCE

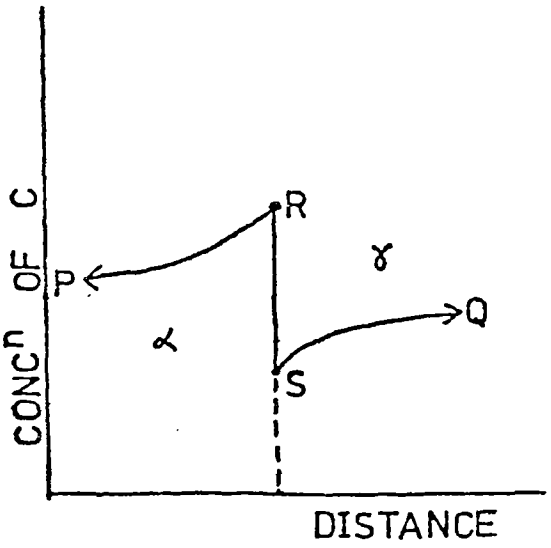
CONCⁿ OF C
R
P
Q
S
α
γ
DISTANCE

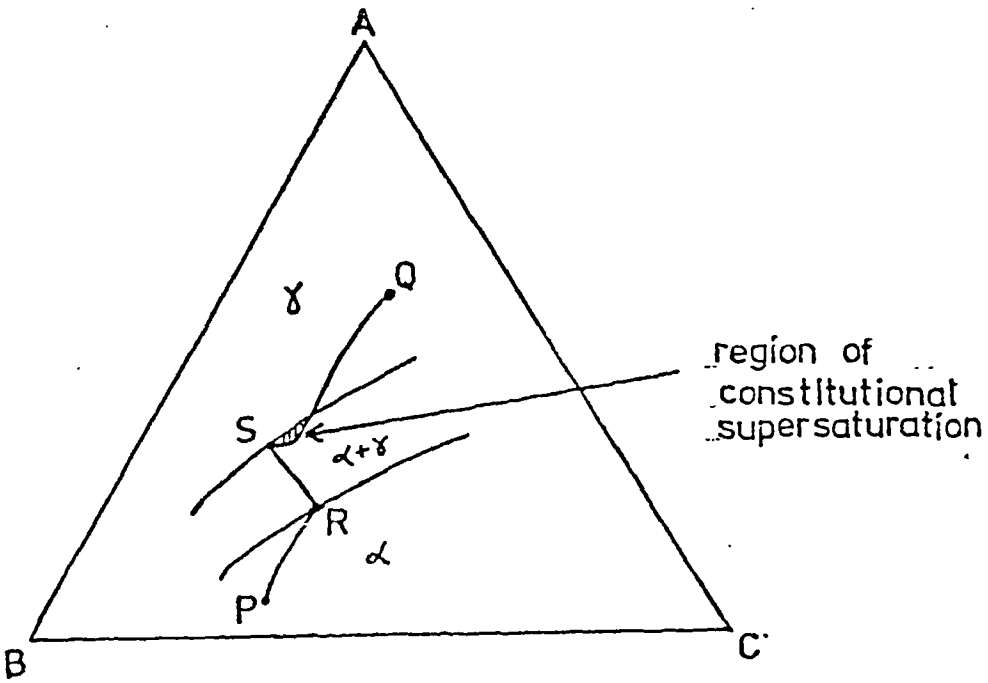
A
B
C
Q
S
R
P
γ
α+γ
α
region of
constitutional
supersaturation